Universidade de Aveiro
2018
Departamento de Química

João Carlos Morais Martins

Desenvolvimento de Microcápsulas Magnéticas como Bioreatores Dinâmicos para Aplicação na Engenharia de Tecidos

Development of Magnetic Microcapsules as Dynamic Bioreactors for Tissue Engineering Applications

Universidade de Aveiro
2018
Departamento de Química

João Carlos Morais Martins

Desenvolvimento de Microcápsulas Magnéticas como Bioreatores Dinâmicos para Aplicação na Engenharia de Tecidos

Development of Magnetic Microcapsules as Dynamic Bioreactors for Tissue Engineering Applications

Dissertação apresentada à Universidade de Aveiro para cumprimento dos requisitos necessários à obtenção do grau de Mestre em Biotecnologia Industrial e Ambiental, realizada sob a orientação científica do Doutor Vítor Gaspar e do Professor Doutor João Mano, Professor Catedrático do Departamento de Química da Universidade de Aveiro

O júri

Presidente

Professora Doutora Ana Maria Rebelo Barreto Xavier

Professora Auxiliar do Departamento de Química da Universidade de Aveiro

Doutor Vítor Manuel Abreu Gaspar

Investigador de Pós-Doutoramento do Departamento de Química da Universidade de Aveiro

Professora Doutora Maria Filomena Filipe Barreiro

Professora Coordenadora na Escola Superior de Tecnologia e Gestão do Instituto Politécnico de Bragança

Acknowledgments Firstly, I would like to thank Professor João Mano for the opportunity to be a part of COMPASS research group which allowed the participation in an international symposium as well as the participation in interesting lectures from national and international researchers. To my supervisor, Doctor Vítor Gaspar, I would like to thank for all the mentoring and explanations in all laboratory tasks and for his tireless personality regarding discussing any problems or mistakes made in the several experiments along the way as well as point out and suggest possible ways to overcome those obstacles. Besides, I am also grateful to him for always being available even after working hours.

I would also like to express my gratitude to Doctor Clara Correia for all the guidance in the capsules production procedures, assays and tutoring.

I thank all my life long friends for all their support throughout this year.

I thank all my family for their unconditional support, specially my parents for all their hard-work and sacrifice over the years. I also thank my sister for cheering me up. I thank my grandmother, even though she says she is kind of illiterate, she gives the wisest advices.

Lastly, I would like to thank Beatriz for raising me up and when I felt down, for not letting me give up, for always being by my side and always helping me move forward.

Palavras-chaves Regeneração óssea, Nanopartículas, Micropartículas, Alginato, Encapsulação Celular, Sistema Compartimentalizado

Resumo

As doenças ósseas são um problema que afeta grande parte da população mundial e têm tendência a aumentar no futuro. Apesar de o tecido ósseo ter capacidade de regeneração, quando uma fratura ultrapassa um ponto crítico o osso não possui capacidade de autorreparar esse defeito. Atualmente estes defeitos são tratados a nível médico através da utilização de implantes cerâmicos ou metálicos que originam respostas imunológicas por parte do hospedeiro e como consequência são rejeitados ao fim de algum tempo pós implantação. Além deste facto, a não bioatividade destes biomateriais restringe a reparação total do tecido e a recuperação das suas propriedades biológicas e funcionais. Terapias como a injeção *in situ* de células encapsuladas em biomateriais bioativos e biodegradáveis para aplicação na regeneração óssea têm surgido nos últimos anos como uma abordagem alternativa e vantajosa. Neste contexto, os sistemas capsulares apresentam-se como os mais vantajosos pois não só protegem as células administradas, mas também permitem a troca de nutrientes/metabolitos de uma forma eficaz. Este facto garante a viabilidade do sistema ao longo de maiores períodos de tempo, contribuindo assim para uma melhor regeneração do tecido lesado. No entanto, a implantação de microcápsulas contendo células tem-se revelado bastante desafiante devido à sua fraca interação com os tecidos circundantes, sendo comum o seu deslocamento do local inicial da implantação. Como forma de ultrapassar estas limitações, este trabalho teve como objetivo desenvolver uma cápsula magneticamente responsiva como sistema de entrega de células aderidas a micropartículas. A inclusão de reposta a estímulos magnéticos tem como objetivo permitir a fixação das cápsulas *in situ* no local de implantação através da utilização de um campo magnético externo. Para tal foram inicialmente produzidas nanopartículas magnéticas de óxido de ferro (≈42.69 nm), que foram ressuspendidas numa solução de Policaprolactona que por emulsão óleo-em-água deram origem a micropartículas magneticamente responsivas (µPCL[MNPs]) cujo tamanho médio foi de 40.5±13.2 µm antes de serem peneiradas. A gama de tamanhos a ser utilizada foi de 40-63µm para potenciar a adesão celular daí a necessidade de peneirar as partículas (55.3±9.00 µm). As micropartículas µPCL[MNPs] foram depois sujeitas a um revestimento de colagénio I para promover a adesão de células pre-osteoblásticas (MC3T3-E1) após a encapsulação. A encapsulação foi feita utilizando uma mistura de alginato, µPCL[MNPs] e células, que por gelificação ionotrópica originou a formação de estruturas esféricas como demonstrado pelas imagens de microscopia ótica. As microesferas foram posteriormente sujeitas a um processo de revestimento por deposição sequencial de polielectrólitos utilizando a técnica camada-a-camada (LBL). Esta abordagem permitiu a obtenção de cápsulas com um núcleo liquefeito e com integridade devido ao seu revestimento LBL. De seguida foi avaliada a viabilidade celular e a atividade metabólica das células encapsuladas. Resumindo, as cápsulas produzidas mantiveram a viabilidade celular e atividade metabólica ao longo de 7. Estudos *ex vivo* demonstraram que a utilização de um campo magnético externo permite a fixação das cápsulas no local onde foram colocadas mesmo quando sujeitas a lavagem com um fluído. Os resultados obtidos evidenciam que é possível fixar as cápsulas *in situ* após serem implantadas e abrem a oportunidade de utilizar estes sistemas em aplicações biomédicas no futuro próximo.

Keywords Bone regeneration, Nanoparticles, Microparticles, Alginate, Cell encapsulation, Compartmentalized system

Abstract

Bone related disorders are a problem which affects most of the world population with a tendency to increase. Although the bone tissue has regenerative capacity, when a fracture exceeds a critical point the bone does not have the capacity to self-repair this defect. Currently these defects are treated at the medical level using ceramic or metallic implants which give rise to immune responses by the host and as a consequence are rejected after some time after implantation. Furthermore, the non-bioactivity of these biomaterials restricts the total repair of the tissue and the recovery of its biological and functional properties. Therapies such as the *in situ* injection of cells encapsulated in bioactive and biodegradable biomaterials have emerged in recent years as an alternative and advantageous approach for bone regeneration. In this context, capsular systems are the most advantageous because they not only protect the cells administered, but also allow the exchange of nutrients / metabolites in an effective way. This ensures the viability of the system over longer periods of time, thus contributing to a better regeneration of the damaged tissue. However, the implantation of microcapsules containing cells has proved to be quite challenging because of its poor interaction with surrounding tissues, and its displacement from the initial site of implantation is common. As a way of overcoming these limitations, this work aimed to develop a magnetically responsive capsule as a delivery system for cells adhered to microparticles. The inclusion of a response to magnetic stimuli aims to allow the capsules to be fixed *in situ* at the implantation site through an external magnetic field. For this purpose, iron oxide magnetic nanoparticles (≈42.69 nm) were initially produced, which were resuspended in a solution of polycaprolactone which, by oil-in-water emulsion, gave rise to magnetically responsive microparticles (μPCL [MNPs]) with an average size of 40.5 ± 13.2 μm. The range of sizes to be used was 40-63μm to enhance cell adhesion, hence the need to sieve the particles (55.3 ± 9.00 μm). Microparticles μPCL [MNPs] were then subjected to a coating of collagen I to promote adhesion of pre-osteoblastic cells (MC3T3-E1) after encapsulation. The encapsulation was done using a mixture of alginate, μPCL [MNPs] and cells, which by ionotropic gelation gave rise to the formation of spherical structures as demonstrated by optical microscopy images. The microspheres were then subjected to a coating process by sequential deposition of polyelectrolytes using the layer-by-layer (LBL) technique. This approach allowed to obtain capsules with a liquefied nucleus and with integrity due to their coating LBL. Cell viability and metabolic activity of the encapsulated cells were then evaluated. In summary, the capsules produced maintained cell viability and metabolic activity over 7 years. *Ex vivo* studies demonstrated that the use of an external magnetic field allows the capsules to be fixed where they were placed even when subjected fluid wash. The results show that it is possible to fix the capsules *in situ* after being implanted and open the opportunity to use these systems in biomedical applications in the near future.

Contents

List of Figures

1.Introduction

3. Materials and Methods

4. Results and Discussion

List of tables

1.Introduction

4. Results and Discussion

7. Annexes

List of Abbreviations and Acronyms

µPCL	PCL microparticles
µPCL[MNPs]	Magnetic nanoparticles-laden PCL microparticles
µPCL[MNPs]@ALG	µPCL[MNPs]-laden alginate beads
2D	Two-dimensional
3D	Three-dimensional
ALG	Alginate
ALP	Alkaline phosphatase
BMP2	Bone morphogenic protein 2
CHT	Chitosan
DNA	Deoxyribonucleic acid
DPBS	Dulbecco's phosphate-buffered saline
ECM	Extracellular Matrix
EDS	Energy-dispersive X-ray spectroscopy
ELISA	Enzyme-linked immunosorbent assay
EMA	European Medicines Agency
EVs	Extracellular vesicles
FBR	Foreign body response
FDA	Food and Drug Administration
GFP	Green fluorescent protein
hMSCs	Human Mesenchymal stem cells
IBE	Ischemic brain extract
LBL	Layer-by-layer
MC3T3-E1	Murine pre-osteoblast cell
MES	2-(N-morpholino)ethanesulfonic acid
miRNA	Micro-ribonucleic acid
MNPs	Magnetic nanoparticles
mRNA	Messenger ribonucleic acid
NIH	National Institutes of Health
PBS	Phosphate buffer saline
PCL	Polycaprolactone
PDI	Polydispersity index
PDMS	Polydimethylsiloxane
PEG	Polyethylene glycol
PLL	Poly-L-Lysine
PVA	Polyvinyl alcohol
qPCR	Quantitative Polymerase Chain Reaction
RAW 264.7	Mouse monocyte macrophage
RFP	Red fluorescent protein
RGD	Arginine-glycine-aspartate
RNA	Ribonucleic acid
RT	Room temperature
TGFB	Transforming growth factor Beta 3
VEGF	Vascular endothelial growth factor
α-MEM	Minimum essential medium α-modification

List of Publications

I Review article: "*Advances in In vitro Cell Culture Platforms– From Therapeutics Testing Models to Cell-Delivery Systems"(manuscript in preparation)*

II Article : "*In situ magnetically fixable hydrogel-microcapsular hybrid for bottom-up bone tissue engineering"(manuscript in preparation)*

1.Introduction

Advances in *In vitro* Cell Culture Platforms– From Therapeutics Testing Models to Cell-Delivery Systems

João C.M. Martins, Vítor M. Gaspar[#], and João F. Mano[#]

Department of Chemistry, CICECO – Aveiro Institute of Materials, University of Aveiro, Campus Universitário de Santiago, 3810-193, Aveiro, Portugal

[#]Corresponding authors:

Professor João F. Mano
Department of Chemistry, CICECO – Aveiro Institute of Materials
University of Aveiro, Campus Universitário de Santiago
3810-193, Aveiro, Portugal
E-mail: jmano@ua.pt
Telephone: +351 234370733

Dr. Vítor Gaspar
Department of Chemistry, CICECO – Aveiro Institute of Materials
University of Aveiro, Campus Universitário de Santiago
3810-193, Aveiro, Portugal
E-mail: vm.gaspar@ua.pt
Telephone: +351 234370733

Abstract

Presently, *in vitro* cell culture systems are rapidly evolving away from simplistic 2D monocultures towards the establishment of tissue mimicking multi-populational clusters that can be used either for disease modeling or in advanced stem cell delivery systems. Particularly, with the dawn of biomimetic 3D cell co-cultures, more insights into tissue pathophysiology and cell-cell communication, as well as more correlative features to those of *in vivo* settings have begun to be paved. In this context, different approaches for developing advanced 3D culture systems including the incorporation of ECM-mimetic biomaterials and compartmentalized co-cultures have been increasingly proposed. However, the field is still a long way from the ideal organ-like cell culture system. Herein, insights on compartmentalized co-culture systems are summarized and critically discussed in the context of their advantages and widespread applications both as pathophysiology modelling tools or as advanced cell delivery systems for regenerative medicine. It is envisioned that improvements on the culture conditions for multiple cell populations in 3D co-culture systems under dynamic conditions that mimic those of human tissues will increase models *in vitro/in vivo* correlation, as well as their medical applicability as advanced cell-rich implants.

Introduction

Currently, the steady rising in life expectancy is leading to an increase in the percentage of elder population and higher prevalence of age-related disorders. In elder people cancer, bone/joint diseases, as well as cardiovascular, respiratory and central nervous system pathologies are presently among the most prevalent ones[1–3].

Among bone disorders osteoporosis is one of the most prevalent worldwide. The pathophysiology of this disease is characterized by the existence of brittle bones, as a consequence of demineralization and cartilage damage, or even in more severe cases total cartilage loss. From a clinical perspective metals and ceramics have been widely used in bone implants, but their grafting bears significant disadvantages [4] and co-morbidities that can lead to infection or full rejection from the host.

Regarding the central nervous system, nerves and neurons (including motor neurons), are also generally affected in older individuals, making them more susceptible to degenerative diseases, such as Alzheimer's disease and Parkinson [1,5]. To tackle these problems, present treatments involve physical therapy in combination with pharmacotherapy *via* administration of approved medicines (e.g., Donepezil, Rivastigmine, Galantamine [6]). However, the latter are only administered with a palliative objective, since no curative treatment is available for these diseases. Moreover, such administration of drug cocktails to manage neurologic disease generally triggers deleterious side effects in patients' healthy organs, a major factor that can contribute for a poorer disease prognosis, decreased life-expectancy and day-to-day morbidity.

Heart diseases are also another common type of disease that is not only increasing in incidence in elderly populations but in general populations as well[3]. Heart disease could be hereditary but most of the times is a consequence of a sedentary lifestyle and bad eating habits[7]. These conditions may lead to myocardium infarctions damaging heart tissue and are incurable and life-threatening.

From these examples of incurable or debilitating diseases, it becomes clear that the development of more effective and curative treatments is a critical requirement. However, the discovery of new therapeutics is a highly complex and multi-stage process which often involves a high attrition rate. In fact, it is estimated that only one marketable drug emerges from the screening of one million candidate compounds[8]. Such scenario is mainly attributed to the lack of sufficiently realistic preclinical testing models that can offer a robust *in vitro/in vivo* performance correlation.

Pre-clinical discovery is a crucial process of new treatments discovery. Particularly, preclinical validation generally involves the use of 2D *in vitro* cell cultures and *in vivo* laboratory animal models, as recommended by major regulatory agencies (e.g., Food and Drug Administration (FDA) and European Medicines Agency (EMA). From these two approaches, *in vitro* cell culture techniques are among the cornerstones of scientific research due to their potential to reproduce features of human biology in healthy and disease states, at a laboratorial level, with low cost and with an acceptable degree of reproducibility. In addition to drug screening, *in vitro* monolayer cell cultures have been extensively used for fundamental biology studies and for the development of tissue engineering and regenerative medicine-based approaches to improve the outcome of heart [9,10] and neurological diseases [11,12], as well as bone disorders [13,14].

However, it is important to emphasize that this is a fairly simplistic approach considering the complexity and multicellular nature of human tissues and organs. To surpass this over simplification, heterogenic 2D cell co-cultures established under static and dynamic conditions, as well as 3D culture models have been introduced. Such models better convey the interactions that are established between different cell populations allowing to explore cell-to-cell communication and their overall response to different therapeutics. From a perspective of cell delivery systems these advanced cultures may also have increased potential to give rise to fully functional tissue-like constructs.

In this context, herein we showcase the development of different cell culture systems that focus on modelling of cell interactions in a co-culture setting both in 2D and 3D. Moreover, various examples of co-culture and compartmentalized/close cell-to-cell communication models are presented and their applicability as *in vitro* models, as well as cell-rich implants is discussed.

2.1.1. Cell culture systems

Historically, the first-time that eukaryotic cells were cultured *in vitro* was in 1907, when Harrison studied frog neurons monocultured in hanging drops [15]. Since then, countless studies were performed as well as numerous techniques were developed. As the general designation suggests, monoculture cell systems consist on expanding only a single cell type in culture medium. These systems were widely used at the dawn of cell culture systems and unravelled important cell mechanisms, cellular behaviour and responses to different stimuli. 2D flat monolayer cultures of a single cell type are

reproducible, robust, relatively inexpensive and can be used in a broad range of studies owing to their versatility. Moreover, these models also avoid the economic and ethical restrictions associated with the use of *in vivo* models [16].

However, the use of single cultures with a single cell type does not properly mimic the *in vivo* scenario, nor the cellular behaviour and cellular responses observed in heterotypic cultures [17–19]. In the tissue microenvironment, cells interact constantly with neighbouring cells, either mechanically or biochemically, and with the extracellular matrix (ECM). Moreover, these parameters regulate all cellular mechanisms (physiology, phenotype and cellular fate, especially in what concerns stem cells) [20]. Co-cultures, however, replicate tissues microenvironment in a more reliable fashion since they account for the cellular heterogeneity found *in vivo*.

Unlike monocultures, in co-culture cell systems, distinct cell types are seeded and generally grown in the same culture medium (except for conditioned medium experiments), in a specific container according to the purpose of the study. Co-culture systems have been extensively used as tools to investigate and understand short and longer distance interactions between cell populations and have a key role in cell-cell interactions studies [17]. To date, *in vitro* co-culture methods comprise: (i) direct and (ii) indirect culture systems.

In direct co-culture, multiple cell types make direct contact with each other within the same culture medium, whereas in indirect co-culture, cells are kept separated in different compartments depending on their type. Consequently cell-cell interactions is mainly established via soluble mediators including growth factors, cytokines or via extracellular vesicles [21].

In tissue engineering, co-culture methods may be used to promote tissue formation with the aid of multiple cell types and to maintain the viability and guide the capacity of stem cells [22]. The types of cells involved in a co-culture system for tissue engineering and regenerative medicine applications are named target cells and assisting cells[22]. If successful, the engineered tissue will be composed with target cells which support stem cells differentiation. Assisting cells help target cells to express a desired behaviour which includes proliferation, differentiation, ECM components production (e.g., collagen), cell adhesion and/or secretion of signalling molecules. This is therefore an active feedback control system according to the target cells needs [22].

ECM is the substrate in which most cells in living tissues reside. This three-dimensional matrix has a complex and dynamic molecular composition and fibres that

provide structural support for growing cells [23,24]. Moreover , this matrix is essential to biochemical and biomechanical signalling that mediate tissue morphogenesis, differentiation and homeostasis [25]. Figure 1 represents the normal tissue ECM.

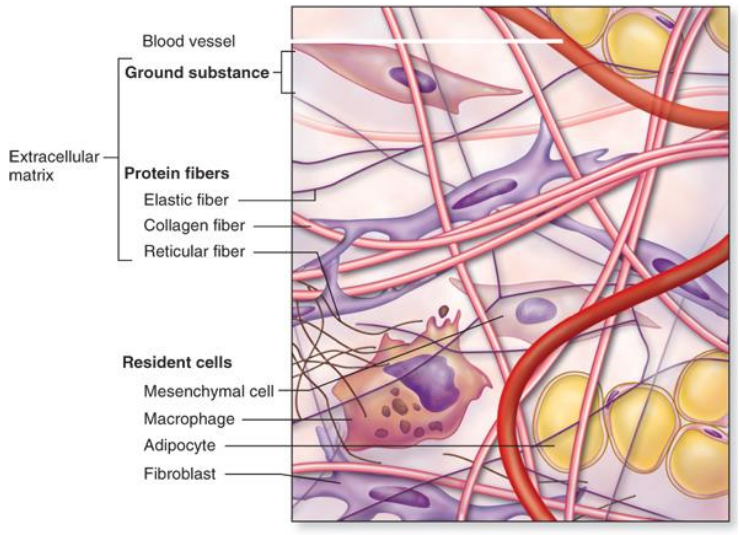

***Figure* 1.** Schematics of extracellular matrix (ECM) components and resident cell types. Adapted from King [26]

The inclusion of tissues ECM could therefore provide an added layer of spatial complexity and more *in vivo* like conditions to these models as it will be further discussed. In general when cultured in 2D monolayers cells do not resemble the conditions found *in vivo* namely: (i) ECM presence, (ii) cell morphology, (iii) physiology and (iv) gene expression, and therefore some of these studies might be misleading [23,24,27]. Differences in gene expression and hence protein synthesis is affected by cell adhesion to glass or plastic surface causing nuclei flattening [28].

Overall, *in vitro* heterotypic co-culture systems including ECM components simulate better the regenerative process than their monotypic cultures [29]. Tissue culture flasks, petri dishes and micro-well plates were used to date for establishing such models [27]. In the following chapter the importance of close or distant cell-cell communication, as well as their mechanisms are described in the context of their importance for *in vitro* models and regenerative medicine applications.

3. Cell-cell routes of communication at the distance

3.1. Cell signalling cues and interactions

Cells are regulated by different stimuli and signals which trigger different responses for cell proliferation, differentiation and function [30]. Cell signalling is an indispensable mechanism to maintain homeostasis and function. Multicellular organisms

rely on a variety of molecules as signals (e.g., peptides, large proteins, amino acids, nucleotides, steroids and other lipids) and their pathways to assure homeostasis or to promote tissue regeneration upon sustaining an injury [31].

In general, the biochemical microenvironment is comprised by cytokines, growth factors and hormones, which combined, form the signalling pathways that decide the fate of a particular cell[32,33].

There are four basic mechanisms of cell-cell signalling: (i) direct contact, (ii) synaptic signalling, (iii) endocrine signalling and (iv) paracrine signalling. Soluble factors and also exosomes[34] are more involved in paracrine processes, which depend on the diffusion of molecules to neighbouring cell of the same or different types.

Endocrine signalling: Often relies on the transport of hormones from distant locations to the local tissue microenvironment. **Autocrine signalling**: involves the production and secretion of an signalling molecule by a cell and then the molecule binds to the same cell triggering signal transduction [35]. In **paracrine signalling**: a myriad of molecules and exosomes released by cells are diffused to the extracellular fluid where they move generally by diffusion, toward other cells. Those soluble biomolecules may be taken up by neighbouring cells, degraded by enzymes, or removed from the extracellular fluid. In either way, the influence of these molecules, which are released at very low concentrations (pg/mL) in a gradient type manner, is restricted to the cells in the vicinity of the releasing cell. This pathway is important to coordinate the activities of clusters of neighbouring cells, in early tissue development and also during tissue regeneration, particularly in the recruitment of cells to the injured site [36]. From a tissue engineering perspective cells that are in contact with ECM protein coated biomaterials are also in contact with neighbouring cells by direct cell-cell contact or to more distant cells by paracrine signalling as shown in the Figure 2.

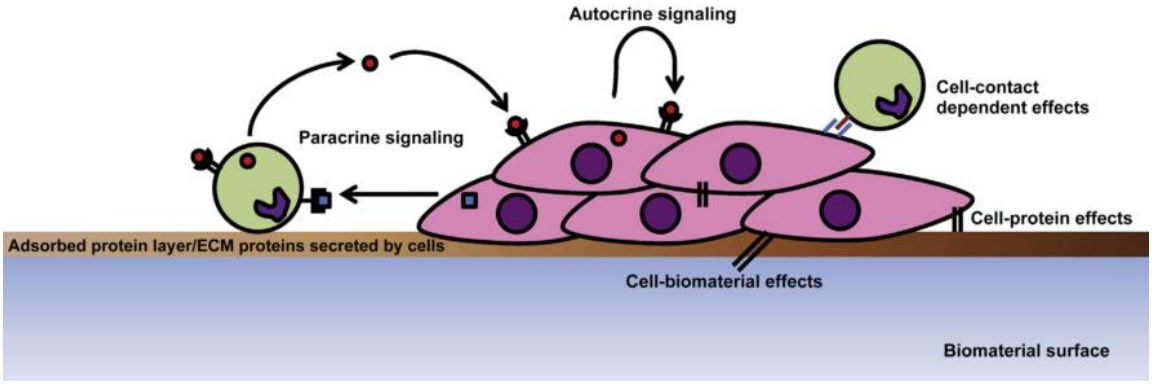

Figure 2. Different interactions in a co-culture system where cells are in contact with a given biomaterial scaffold that can also be an ECM-type material. (Adapted from Battiston *et al* [37]**)**

For example. the mechanisms of bone remodelling, either bone formation or bone resorption, are crucial to keep the structural integrity of one's skeleton throughout the years and for that paracrine signalling, as well as, endocrine signalling have a key part on establishing homeostasis. Focusing on paracrine signalling, osteoblasts, osteoclasts, osteocytes and even bone marrow macrophages secrete molecules (growth factors, cytokines and chemokines) which are responsible for the remodelling process [33].

3.1.1 Paracrine signalling – Unique extracellular vesicles

Extracellular vesicles (EVs) have raised interest due to their potential as intercellular communication mediators or as drug delivery vehicles[38] that are able to modulate physiological and pathological pathways. EVs comprise a variety enclosed spherical subcellular structures, whose membrane is comprised by a lipid bilayer, with sizes ranging between several nanometres to few micrometres[39]. EVs can be categorized according to their biogenesis processes as exosomes, ectosomes (also named shedding vesicles and microvesicles[40]) and apoptotic bodies (Figure 3) . Further information about these processes is reviewed excellently in the literature [41–43].

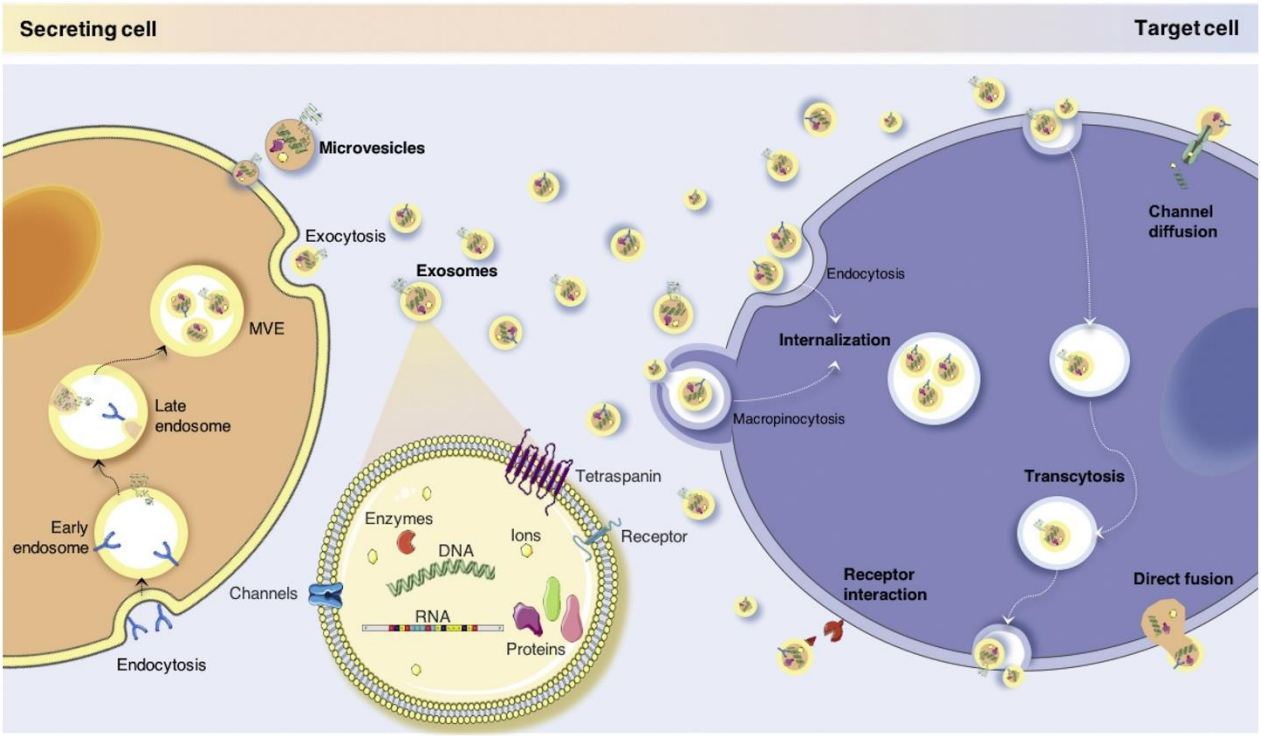

Figure 3 EV biogenesis and interaction mechanisms. Exosomes can carry nucleic acids including DNA and RNA, as well as other signaling mediators such as proteins. They are rapidly internalized by target cells and can be entrapped in cells intracellular space or be excreted by exocytosis once more. Due to their natural lipid nature and sub-cellular size, exosomes can be internalized by a number of different routes including micropinocytosis or direct fusion with the

membrane. The latter leads to rapid contents release in target cells cytoplasm (Adapted from Pinheiro *et al*[44])..

A standardised technique for EVs isolation from fluids is yet to be established, since in numerous studies different approaches are explored. Essentially, isolation is carried out through centrifugation (described as the gold standard technique [45]), polymeric precipitation, immunoaffinity isolation, microfluidics or size exclusion methods (either chromatography or filtration). More detailed information about this topic as well as quantitative and qualitative evaluation of EVs is available in the recent review by Witwer and *et al*[46].

As aforementioned, intercellular communication has a paramount importance in maintaining homeostasis and EVs are key players on paracrine signalling transporting proteins, lipids, DNA, mRNA and miRNA [43,47].

Recently, a study performed by Cha and colleagues[48] proposed an efficient scaled-up production model of microvesicles from human mesenchymal stem cells (hMSCs) for therapeutic purposes. Five production scenarios were evaluated: 2D, 2D w/shaking, 3D, 3D w/shaking and exosome-free 3D culture (exo-free 3D) where 2D culture was made in culture flasks and the 3D culture was performed in specially designed PEG hydrogel microwell, (which had complete resistance to cellular attachment) that were fitted in a six-well plate. Vesicles production was characterized by isolation through centrifugation, followed by quantification by using flow cytometry in which the microvesicles were stained with anti-CD105 and anti-annexin V to ensure that hMSCs were the cells of origin. These researchers also assessed gene expression comparing 2D- and 3D-dynamic conditions and concluded that hMSCs maintained stemness in 3D-dynamic conditions and that chondrogenesis and osteogenesis genes (TGFB3 and BMP2, respectively) were upregulated. The authors then tested the therapeutic inclusion of ischemic brain extract (IBE) to evaluate an increase of production of various paracrine factors related to angiogenesis and neurogenesis which were assessed by several cytokine assay kits and gene expression was evaluated using qPCR (Figure 4).

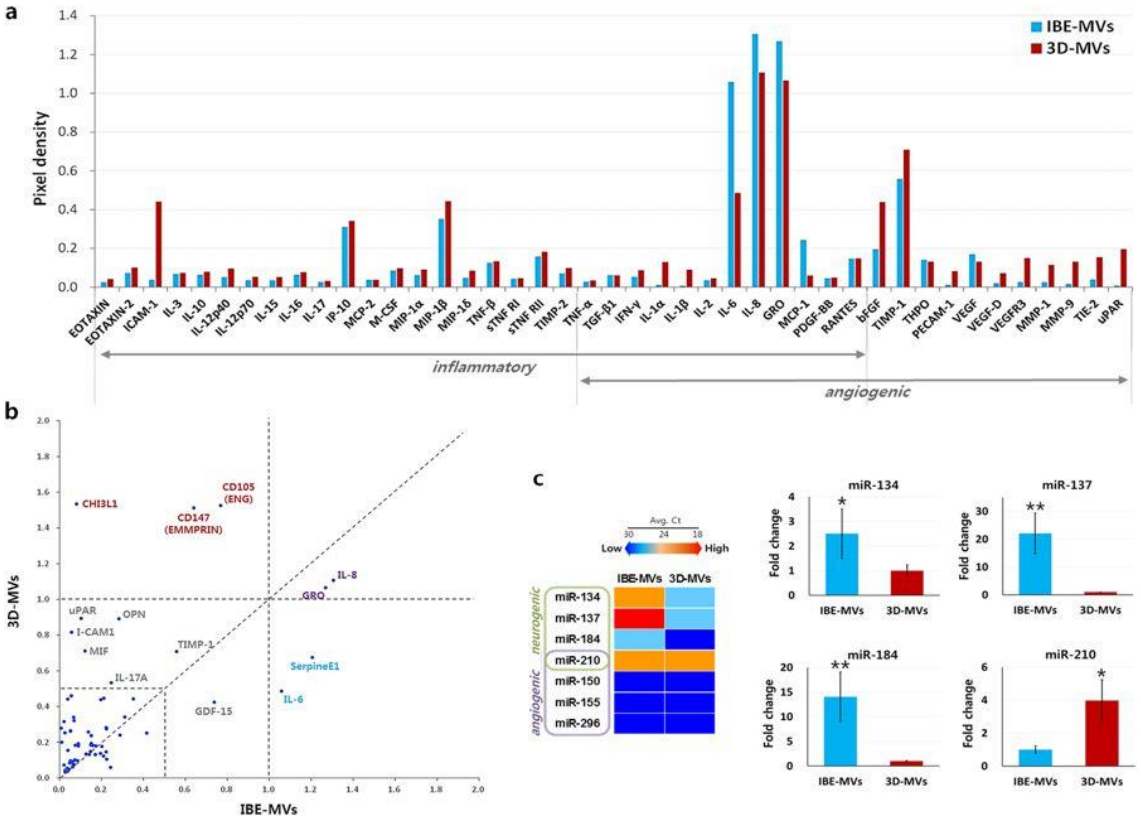

Figure 4. Cytokine profile contained in microvesicles excreted from hMSCs treated a priori with IBE and microvesicles from 3D cultures, as assessed by using several cytokine array kits (a) cytokine production from the two groups (b). Micro-RNAs included in microvesicles were evaluated using qPCR assays. These micro-RNAs are known for their key role in neurogenic and/or angiogenic molecular signalling (c). (Adapted from Cha *et al*[48])

As already mentioned, cells when cultured in 2D single cell type monolayers do not resemble the *in vivo* environment and therefore the secretion of microvesicles observed was lower in this environment. On the other hand, when hMSCs were cultured as a 3D spheroid platform cytokine production was 100-fold higher than when cultured in 2D. This is a promising approach to produce extracellular vesicles, such as microvesicles, however the production is still low for therapeutic applications. Furthermore, more pre-treatments with other trophic factors should be considered to extend the number of applications of the microvesicles.

Even though stem cell therapies have produced positive results, the transplantation of such cells is challenging due to limited cell sources, the administration must fall on an optimal time window, tumour formation or undesirable ossification, hence safety concerns have been raised [49]. Furthermore, the therapeutic effects of stem cells have been attributed to paracrine signalling involving EVs, specially exosomes, to promote intercellular communication[50]. In a nutshell, this therapy must overcome the obstacles of:

i) low production yield, ii) no standard method for EVs isolation and iii) the need for personalised and localised therapy on other organs or tissues.

To further understand paracrine signalling mechanisms, models mimicking such interactions are crucial. Recently, Ansorge *et al* reviewed systems specially designed to establish biomolecule release gradients *in vitro* to mimic paracrine communications. These models ranged from the simple and well established transwells platforms to more complex microfluidic devices including the use of microparticles as tools to generate short-ranged gradients as it will be addressed in subsequent chapters. [51]

4. 2D *in vitro* co-culture models

4.1. Static *in vitro* models - Transwells

These systems rely on a porous membrane comprised of either polycarbonate, polyester or polyethylene terephthalate or polytetrafluorethylene to physically separate different cell lines which allows reciprocal cell signalling [52].

In this context, recently, Saleh *et al*[53] aimed to study *in vitro* the effects of macrophages on the osteogenic capacity of murine pre-osteoblastic cell line MC3T3-E1 using a Transwell system. The specific aims of this co-culture were the evaluation of a cell-laden poly(ethylene glycol) (PEG) hydrogel for evaluation of cellular apoptosis, cellular morphology and also to determine its ability to induce osteogenic capacity and ECM deposition in *in vitro*. The immune cells selected were RAW 264.7 and primary derived macrophages. Hydroxyapatite nanoparticles were also included on the PEG hydrogel as wells as the adhesion peptide RGD and metalloproteinases (MMP). The MC3T3-E1 cell-laden hydrogel was set on the apical side of the transwell and the macrophages were set on bottom of the well according to the test. Firstly, the authors evaluated the morphology of MC3T3-E1 cells immediately after the encapsulation on the hydrogel and 10 days after culture. Immunohistochemical and histological analyses were performed at day 0,10 and 28 to evaluate collagen I deposition, mineralization and the existence of apoptotic cells, the latter by confocal microscopy. Media samples were collected and assessed for cytokines interleukin-6 (IL-6) and tumour necrosis factor alpha (TNF-a) using standard enzyme-linked immunosorbent assay kit (ELISA) and ALP activity was also evaluated from day 8 to day 28. DNA was quantified for the same time points. The major findings of this study were that macrophages increased MC3T3-E1 cell apoptosis, reduced cell spreading delayed or inhibited alkaline phosphatase activity, and

decreased collagen deposition, however it did not affect mineralization. Such example of long-distance co-culture emphasizes the influence of these settings in the cells of interest. In Table 1, additional examples of studies performed with Transwells are summarized.

Table 1. Studies performed using Transwells either with two different cell lines or more. The columns represent the cell lines, possible applications and references.

Cells	Application	Reference
Human amniotic membrane derived epithelial and mesenchymal cells, monocytes	Immunomodulatory activity studies	54
Human mesenchymal stem cells (hMSCs) and human pulmonary microvascular endothelial cells	Restoring the integrity of alveolar-capillary membranes	55
H292 cell line and human airway basal cells	Inflamed airway mucosa model	56
hBMSCs and HUVECs	Osteogenic and angiogenic differentiation study	57
Human keratinocytes and fibroblasts	Studying the mechanisms of wound healing	58
Multiple cell lines (three human cell lines and one bovine cell line)	Cartilaginous grafts	59
Naïve and infected macrophages	Study of the interactions between naïve and *Mycobacterium tuberculosis* infected macrophages	60
HUVECs and human retinal pigment epithelial cells	Study the interactions between cell lines to further understand retinal homeostasis mechanisms	61
Mice MSCs, MC3T3-E1 and MLO-Y4 cell lines	Osteogenic differentiation	62
Multiple cell lines (human and mice)	Treatment of inflammatory corneal surfaces diseases with stem cells	63

Rat bone marrow mesenchymal stem cells and rat bone marrow-derived macrophages	Cardiac tissue repair	[64]
Human gastric cancer cell lines (BGC-823 and MKN-28) and gastric cancer-derived mesenchymal stem cells	Study the role of MSCs in gastric cancer	[65]
Human breast cancer-derived mesenchymal stem cells and MCF7 cells	Study of the role of MSCs in breast cancer	[66]

Despite the fact that transwells are a widely used model only the interaction and behaviour of two or three types of cells are generally studied [18,21,67–69], such could be restrictive if one aims to fully recapitulate disease states or human tissues complexity *in vitro*. Moreover, in transwell platforms, cells are cultured in 2D flat substrates and in static conditions, since these models are unable to mimic the flow of culture medium during *in vitro* culture. The latter is one of the most important factors since it has been shown to influence cell alignment and gene expression [70].

4.2. Layer-by-layer cell stacked assemblies

The controlled fabrication of thin polymeric films on the micrometric or nanometric scale onto solid substrates is potentially applicable in the fields of biology and medicine. Langmuir–Blodgett deposition and self-assembled monolayers (SAMs) are predominant techniques in this research field, however both have advantages and disadvantages as stated in the seminal review of Tang *et al*[71].

The Layer-by-layer (LBL) deposition method was introduced over 25 years ago by Decher *et al*[72]. This methodology is based on the coating of a material's surface by polyelectrolytes sequential adsorption and ultimately lead to the formation of multi-layered thin films. Layers assembly consists on using opposite charged polyelectrolytes that can be of natural or synthetic origin[73]. The formation of layers is mediated by the charges of material surface and the polyelectrolytes, so to produce another layer the polyelectrolyte used the charges must be complementary (Figure 5). A rinsing step is also important to remove unbound polyelectrolytes [71]. LBL has numerous applications as

biomimetic constructs, biosensors, in drug delivery, for protein and cell adhesion, for mediation of cellular functions and as implantable materials as reviewed elsewhere [71,74–76].

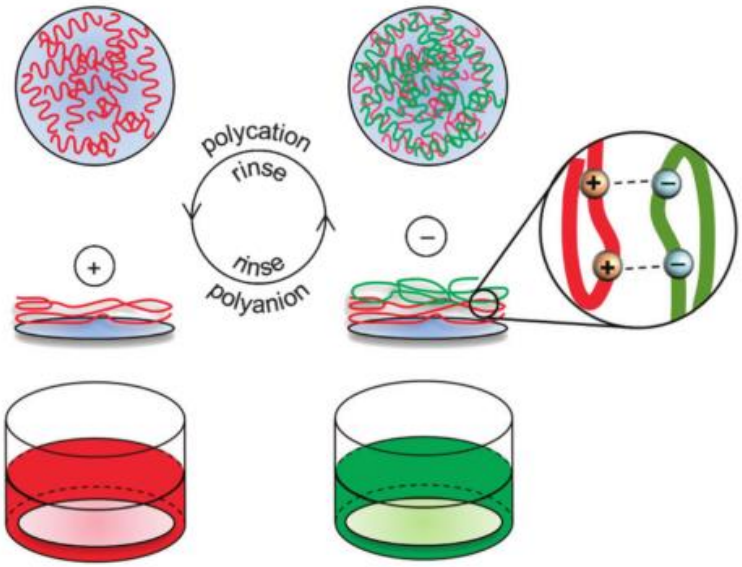

Figure 5. Schematic representation of layer-by-layer adsorption of polyelectrolytes. The first layer is positively charge so the polyelectrolyte added to produce another layer must be negatively charge. After each adsorption, a rinsing step must be used to remove the loosely adsorbed polyelectrolytes. (Adapted from Costa and Mano [77])

Inspired by the polyelectrolyte adsorption process, a few years ago, two new techniques have risen: (i) hierarchical cell manipulation and (ii) cell accumulation technique, which were developed by Matsusaki *et al*[78] and Nishiguchi *et al*[79], respectively.

The **hierarchical cell manipulation** consisted on the use of fibronectin-gelatin nanofilms prepared directly on the cell surface via LBL assembly (Figure 6). Fibronectin was selected by these researchers because of its abundance on the ECM and because of its key role in cell adhesion. Using human umbilical artery smooth muscle cells (SMCs) and human umbilical vascular endothelial cells (HUVECs), the authors developed a 3D-layered blood vessel co-culture construct that without the structural support from fibronectin-gelatin films it would not be possible due to the lack of cell adhesion in stacks. This primordial blood vessel can be applied for tissue engineering and drug-screening applications.

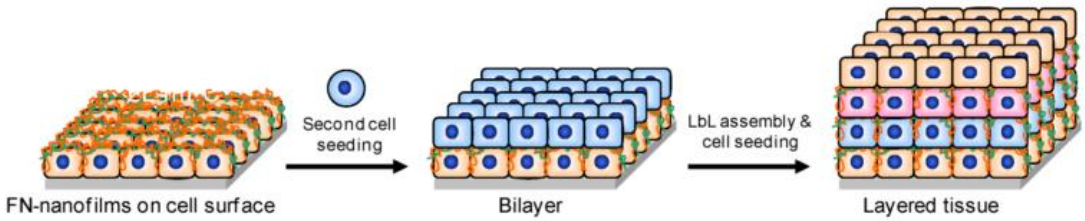

Figure 6. Schematic representation of the hierarchical cell manipulation process. Adapted from Matsusaki *et al* [78].

In the **cell-accumulation technique**, fibronectin-gelatin nanofilms are prepared on each individual cell surface and then cell-cell adhesion is induced (Figure 7).

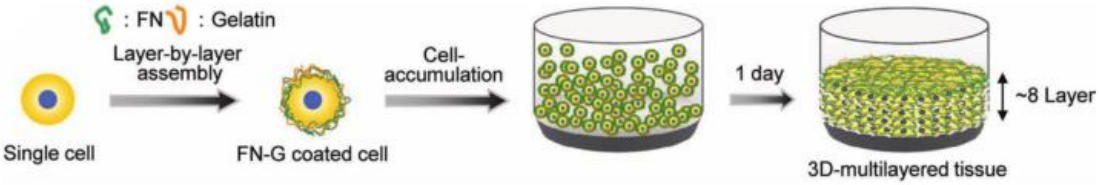

Figure 7. Schematic illustration 3D multi-layered tissues assembled by the cell-accumulation technique. Adapted from Nishiguchi *et al*[79]

Recently, Lazzari *et al* used the described cell accumulation technique to assemble triple co-culture multicellular tumour spheroids(MCTS) to mimic pancreatic tumour. [80] The cells lines employed in the assembly of this complex tumour environment whose mortality in five years reaches 97-98% once it reaches metastatic stage [81] were human pancreatic cancer cells PANC-1), human lung fibroblasts (MRC-5) and HUVECs. The authors assembled mono cultured 3D spheroids with PANC-1, double co-culture spheroids with PANC-1 and MRC-5 and triple co-culture with PANC-1, MRC-5 and HUVECs, as well as tested several cell ratios which were cultured in round bottomed 96-plates. After the assembly of 3D spheroids, they were characterized by optical imaging, Selective Plain Illumination Microscopy (SPIM) (Figure 8) and histological analysis. The preliminary results of triple co-culture 3D spheroid assemblies showed that HUVEC integration was poor and hence, MRC-5 were coated with fibronectin and gelatin to promote such integration. Although, the integration and residence of HUVECs was improved after two days of culture, on the outer boundaries of the spheroid, cancer cells were loosely attached. The spatial distribution of cells involved in the assembly of the multiple cell type 3D spheroids is shown in Figure 8 after four and seven days of culture through SPIM. The different fluorescence represented is the result of GFP-expressing MRC-5 fibroblasts and RFP-expressing HUVECs.

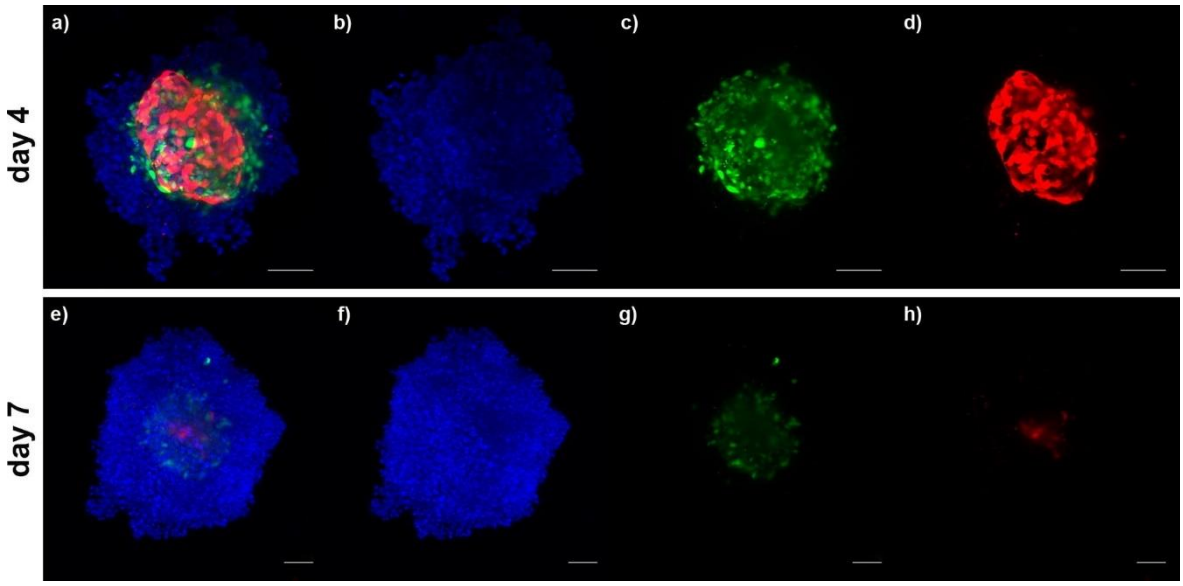

Figure 8. SPIM 3D topography of MCTS comprised of PANC-1:MRC-5(coated with fibronectin and gelatin) :HUVECs at day 4 and day 7. (a, e) Overlay of blue (Hoechst 33342, nuclei), green (GFP-expressing MRC-5 fibroblasts) and red (RFP-expressing HUVECs) fluorescence; (b, f) single blue channel (λ_{exc} / λ_{em} 405/440 nm) showing all cell nuclei; (c, g) single green channel (λ_{exc}/ λ_{em} 488/525 nm) showing GFP-expressing MRC-5 fibroblasts; (d, h) single red channel (λ_{exc} / λ_{em} 561/605 nm) with RFP-expressing HUVECs. Scale bars: 100 µm. Adapted from Lazzari *et al* [80]

After 3D MCTS assembly, the authors sought to evaluate the different resistance patterns to doxorubicin and gemcitabine concluding that the MCTS assembled in triple co-culture displayed higher resistance the anticancer drugs tested. To corroborate the data acquired, another pancreatic cancer cell line (BxPC-3) was chosen and the assembly methods were the same. However, BxPC-3 monoculture spheroid showed more resistance to the anticancer drugs than the BxPC-3 triple co-culture MCTS related to the denser and more compact of the BxPC-3 monoculture spheroid causing lower diffusion of the drugs.

The work developed is a breakthrough on assembling a complex pancreatic tumour microenvironment allowing to understand the influence of such environment on the drug efficacy replicating *in vivo* environment. The authors pointed out a limitation of this study which was the use of gelatin instead of collagen in MRC-5 coating since collagen is a main component of pancreatic tumour ECM however, the use of collagen would mean lowering the pH which would ultimately affect cell viability.

Several works involving cell LBL have been developed recently to assemble vascularized networks(blood vessels or lymphatic vessels)[82–85], pancreatic β-cell spheroids[86], multi-layered fibroblast cell sheets[87], liver tissues[88], high-throughput drug screening models [89] and even induced pluripotent stem cells derived cardiac tissues[90,91]

This approach could be useful to assemble *in vitro* tissues which could be then transplanted to a patient injured area or act as a model to study the microenvironment and drug screening.

4.3. Dynamic Co-culture systems

4.3.1. Microfluidic 2D and 3D Platforms

Microfluidic chips are precisely engineered platforms with interconnected reservoirs and/or channels that allow both the passage of fluids and also cells culture and adhesion into the chip if the surface is permissive or coated with macromolecules that promote cell adhesion and proliferation [92,93]. Microfluidic chips have a large spectrum of applications as dynamic cell cultivation set-ups (Figure 9). They can be used for: high-throughput screening of cell metabolites, organ-on-chip drug screening assays, single cell encapsulation and biomolecular analysis. Moreover, microfluidic chips can be used to produce drug delivery systems encapsulating advanced therapeutic molecules, can also be used for cell culture and establishment of cancer models[20,93–102]. The latter could be particularly useful since it can contribute to reduce animal testing and provide faster and more reliable *in vitro/in vivo* correlation.

Earlier microfluidic chips only relied on 2D cell cultures while depending on the chip surface to be coated with a material which allowed cell adhesion in order to provide cell proliferation. However, these systems did not ensure an adequate environment to recapitulate cell-cell interactions *in vivo* since there was no perfusion which is paramount for nutrients, metabolites and waste products and dissolved gases to flow in accordance to a correct cellular environment, despite having reservoirs whose efficiency is not the ideal to recapitulate such environment[103].

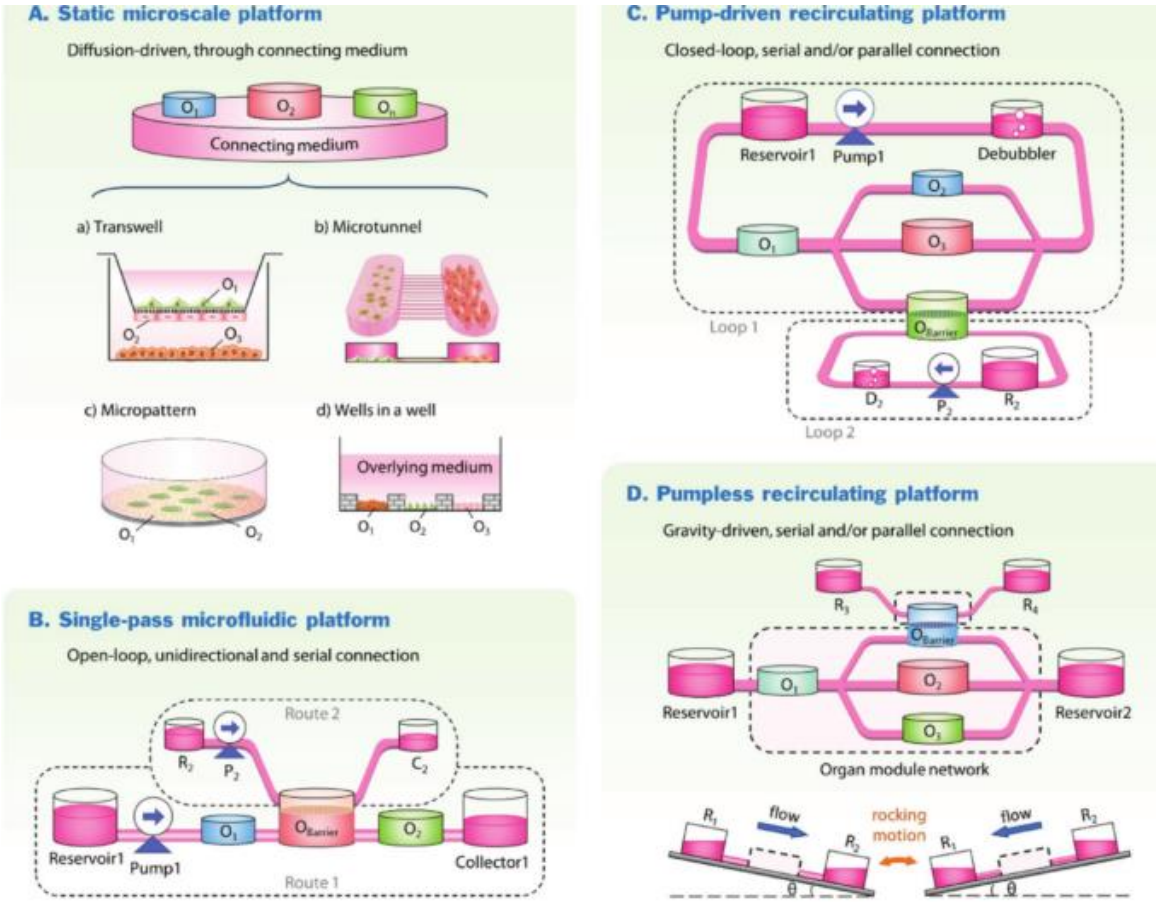

Figure 9. Organ-organ in vitro interactions platforms. A) Static microscale platforms are comprise a) transwell platform; b) microtunnel platform; c) micropattern platform; d) wells in a well platform B) In single-pass microfluidic platforms, the organ modules are connected in series in one fluid route (route 1) or with additional routes (e.g., route 2) connects all organ modules in series in one fluid route (route 1), or with additional routes (e.g., route 2) if barrier tissues are involved C) In pump-driven recirculating platforms, the organ models are interconnected in serial and or parallel in a closed-loop circuit (loop 1). Separate fluidic pools or loops (e.g., loop 2) are needed for barrier tissues D) The fluid circulation to organ modules connected in serial and/or in parallel in pumpless recirculating platform is driven by gravity and rocking motion. O_n – organ module; P_n – pump; R_n – reservoir; C_n – medium collector; D_n – debubbler. n represents the index of a specific module. Adapted from Wang *et al*[102].

As a specific example, recently, Choi *et al*[104] developed an early-stage breast cancer model using a PDMS microfluidic device using three cell lines: human mammary epithelial cells (HMT-3522), human primary mammary fibroblasts and breast ductal carcinoma *in situ* (DCIS). The fibroblasts and the epithelial cells lines were cultured on opposite sides of a vitrified collagen membrane dividing the system in an upper and lower chamber (mammary fibroblasts are cultured in the lower and mammary epithelial cells were cultured in the lower chamber, Figure 10). The DCIS, which were seeded into a 96-well hanging drop plate, were then injected in the upper channel to attach to the epithelial cell layer (without media perfusion) to allow spheroid attachment. This device was then

used as a preclinical cancer model to evaluate responses to an anti-cancer drug (Paclitaxel).

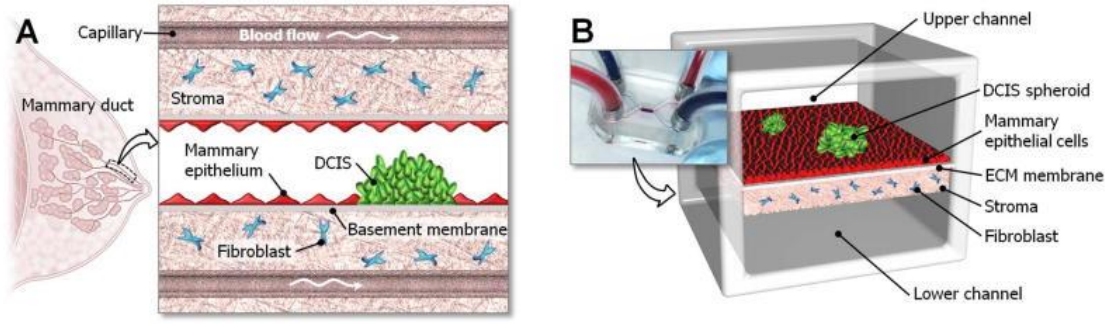

Figure 10. *In vivo* breast cancer microenvironment (A) compared with the microfluidic device developed by Choi *et al* to model of an early-stage breast cancer (B) (Adapted from Choi and colleagues [104]).

This system paved the way to the possibility to simulating, understanding how tumour cells interact with other cell types, which has a critical importance in the progression and metastasis of breast cancer cells. Despite, this breakthrough, the authors referred that these system's physiological relevance must be improved by adding more cell lines to closely resemble the breast cancer environment. Some examples of studies performed using microfluidic devices are shown in Table 2.

There is also the possibility of using microfluidic platforms in indirect cell culture due to the controllable co-culturing of cells, the control and generation of signalling gradients and lastly the integration of perfusion/flow [105]. To date most of the microfluidic devices are produced with polydimethylsiloxane (PDMS) although chips made from glass, silicon or quartz can be built [106].

Table 2. Examples of studies performed using a microfluidic device. Which cell types were used, the device (material used during construction), application and reference.

Cells	Device	Applications	References
Multiple human cell lines (intestine, liver, kidney and skin)	PDMS	Organs-on-chip for drug toxicity tests	[107]
NT2, HepaRG and primary human hepatic stellate cells	PDMS	Organs-on-chip for substance testing	[108]
Human non-small lung cancer cells (SPCA-1) Human lung fibroblasts (HFL1)	PDMS	Lung cancer treatment drug sensitivity evaluation	[109]
HepG2 cells NIH-3T3 cells	Glass	Drug screening on hepatic tissue model	[110]
Rat neurons and glia cells	PDMS	Study axon-glia interactions	[111]
Multiple cell lines	PDMS	Bladder cancer microenvironment model for drug screening assays	[112]
Human stem cells from exfoliated deciduous teeth, gingival fibroblasts and periodontal ligament stem cells	PDMS	Tooth mineralization assay	[113]
Multiple human cell lines	PDMS	Characterization of the biology of circulating tumour cells from early-stage lung cancer to unravel metastasis mechanisms	[114]
Multiple human cell lines	PDMS	Organs-on-chips with multiple sensors for drug screening of cancer treatment drugs	[115]

Although most of the devices displayed in Table 2 are constructed from PDMS and despite PDMS's transparency, gas permeability, easy prototyping and low cost, hydrophobic small molecules and drugs may be subjected to adsorption or absorption on this material [116]. This is an important drawback and must be taken into consideration in the future.

Microfluidic cell culture is a crucial tool to design cell culture systems which offer flexibility of chip design, on chip analysis, single cell handling, a low number of cells is sufficient, controlled co-culture, reduced reagent consumption, perfusion culture is possible, real time, automation and experimental flexibility and control [117].

Microfluidic cell cultures systems allow the establishment of a precisely controllable environment suitable for drug screening tests by fabricating a specific chip designed fitting the desired format which can then be used to establish a specific cell culture system by building multiple channels for example [118]. To potentiate the capabilities of a chip, it can be paired up with a high throughput analysing system which will be capable of acquiring more data on drug combinations efficacy as well as cell culture shape changes, simplifying the method and using it in a more cost-effective manner.

Considering cancer drug screening, due to the complexity of some tumours and even the different responses given by the same type of tumour cells on different patients, using those patient-specific cells to perform personalized drug screening study could highlight different responses and determine to most efficient treatment to treat that pathology. However, these systems are still on an early stage of development meaning that there's yet to be microfluidic model suitable for testing a myriad of possibilities of drug combinations to reduce the costs and time spent on a trial/error fashion [119].

However, the challenges were also stated: non-standard culture protocols, chip design, the surface is different from the standard culturing methods, small volumes and consequent analytical chemistry and complex operational control which requires a study of the systems' perfect conditions.

5. Hydrogel-based cell culture/cell delivery systems

3D Hydrogels can be classified according to their origin as: (i) natural, (ii) synthetic or (iii) natural/synthetic hybrid cross-linked polymeric networks with the ability to mimic the ECM microenvironment because their properties resemble soft

natural tissues and their structure is permeable to water, ions, molecules and even proteins [120–123].. These systems promote cell proliferation and cell differentiation, as well as increase cell viability [124]. The performance of hydrogels is highly dependent on their building blocks (e.g., proteins, natural/synthetic polymers, etc[125]) , on their crosslinking methods as extensively reviewed in the literature [125–128]. Figure 11 presents a comprehensive scheme on the different hydrogel crosslinking mechanisms.

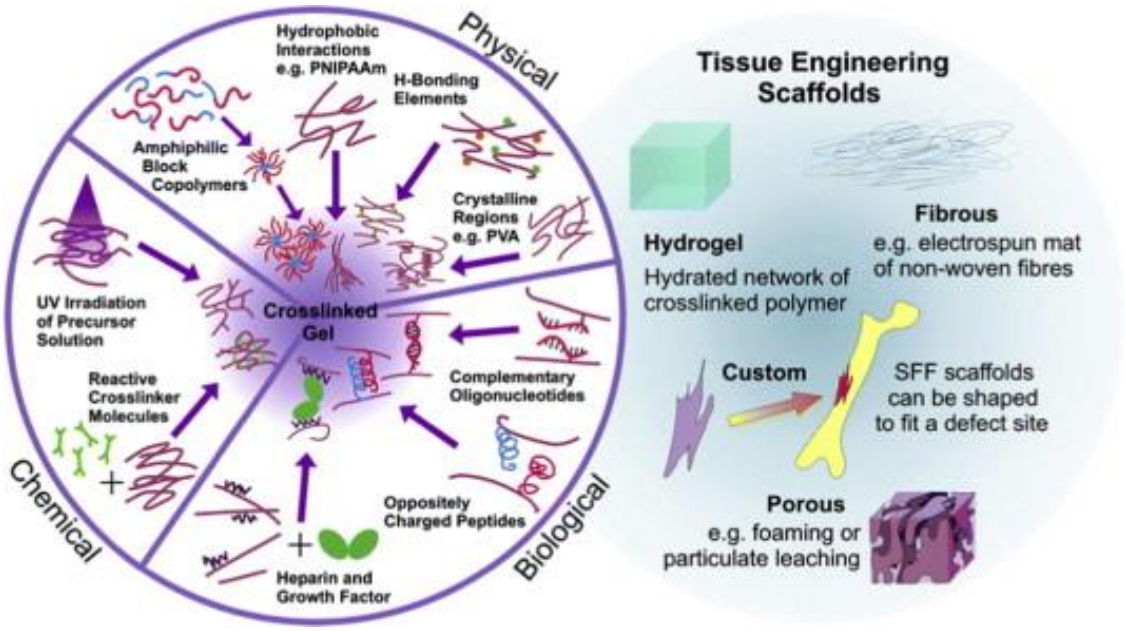

Figure 11. Scheme of hydrogel crosslinking mechanisms and hydrogels applications (Adapted from Caló *et al*[129]).

In general, for ECM mimicking applications and advanced cell cultures the material of which the hydrogel is comprised should be biocompatible and biodegradable [130]. Hydrogels aqueous environment can protect cells and can be easily modified with cell adhesion ligands to provide specific cell adhesion (e.g., RGD[131]). However, some of these gels can be mechanically weak, may be difficult to cells and then crosslink and may be difficult to sterilise [122].

Gradient hydrogels have been studied to recapitulate more complex cellular niches , for example mimicking the cartilage environment which transitions from ECM lower stiffness on the superficial zone to a stiffness increase onward to the deeper zones characterized by higher amounts of glycosaminoglycans [132]. These systems have served as well to mimic spatiotemporal changes in cellular communication [133]. Moreover, these biochemical and biomechanical gradients in such hydrogels support different cell phenotypes allowing more replicable *in vivo* conditions *in vitro* establishing reliable

tissue models which have paramount importance on understanding cell regeneration mechanisms and promoting damaged tissues regeneration in heterotypical environments and also play a crucial role on drug screening and cytotoxicity assays[134] The simpler method to fabricate gradient hydrogels is varying the photo-crosslinking intensity along the hydrogel exposing sections for longer periods of time and others for shorter periods and hence causing different stiffness which is useful to study cell proliferation and differentiation profiles through mechanically different matrixes[135]

Recently, hydrogels have been raising interest also as 3D bioinks for bioprinting, resulting in a major increase on research on this subject. Bioprinting consists on using cell-laden hydrogels dispensed through a bioprinter which allows the design of complex structures. 3D Bioprinted models have been used for cell transplantation, drug screening and chemical, biological and toxicological agents analysis[136,137]. To date different printing mechanisms are comprise multi-cell bioprinting: inkjet bioprinting, micro-extrusion bioprinting (also named robotic dispensing) and laser assisted bioprinting; cell aggregate bioprinting and single-cell bioprinting as described elsewhere.[136–139].

Considering their versatility, hydrogels have a wide range of applications as scaffolds for cell culture as shown in Table 3. Gradient hydrogels are indicated by (1) and bioprinted systems by (2).

Table 3. Studies performed using hydrogels. The columns divide the studies by gel components, cell lines, possible application and references.

Components	Cells	Applications	References
N-carboxyethyl chitosan, oxidized acrylated hyaluronic acid and matrix metalloproteinase (1)	Murine sarcoma GFP expressing cells	Injectable hydrogel for tissue regeneration	140
PEG (1)	Neonatal bovine chondrocytes	Cartilage regeneration	133
Gelatin methacrylate(GelMA), kappa-carrageenan methacrylate and nanosilicates (1)	hBMSCs	Replicate bone-cartilage interface	141
Agarose and glycosylated SPIONs loaded with BMP-2 (1)	hMSCs	Interfacial tissue engineering	142

Collagen, alginate and fibrin	murine fibroblasts (L929), murine pancreatic β-cells (MIN6) and human-TERT mesenchymal stem cells (Y201 hMSCs)	Replicate soft tissues properties for regeneration purposes	143
Methacryloyl modified human platelet lysates	L929 and hASCs	Alternative to animal derived hydrogels for cell culture	123
Alginate and polyethylene glycol monoacrylate-fibrinogen(2)	HUVECs and iPSC-derived cardiomyocytes	Revascularization of damaged organs promoting regeneration	144
Alginate and hyaluronic acid (HA)	Human periodontal ligament and gingival derived mesenchymal stem cells	Neurogenic tissues regeneration	145
Porcine liver decellularized extracellular matrix and GelMA (2)	Human liver cancer cell line (HepG2)	Recapitulate cirrhotic liver pathophysiology	146
Silk fibroin	Primary rat islets and RIN-5 cells	Injectable pancreatic islet transplantation and immunomodulatory regulation	147
Fibrogen, gelatin, HA and glycerol (2)	Human muscle progenitor cells	Muscle tissue regeneration	148
Chitosan,chondroitin sulfate and chitosan microspheres	Bovine articular chondrocytes	Injectable drug delivery system	149

As evidenced in Table 3, hydrogels support cell growth of a great variety of cell lines, as well as stem cells and have proven their worth in numerous applications ranging from replicating cellular microenvironments for pathophysiological studies to tissue regeneration and drug-screening. Taken these application into consideration, hydrogels are a useful tool to relieve patients' pain from their damaged tissues by administrating more accurately a specific type of drug maximizing treatment efficiency and even inject cells *in situ* to regenerate those injured tissues minimizing the invasiveness of a procedure or as a last resort replace those damaged tissues with *in vitro* constructed tissues which can be tailored according to the *in vivo* conditions albeit these approaches have to be validated for human *in vivo* applications to determine how accurately they recapitulate

the cell niche and their treatment efficacy which could be a consequence of high regulatory procedures and funding limitations[150]

5.2. Spherically structured Hydrogel-based models

Spherically structured hydrogels provide a higher area/volume ratio and hence the nutrients, metabolites and O_2 and CO_2 flow is more efficient, thus rendering an increase on cell survival expectancies. As recently reviewed by Correia *et al*[151], microencapsulation methods may originate different platforms including beads or capsules. Beads comprise a solid spherical hydrogel gel matrix and capsules have a membrane surrounding the core (Figure 12)

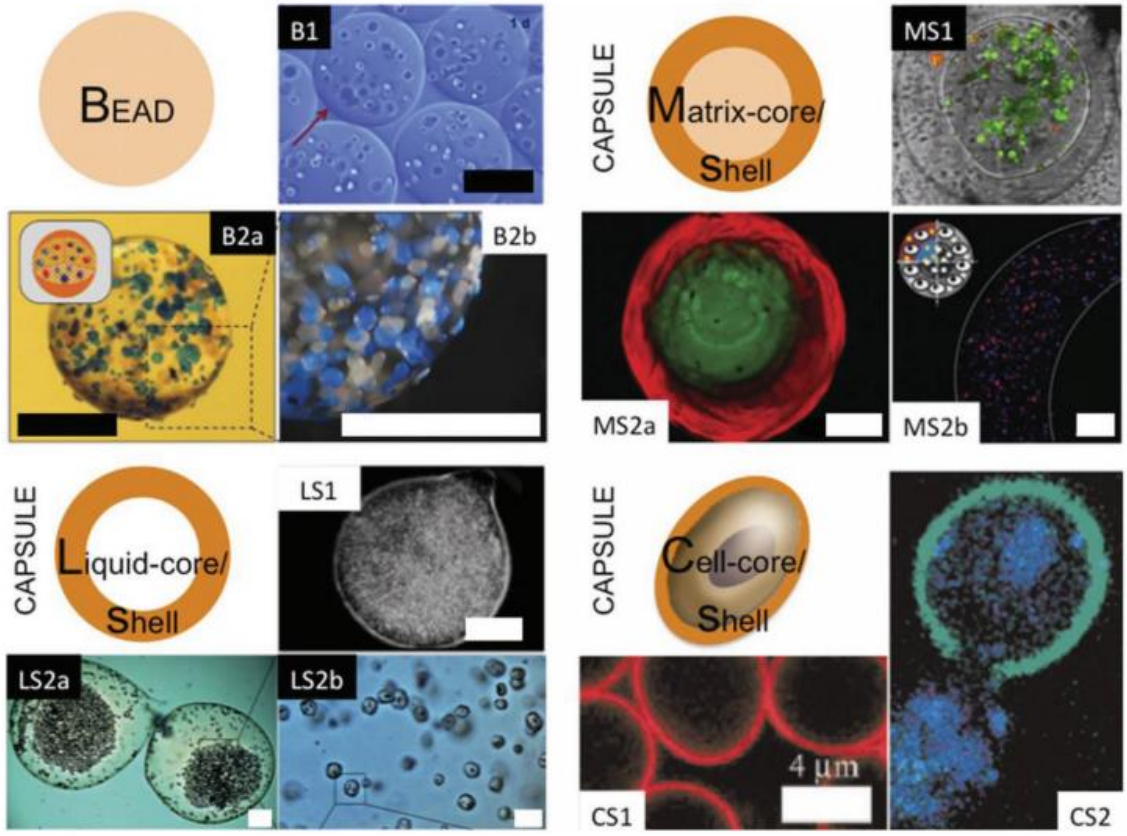

Figure 12.. Schematics of different types of beads and capsules that can be used as cell encapsulation systems. These systems have been used for numerous applications ranging from tissue engineering to in vitro disease modelling. Adapted from Correia *et al*[151].

Over the years these spherical hydrogels have been applied for encapsulation of different cell lines. Capsules produced using alginate and then LBL polyelectrolyte assembly technique have been used to encapsulate L929 cells[152,153] cultured in a customized environment included microparticles on which cell adhered. This system is highly versatile and could be further improved to release growth factors or encapsulate

multiple cell types. In fact, the same system was used as a co-culture system with a self-regulated environment for osteogenic differentiation *in vitro* using adipose tissue-derived stem cells (hASCs) and human adipose microvascular endothelial cells resulting in osteogenic differentiation of hASCs and the release of bone morphogenic protein -2 (BMP-2) and VEGF was observed and hence the system could be used as a cytokine delivery system[154]. In addition, the latter system was tested *in vivo* and no serious immunological response was obtained. Moreover, successful mineralization was reported which is promising for bone regeneration purposes [155]

Another systems which could also be described as co-culture capsule has also been studied as a tool for liver regeneration[156]. This system was bioinspired by the volvox algae colony whose structure is described as a sphere with smaller sphere inside. The authors relied on firstly encapsulating AML12 hepatocytes in an alginate-collagen solution followed by an encapsulation using the same solution however with rat MSCs. The volvox spheres were cultured *in vitro* and then implanted on mice where they promoted improved regeneration[156].

As for spherical hydrogels described as beads, a mussel-inspired system was designed with the intent to promote osteogenic differentiation [157]. Instead of using unmodified alginate as in most of the studies performed, the authors modified alginate with dopamine which was then used to encapsulate mice BMSCs and then the beads were coated with silver nanoparticles. The outcome was a bead which could support osteogenic differentiation and be transplanted causing less chances of infection due to the silver nanoparticles antibacterial properties.

From this context, it is clear that spherical hydrogels have great potential to support different cell co-cultures and provide a suitable environment for cell differentiation in the context of disease modelling or regenerative medicine.

6. Conclusions and Future Perspectives

These compartmentalized cell culture may offer more reliable fundamental biology studies and recapitulate more effectively *in vivo* drug response. Furthermore, these models are suitable to create minimal invasiveness tissue regeneration methods and also create large tissues constructs which could one day be transplanted to a patient to regenerate an injured or damaged site.

However, one of the hallmarks of these transplantations is a low FBR preventing a rejection of the new tissue is yet to be solved or validated and for that reason numerous studies and validations must be performed before human trials. Furthermore, these systems should be easily manufactured and cost-effective to become available to most of the population reducing health costs. Moreover, for drug screening and transplantation purposes these myriads of methods should consider a personalized approach meaning that cells should be harvested from the patient in the least painful manner possible and then using those cells perform such studies paving a way to personalized medicine.

Acknowledgements

The authors would like to acknowledge the support of the European Research Council grant agreement ERC-2014-ADG-669858 for project ATLAS. The authors also acknowledge the financial support by the Portuguese Foundation for Science and Technology (FCT) through a Post-doctoral grant (SFRH/BPD/119983/2016, Vítor Gaspar).

7. References

1. Savica, R., Grossardt, B. R., Bower, J. H., Ahlskog, J. E. & Rocca, W. A. Time Trends in the Incidence of Parkinson Disease. *JAMA Neurol.* **73,** 981–9 (2016).

2. Hernlund, E. *et al.* Osteoporosis in the European Union: medical management, epidemiology and economic burden. *Arch. Osteoporos.* **8,** 136 (2013).

3. Piepoli, M. F. *et al.* 2016 European Guidelines on cardiovascular disease prevention in clinical practice. *Eur. Heart J.* **37,** 2315–2381 (2016).

4. Salgado, A. J., Coutinho, O. P. & Reis, R. L. Bone Tissue Engineering: State of the Art and Future Trends. *Macromol. Biosci.* **4,** 743–765 (2004).

5. Alzheimer's Association and others. *2017 Alzheimer's disease facts and figures*. *Alzheimer's & Dementia* **13,** (Elsevier, 2017).

6. Szeto, J. Y. Y. & Lewis, S. J. G. Current Treatment Options for Alzheimer's Disease and Parkinson's Disease Dementia. *Curr. Neuropharmacol.* **14,** 326–38 (2016).

7. Mozaffarian, D. *et al.* Heart Disease and Stroke Statistics—2016 Update. *Circulation* **133,** (2016).

8. Carnero, A. High throughput screening in drug discovery. *Clin. Transl. Oncol.* **8,** 482–490 (2006).

9. Flanagan, T. C. *et al.* A collagen-glycosaminoglycan co-culture model for heart valve tissue engineering applications. *Biomaterials* **27,** 2233–2246 (2006).

10. Rogozhnikov, D., O'Brien, P. J., Elahipanah, S. & Yousaf, M. N. Scaffold Free Bio-orthogonal Assembly of 3-Dimensional Cardiac Tissue via Cell Surface Engineering. *Sci. Rep.* **6,** 39806 (2016).

11. Li, N. *et al.* Three-dimensional graphene foam as a biocompatible and conductive scaffold for neural stem cells. *Sci. Rep.* **3,** 1604 (2013).

12. Dinh, N.-D. *et al.* Microfluidic construction of minimalistic neuronal co-cultures. *Lab Chip* **13,** 1402 (2013).

13. Lau, T. T., Lee, L. Q. P., Vo, B. N., Su, K. & Wang, D.-A. Inducing ossification in an engineered 3D scaffold-free living cartilage template. *Biomaterials* **33,** 8406–8417 (2012).

14. Choong, C. S. N., Hutmacher, D. W. & Triffitt, J. T. Co-culture of Bone Marrow Fibroblasts and Endothelial Cells on Modified Polycaprolactone Substrates for Enhanced Potentials in Bone Tissue Engineering. *Tissue Eng.* **12,** 2521–2531 (2006).

15. Harrison, R. G. Observations on the living developing nerve fiber. *Exp. Biol. Med.* **4,** 140–143 (1907).

16. Duell, B. L., Cripps, A. W., Schembri, M. A. & Ulett, G. C. Epithelial cell coculture models for studying infectious diseases: benefits and limitations. *J. Biomed. Biotechnol.* **2011,** 852419 (2011).

17. Goers, L., Freemont, P. & Polizzi, K. M. Co-culture systems and technologies: taking synthetic biology to the next level. *J. R. Soc. Interface* **11,** 20140065 (2014).

18. Miki, Y. *et al.* The advantages of co-culture over mono cell culture in simulating *in vivo* environment. *J. Steroid Biochem. Mol. Biol.* **131,** 68–75 (2012).

19. Kasper, J. *et al.* Inflammatory and cytotoxic responses of an alveolar-capillary coculture model to silica nanoparticles: Comparison with conventional monocultures. *Part. Fibre*

Toxicol. **8,** 6 (2011).

20. Yeo, L. Y., Chang, H.-C., Chan, P. P. Y. & Friend, J. R. Microfluidic Devices for Bioapplications. *Small* **7,** 12–48 (2011).

21. Lu, Z. F., Zandieh Doulabi, B., Wuisman, P. I., Bank, R. A. & Helder, M. N. Influence of collagen type II and nucleus pulposus cells on aggregation and differentiation of adipose tissue-derived stem cells. *J. Cell. Mol. Med.* **12,** 2812–2822 (2008).

22. Paschos, N. K., Brown, W. E., Eswaramoorthy, R., Hu, J. C. & Athanasiou, K. A. Advances in tissue engineering through stem cell-based co-culture. *J. Tissue Eng. Regen. Med.* **9,** 488–503 (2015).

23. Cukierman, E., Pankov, R. & Yamada, K. M. Cell interactions with three-dimensional matrices. *Curr. Opin. Cell Biol.* **14,** 633–9 (2002).

24. Griffith, L. G. & Swartz, M. A. Capturing complex 3D tissue physiology in vitro. *Nat. Rev. Mol. Cell Biol.* **7,** 211–224 (2006).

25. Frantz, C., Stewart, K. M. & Weaver, V. M. The extracellular matrix at a glance. *J. Cell Sci.* **123,** 4195–4200 (2010).

26. King, M. W. *Integrative Medical Biochemistry: Examination and Board Review*. (McGraw-Hill Education, 2014). at <https://books.google.pt/books?id=cG6EAwAAQBAJ>

27. Lee, J., Cuddihy, M. J. & Kotov, N. A. Three-Dimensional Cell Culture Matrices: State of the Art. *Tissue Eng. Part B Rev.* **14,** 61–86 (2008).

28. Thomas, C. H., Collier, J. H., Sfeir, C. S. & Healy, K. E. Engineering gene expression and protein synthesis by modulation of nuclear shape. *Proc. Natl. Acad. Sci. U. S. A.* **99,** 1972–7 (2002).

29. Kirkpatrick, C. J., Fuchs, S., Hermanns, M. I., Peters, K. & Unger, R. E. Cell culture models of higher complexity in tissue engineering and regenerative medicine. *Biomaterials* **28,** 5193–5198 (2007).

30. Baker, B. M. & Chen, C. S. Deconstructing the third dimension: how 3D culture microenvironments alter cellular cues. *J. Cell Sci.* **125,** 3015–24 (2012).

31. Alberts, B. *et al. Molecular biology of the cell*. (Garland Science, 2002).

32. Gnecchi, M., Zhang, Z., Ni, A. & Dzau, V. J. Paracrine Mechanisms in Adult Stem Cell Signaling and Therapy. *Circ. Res.* **103,** 1204–1219 (2008).

33. Han, Y., You, X., Xing, W., Zhang, Z. & Zou, W. Paracrine and endocrine actions of bone—the functions of secretory proteins from osteoblasts, osteocytes, and osteoclasts. *Bone Res.* **6,** 16 (2018).

34. Ono, M. *et al.* Exosomes from bone marrow mesenchymal stem cells contain a microRNA that promotes dormancy in metastatic breast cancer cells. *Sci. Signal.* **7,** ra63-ra63 (2014).

35. King, T. C. in *Elsevier's Integrated Pathology* (ed. Mosby, 2007) 59–88 (Elsevier, 2007). doi:10.1016/B978-0-323-04328-1.50009-7

36. Ko, I. K., Lee, S. J., Atala, A. & Yoo, J. J. *In situ* tissue regeneration through host stem cell recruitment. *Exp. Mol. Med.* **45,** e57–e57 (2013).

37. Battiston, K. G., Cheung, J. W. C., Jain, D. & Santerre, J. P. Biomaterials in co-culture systems: Towards optimizing tissue integration and cell signaling within scaffolds. *Biomaterials* **35,** 4465–4476 (2014).

38. Lamichhane, T. N. *et al.* Emerging Roles for Extracellular Vesicles in Tissue Engineering and Regenerative Medicine. *Tissue Eng. Part B Rev.* **21,** 45–54 (2015).

39. Cabral, J., Ryan, A. E., Griffin, M. D. & Ritter, T. Extracellular vesicles as modulators of wound healing. *Adv. Drug Deliv. Rev.* **129,** 394–406 (2018).

40. Bjørge, I. M., Kim, S. Y., Mano, J. F., Kalionis, B. & Chrzanowski, W. Extracellular vesicles, exosomes and shedding vesicles in regenerative medicine – a new paradigm for tissue repair. *Biomater. Sci.* **6,** 60–78 (2018).

41. Akers, J. C., Gonda, D., Kim, R., Carter, B. S. & Chen, C. C. Biogenesis of extracellular vesicles (EV): exosomes, microvesicles, retrovirus-like vesicles, and apoptotic bodies. *J. Neurooncol.* **113,** 1–11 (2013).

42. El Andaloussi, S., Mäger, I., Breakefield, X. O. & Wood, M. J. A. Extracellular vesicles: biology and emerging therapeutic opportunities. *Nat. Rev. Drug Discov.* **12,** 347–357 (2013).

43. Yáñez-Mó, M. *et al.* Biological properties of extracellular vesicles and their physiological functions. *J. Extracell. Vesicles* **4,** 27066 (2015).

44. Pinheiro, A. *et al.* Extracellular vesicles: intelligent delivery strategies for therapeutic applications. *J. Control. Release* **289,** 56–69 (2018).

45. Mol, E. A., Goumans, M.-J., Doevendans, P. A., Sluijter, J. P. G. & Vader, P. Higher functionality of extracellular vesicles isolated using size-exclusion chromatography compared to ultracentrifugation. *Nanomedicine Nanotechnology, Biol. Med.* **13,** 2061–2065 (2017).

46. Witwer, K. W. *et al.* Standardization of sample collection, isolation and analysis methods in extracellular vesicle research. *J. Extracell. Vesicles* **2,** 20360 (2013).

47. Kanada, M. *et al.* Differential fates of biomolecules delivered to target cells via extracellular vesicles. *Proc. Natl. Acad. Sci.* 201418401 (2015). doi:10.1073/pnas.1418401112

48. Cha, J. M. *et al.* Efficient scalable production of therapeutic microvesicles derived from human mesenchymal stem cells. *Sci. Rep.* **8,** 1171 (2018).

49. Mount, S. & Davis, D. R. Electrical effects of stem cell transplantation for ischaemic cardiomyopathy: friend or foe? *J. Physiol.* **594,** 2511–2524 (2016).

50. Toh, W. S., Lai, R. C., Hui, J. H. P. & Lim, S. K. MSC exosome as a cell-free MSC therapy for cartilage regeneration: Implications for osteoarthritis treatment. *Semin. Cell Dev. Biol.* **67,** 56–64 (2017).

51. Ansorge, M. & Pompe, T. Systems for localized release to mimic paracrine cell communication in vitro. *J. Control. Release* **278,** 24–36 (2018).

52. Domenech, M. *et al.* Cellular observations enabled by microculture: paracrine signaling and population demographics. *Integr. Biol.* **1,** 267–274 (2009).

53. Saleh, L. S., Carles-Carner, M. & Bryant, S. J. The in vitro effects of macrophages on the osteogenic capabilities of MC3T3-E1 cells encapsulated in a biomimetic poly(ethylene glycol) hydrogel. *Acta Biomater.* **71,** 37–48 (2018).

54. Magatti, M. *et al.* Human Amniotic Membrane-Derived Mesenchymal and Epithelial Cells Exert Different Effects on Monocyte-Derived Dendritic Cell Differentiation and Function. *Cell Transplant.* **24,** 1733–1752 (2015).

55. Chen, Q.-H., Liu, A.-R., Qiu, H.-B. & Yang, Y. Interaction between mesenchymal stem

cells and endothelial cells restores endothelial permeability via paracrine hepatocyte growth factor in vitro. *Stem Cell Res. Ther.* **6,** 44 (2015).

56. Yonker, L. M. *et al.* Development of a Primary Human Co-Culture Model of Inflamed Airway Mucosa. *Sci. Rep.* **7,** 8182 (2017).

57. Böhrnsen, F. & Schliephake, H. Supportive angiogenic and osteogenic differentiation of mesenchymal stromal cells and endothelial cells in monolayer and co-cultures. *Int. J. Oral Sci.* **8,** 223–230 (2016).

58. Wang, Z., Wang, Y., Farhangfar, F., Zimmer, M. & Zhang, Y. Enhanced Keratinocyte Proliferation and Migration in Co-culture with Fibroblasts. *PLoS One* **7,** e40951 (2012).

59. Acharya, C. *et al.* Enhanced chondrocyte proliferation and mesenchymal stromal cells chondrogenesis in coculture pellets mediate improved cartilage formation. *J. Cell. Physiol.* **227,** 88–97 (2012).

60. Hartman, M. L. & Kornfeld, H. Interactions between Naïve and Infected Macrophages Reduce Mycobacterium tuberculosis Viability. *PLoS One* **6,** e27972 (2011).

61. Spencer, C., Abend, S., McHugh, K. J. & Saint-Geniez, M. Identification of a synergistic interaction between endothelial cells and retinal pigment epithelium. *J. Cell. Mol. Med.* **21,** 2542–2552 (2017).

62. Birmingham, E. *et al.* Osteogenic differentiation of mesenchymal stem cells is regulated by osteocyte and osteoblast cells in a simplified bone niche. *Eur. Cell. Mater.* **23,** 13–27 (2012).

63. Roddy, G. W. *et al.* Action at a Distance: Systemically Administered Adult Stem/Progenitor Cells (MSCs) Reduce Inflammatory Damage to the Cornea Without Engraftment and Primarily by Secretion of TNF-α Stimulated Gene/Protein 6. *Stem Cells* **29,** 1572–1579 (2011).

64. Cho, D.-I. *et al.* Mesenchymal stem cells reciprocally regulate the M1/M2 balance in mouse bone marrow-derived macrophages. *Exp. Mol. Med.* **46,** e70–e70 (2014).

65. Li, W. *et al.* Gastric cancer-derived mesenchymal stem cells prompt gastric cancer progression through secretion of interleukin-8. *J. Exp. Clin. Cancer Res.* **34,** 52 (2015).

66. Yan, X. *et al.* Mesenchymal stem cells from primary breast cancer tissue promote cancer proliferation and enhance mammosphere formation partially via EGF/EGFR/Akt pathway. *Breast Cancer Res. Treat.* **132,** 153–164 (2012).

67. Murdoch, A. D. *et al.* Chondrogenic Differentiation of Human Bone Marrow Stem Cells in Transwell Cultures: Generation of Scaffold-Free Cartilage. *Stem Cells* **25,** 2786–2796 (2007).

68. Luo, Q. *et al.* Indirect co-culture with tenocytes promotes proliferation and mRNA expression of tendon/ligament related genes in rat bone marrow mesenchymal stem cells. *Cytotechnology* **61,** 1–10 (2009).

69. Wada, N., Menicanin, D., Shi, S., Bartold, P. M. & Gronthos, S. Immunomodulatory properties of human periodontal ligament stem cells. *J. Cell. Physiol.* **219,** 667–676 (2009).

70. Rhee, W. J. *et al.* HuR regulates the expression of stress-sensitive genes and mediates inflammatory response in human umbilical vein endothelial cells. *Proc. Natl. Acad. Sci.* **107,** 6858–6863 (2010).

71. Tang, Z., Wang, Y., Podsiadlo, P. & Kotov, N. A. Biomedical Applications of Layer-by-Layer Assembly: From Biomimetics to Tissue Engineering. *Adv. Mater.* **18,** 3203–3224 (2006).

72. Decher, G., Hong, J. D. & Schmitt, J. Buildup of ultrathin multilayer films by a self-assembly process: III. Consecutively alternating adsorption of anionic and cationic polyelectrolytes on charged surfaces. *Thin Solid Films* **210–211,** 831–835 (1992).

73. Borges, J. & Mano, J. F. Molecular Interactions Driving the Layer-by-Layer Assembly of Multilayers. *Chem. Rev.* **114,** 8883–8942 (2014).

74. Gribova, V., Auzely-Velty, R. & Picart, C. Polyelectrolyte Multilayer Assemblies on Materials Surfaces: From Cell Adhesion to Tissue Engineering. *Chem. Mater.* **24,** 854–869 (2012).

75. Boudou, T., Crouzier, T., Ren, K., Blin, G. & Picart, C. Multiple Functionalities of Polyelectrolyte Multilayer Films: New Biomedical Applications. *Adv. Mater.* **22,** 441–467 (2010).

76. Gentile, P., Carmagnola, I., Nardo, T. & Chiono, V. Layer-by-layer assembly for biomedical applications in the last decade. *Nanotechnology* **26,** 422001 (2015).

77. Costa, R. R. & Mano, J. F. Polyelectrolyte multilayered assemblies in biomedical technologies. *Chem. Soc. Rev.* **43,** 3453 (2014).

78. Matsusaki, M. *et al.* Morphological and Histological Evaluations of 3D-Layered Blood Vessel Constructs Prepared by Hierarchical Cell Manipulation. *J. Biomater. Sci. Polym. Ed.* **23,** 63–79 (2012).

79. Nishiguchi, A., Yoshida, H., Matsusaki, M. & Akashi, M. Rapid Construction of Three-Dimensional Multilayered Tissues with Endothelial Tube Networks by the Cell-Accumulation Technique. *Adv. Mater.* **23,** 3506–3510 (2011).

80. Lazzari, G. *et al.* Multicellular spheroid based on a triple co-culture: A novel 3D model to mimic pancreatic tumor complexity. *Acta Biomater.* **78,** 296–307 (2018).

81. Campbell, P. J. *et al.* The patterns and dynamics of genomic instability in metastatic pancreatic cancer. *Nature* **467,** 1109–1113 (2010).

82. Bertlein, S. *et al.* Development of Endothelial Cell Networks in 3D Tissues by Combination of Melt Electrospinning Writing with Cell-Accumulation Technology. *Small* **14,** 1701521 (2018).

83. Asano, Y., Shimoda, H., Matsusaki, M. & Akashi, M. Transplantation of artificial human lymphatic vascular tissues fabricated using a cell-accumulation technique and their engraftment in mouse tissue with vascular remodelling. *J. Tissue Eng. Regen. Med.* **12,** e1501–e1510 (2018).

84. Choi, D. *et al.* Vascular Endothelial Growth Factor Incorporated Multilayer Film Induces Preangiogenesis in Endothelial Cells. *ACS Biomater. Sci. Eng.* **4,** 1833–1842 (2018).

85. Masuda, T. *et al.* Fabrication of engineered tubular tissue for small blood vessels via three-dimensional cellular assembly and organization ex vivo. *J. Biotechnol.* **276–277,** 46–53 (2018).

86. Fukuda, Y. *et al.* Layer-by-layer cell coating technique using extracellular matrix facilitates rapid fabrication and function of pancreatic β-cell spheroids. *Biomaterials* **160,** 82–91 (2018).

87. Lee, Y. Bin *et al.* One-step delivery of a functional multi-layered cell sheet using a thermally expandable hydrogel with controlled presentation of cell adhesive proteins. *Biofabrication* **10,** 025001 (2018).

88. Sasaki, K. *et al.* Construction of three-dimensional vascularized functional human liver tissue using a layer-by-layer cell coating technique. *Biomaterials* **133,** 263–274 (2017).

89. Hikimoto, D., Nishiguchi, A., Matsusaki, M. & Akashi, M. High-Throughput Blood- and Lymph-Capillaries with Open-Ended Pores Which Allow the Transport of Drugs and Cells. *Adv. Healthc. Mater.* **5,** 1969–1978 (2016).

90. Narita, H. *et al.* Engraftment and morphological development of vascularized human iPS cell-derived 3D-cardiomyocyte tissue after xenotransplantation. *Sci. Rep.* **7,** 13708 (2017).

91. Takeda, M. *et al.* Development of *In Vitro* Drug-Induced Cardiotoxicity Assay by Using Three-Dimensional Cardiac Tissues Derived from Human Induced Pluripotent Stem Cells. *Tissue Eng. Part C Methods* **24,** 56–67 (2018).

92. Meyvantsson, I. & Beebe, D. J. Cell Culture Models in Microfluidic Systems. *Annu. Rev. Anal. Chem.* **1,** 423–449 (2008).

93. Young, E. W. K. & Beebe, D. J. Fundamentals of microfluidic cell culture in controlled microenvironments. *Chem. Soc. Rev.* **39,** 1036 (2010).

94. Bhatia, S. N. & Ingber, D. E. Microfluidic organs-on-chips. *Nat. Biotechnol.* **32,** 760–772 (2014).

95. Song, H., Chen, D. L. & Ismagilov, R. F. Reactions in Droplets in Microfluidic Channels. *Angew. Chemie Int. Ed.* **45,** 7336–7356 (2006).

96. Wu, J., Chen, Q., Liu, W., He, Z. & Lin, J.-M. Recent advances in microfluidic 3D cellular scaffolds for drug assays. *TrAC Trends Anal. Chem.* **87,** 19–31 (2017).

97. Rothbauer, M., Zirath, H. & Ertl, P. Recent advances in microfluidic technologies for cell-to-cell interaction studies. *Lab Chip* (2017). doi:10.1039/C7LC00815E

98. Gao, D. *et al.* Recent developments in microfluidic devices for in vitro cell culture for cell-biology research. *TrAC Trends Anal. Chem.* **35,** 150–164 (2012).

99. Ziółkowska, K., Kwapiszewski, R. & Brzózka, Z. Microfluidic devices as tools for mimicking the *in vivo* environment. *New J. Chem.* **35,** 979 (2011).

100. Huh, D., Hamilton, G. A. & Ingber, D. E. From 3D cell culture to organs-on-chips. *Trends Cell Biol.* **21,** 745–754 (2011).

101. Esch, E. W., Bahinski, A. & Huh, D. Organs-on-chips at the frontiers of drug discovery. *Nat. Rev. Drug Discov.* **14,** 248–260 (2015).

102. Wang, Y. I., Carmona, C., Hickman, J. J. & Shuler, M. L. Multiorgan Microphysiological Systems for Drug Development: Strategies, Advances, and Challenges. *Adv. Healthc. Mater.* 1701000 (2017). doi:10.1002/adhm.201701000

103. Kieninger, J., Weltin, A., Flamm, H. & Urban, G. A. Microsensor systems for cell metabolism – from 2D culture to organ-on-chip. *Lab Chip* **18,** 1274–1291 (2018).

104. Choi, Y. *et al.* A microengineered pathophysiological model of early-stage breast cancer. *Lab Chip* **15,** 3350–3357 (2015).

105. van Duinen, V., Trietsch, S. J., Joore, J., Vulto, P. & Hankemeier, T. Microfluidic 3D cell culture: from tools to tissue models. *Curr. Opin. Biotechnol.* **35,** 118–126 (2015).

106. El-Ali, J., Sorger, P. K. & Jensen, K. F. Cells on chips. *Nature* **442,** 403–411 (2006).

107. Maschmeyer, I. *et al.* A four-organ-chip for interconnected long-term co-culture of human intestine, liver, skin and kidney equivalents. *Lab Chip* **15,** 2688–2699 (2015).

108. Materne, E.-M. *et al.* A multi-organ chip co-culture of neurospheres and liver equivalents for long-term substance testing. *J. Biotechnol.* **205,** 36–46 (2015).

109. Xu, Z. *et al.* Application of a microfluidic chip-based 3D co-culture to test drug sensitivity for individualized treatment of lung cancer. *Biomaterials* **34,** 4109–4117 (2013).

110. Au, S. H., Chamberlain, M. D., Mahesh, S., Sefton, M. V. & Wheeler, A. R. Hepatic organoids for microfluidic drug screening. **14,** 3290–3299 (2014).

111. Park, J., Koito, H., Li, J. & Han, A. Multi-compartment neuron–glia co-culture platform for localized CNS axon–glia interaction study. *Lab Chip* **12,** 3296 (2012).

112. Liu, P. *et al.* A bladder cancer microenvironment simulation system based on a microfluidic co-culture model. *Oncotarget* **6,** 37695–37705 (2015).

113. Kang, K.-J., Ju, S. M., Jang, Y.-J. & Kim, J. Indirect co-culture of stem cells from human exfoliated deciduous teeth and oral cells in a microfluidic platform. *Tissue Eng. Regen. Med.* **13,** 428–436 (2016).

114. Zhang, Z. *et al.* Expansion of CTCs from early stage lung cancer patients using a microfluidic co-culture model. *Oncotarget* **5,** 12383–12397 (2014).

115. Zhang, Y. S. *et al.* Multisensor-integrated organs-on-chips platform for automated and continual *in situ* monitoring of organoid behaviors. *Proc. Natl. Acad. Sci. U. S. A.* **114,** 2293–2302 (2017).

116. Toepke, M. W. & Beebe, D. J. PDMS absorption of small molecules and consequences in microfluidic applications. *Lab Chip* **6,** 1484 (2006).

117. Halldorsson, S., Lucumi, E., Gómez-Sjöberg, R. & Fleming, R. M. T. Advantages and challenges of microfluidic cell culture in polydimethylsiloxane devices. *Biosens. Bioelectron.* **63,** 218–231 (2015).

118. Akay, M. *et al.* Drug Screening of Human GBM Spheroids in Brain Cancer Chip. *Sci. Rep.* **8,** 15423 (2018).

119. Mazzocchi, A. R., Rajan, S. A. P., Votanopoulos, K. I., Hall, A. R. & Skardal, A. In vitro patient-derived 3D mesothelioma tumor organoids facilitate patient-centric therapeutic screening. *Sci. Rep.* **8,** 2886 (2018).

120. Hunt, N. C., Shelton, R. M. & Grover, L. An alginate hydrogel matrix for the localised delivery of a fibroblast/keratinocyte co-culture. *Biotechnol. J.* **4,** 730–737 (2009).

121. Brunsen, A. *et al.* Photocrosslinkable dextran hydrogel films as substrates for osteoblast and endothelial cell growth. *J. Mater. Chem.* **22,** 19590 (2012).

122. Hoffman, A. S. Hydrogels for biomedical applications. *Adv. Drug Deliv. Rev.* **54,** 3–12 (2002).

123. Santos, S. C., Custódio, C. A. & Mano, J. F. Photopolymerizable Platelet Lysate Hydrogels for Customizable 3D Cell Culture Platforms. *Adv. Healthc. Mater.* 1800849 (2018). doi:10.1002/adhm.201800849

124. Tibbitt, M. W. & Anseth, K. S. Hydrogels as extracellular matrix mimics for 3D cell culture. *Biotechnol. Bioeng.* **103,** 655–663 (2009).

125. Zhu, J. & Marchant, R. E. Design properties of hydrogel tissue-engineering scaffolds. *Expert Rev. Med. Devices* **8,** 607–626 (2011).

126. Van Vlierberghe, S., Dubruel, P. & Schacht, E. Biopolymer-Based Hydrogels As Scaffolds for Tissue Engineering Applications: A Review. *Biomacromolecules* **12,** 1387–1408 (2011).

127. Lee, K. Y. & Mooney, D. J. Hydrogels for Tissue Engineering. *Chem. Rev.* **101,** 1869–1880 (2001).

128. Peppas, N. A., Hilt, J. Z., Khademhosseini, A. & Langer, R. Hydrogels in Biology and Medicine: From Molecular Principles to Bionanotechnology. *Adv. Mater.* **18,** 1345–1360 (2006).

129. Caló, E. & Khutoryanskiy, V. V. Biomedical applications of hydrogels: A review of patents and commercial products. *Eur. Polym. J.* **65,** 252–267 (2015).

130. Hwang, C. M. *et al.* Fabrication of three-dimensional porous cell-laden hydrogel for tissue engineering. *Biofabrication* **2,** 035003 (2010).

131. Jeon, O. & Alsberg, E. Photofunctionalization of alginate hydrogels to promote adhesion and proliferation of human mesenchymal stem cells. *Tissue Eng. Part A* **19,** 1424–32 (2013).

132. Sharma, B. *et al.* Designing Zonal Organization into Tissue-Engineered Cartilage. *Tissue Eng.* **13,** 405–414 (2007).

133. Zhu, D., Trinh, P., Liu, E. & Yang, F. Biochemical and Mechanical Gradients Synergize To Enhance Cartilage Zonal Organization in 3D. *ACS Biomater. Sci. Eng.* **4,** 3561–3569 (2018).

134. Seidi, A., Ramalingam, M., Elloumi-Hannachi, I., Ostrovidov, S. & Khademhosseini, A. Gradient biomaterials for soft-to-hard interface tissue engineering. *Acta Biomater.* **7,** 1441–1451 (2011).

135. Marklein, R. A. & Burdick, J. A. Spatially controlled hydrogel mechanics to

modulate stem cell interactions. *Soft Matter* **6,** 136–143 (2010).

136. Murphy, S. V & Atala, A. 3D bioprinting of tissues and organs. *Nat. Biotechnol.* **32,** 773–785 (2014).

137. Mandrycky, C., Wang, Z., Kim, K. & Kim, D.-H. 3D bioprinting for engineering complex tissues. *Biotechnol. Adv.* **34,** 422–434 (2016).

138. Jakab, K. *et al.* Tissue engineering by self-assembly and bio-printing of living cells. *Biofabrication* **2,** 022001 (2010).

139. Malda, J. *et al.* 25th Anniversary Article: Engineering Hydrogels for Biofabrication. *Adv. Mater.* **25,** 5011–5028 (2013).

140. Wei, Z., Lewis, D. M., Xu, Y. & Gerecht, S. Dual Cross-Linked Biofunctional and Self-Healing Networks to Generate User-Defined Modular Gradient Hydrogel Constructs. *Adv. Healthc. Mater.* **6,** 1700523 (2017).

141. Cross, L. M., Shah, K., Palani, S., Peak, C. W. & Gaharwar, A. K. Gradient nanocomposite hydrogels for interface tissue engineering. *Nanomedicine Nanotechnology, Biol. Med.* **14,** 2465–2474 (2018).

142. Li, C. *et al.* Glycosylated superparamagnetic nanoparticle gradients for osteochondral tissue engineering. *Biomaterials* **176,** 24–33 (2018).

143. Montalbano, G. *et al.* Synthesis of bioinspired collagen/alginate/fibrin based hydrogels for soft tissue engineering. *Mater. Sci. Eng. C* **91,** 236–246 (2018).

144. Maiullari, F. *et al.* A multi-cellular 3D bioprinting approach for vascularized heart tissue engineering based on HUVECs and iPSC-derived cardiomyocytes. *Sci. Rep.* **8,** 13532 (2018).

145. Ansari, S. *et al.* Human Periodontal Ligament- and Gingiva-derived Mesenchymal Stem Cells Promote Nerve Regeneration When Encapsulated in Alginate/Hyaluronic Acid 3D Scaffold. *Adv. Healthc. Mater.* **6,** 1700670 (2017).

146. Ma, X. *et al.* Rapid 3D bioprinting of decellularized extracellular matrix with regionally varied mechanical properties and biomimetic microarchitecture. *Biomaterials* **185,** 310–321 (2018).

147. Kumar, M., Gupta, P., Bhattacharjee, S., Nandi, S. K. & Mandal, B. B. Immunomodulatory injectable silk hydrogels maintaining functional islets and promoting anti-inflammatory M2 macrophage polarization. *Biomaterials* **187,** 1–17 (2018).

148. Kim, J. H. *et al.* 3D Bioprinted Human Skeletal Muscle Constructs for Muscle Function Restoration. *Sci. Rep.* **8,** 12307 (2018).

149. Fan, M. *et al.* Covalent and injectable chitosan-chondroitin sulfate hydrogels embedded with chitosan microspheres for drug delivery and tissue engineering. *Mater. Sci. Eng. C* **71,** 67–74 (2017).

150. Foyt, D. A., Norman, M. D. A., Yu, T. T. L. & Gentleman, E. Exploiting Advanced Hydrogel Technologies to Address Key Challenges in Regenerative Medicine. *Adv. Healthc. Mater.* **7,** 1700939 (2018).

151. Correia, C. R., Reis, R. L. & Mano, J. F. Design Principles and Multifunctionality

in Cell Encapsulation Systems for Tissue Regeneration. *Adv. Healthc. Mater.* **7,** 1701444 (2018).

152. Correia, C. R., Sher, P., Reis, R. L. & Mano, J. F. Liquified chitosan–alginate multilayer capsules incorporating poly(l -lactic acid) microparticles as cell carriers. *Soft Matter* **9,** 2125–2130 (2013).

153. Correia, C. R., Reis, R. L. & Mano, J. F. Multilayered Hierarchical Capsules Providing Cell Adhesion Sites. *Biomacromolecules* **14,** 743–751 (2013).

154. Correia, C. R. *et al.* Semipermeable Capsules Wrapping a Multifunctional and Self-regulated Co-culture Microenvironment for Osteogenic Differentiation. *Sci. Rep.* **6,** 21883 (2016).

155. Correia, C. R. *et al. In vivo* osteogenic differentiation of stem cells inside compartmentalized capsules loaded with co-cultured endothelial cells. *Acta Biomater.* **53,** 483–494 (2017).

156. Chang, S. H. *et al.* In vitro and *in vivo* study of the application of volvox spheres to co-culture vehicles in liver tissue engineering. *Acta Biomater.* **63,** 261–273 (2017).

157. Zhang, S., Xu, K., Darabi, M. A., Yuan, Q. & Xing, M. Mussel-inspired alginate gel promoting the osteogenic differentiation of mesenchymal stem cells and anti-infection. *Mater. Sci. Eng. C* **69,** 496–504 (2016).

2. Aims

In a nutshell, the global aim of this thesis was the production of a hierarchic system comprising magnetically responsive iron oxide nanoparticles loaded into collagen-coated microparticles and on which cells would adhere after encapsulation in a bigger liquefied layer-by-layer (LBL) assembled microcapsule. The specific aims were sectioned as follows:

- Synthesis and characterization of magnetic iron oxide nanoparticles;
- Production, optimization and physicochemical characterization of blank or nanoparticle loaded polymeric PCL microparticles;
- Surface modification via plasma and collagen coating of nanoparticle containing PCL microparticles;
- Production, optimization and characterization of alginate microbeads with and without microparticles by using the electrospray technique;
- Production of cell-laden capsules containing iron oxide nanoparticle loaded PCL microparticles and MC3T3-E1 pre-osteoblasts attached on their surface.
- Cell laden magnetic microcapsules characterization *via* microscopy techniques;
- Evaluation of *in situ* magnetically assisted fixation of cell laden microcapsules;
- Evaluation of MC3T3-E1 pre-osteoblasts metabolic, cell viability and cell adhesion upon adhesion to magnetic microparticles loaded in LBL microcapsules.
-

3. Materials and Methods

3.1 Materials

$FeCl_3.6H_2O$ (≥99%), $FeCl_2.4H_2O$ (98%) and ammonia solution 25% were purchased from Laborspirit (Loures, Portugal) and produced by Sigma Aldrich, Alfa Aesar and LabChem respectively. Oleic acid (Sigma, ≥99%) was purchased from Laborspirit (Loures, Portugal) Neodymium magnet was purchased from Supermagnete (Germany)

Polycaprolactone (PCL; Mn 80,000) and polyvinyl alcohol (PVA; 87-90% hydrolysed, Mw-30,000-70,000 and produced by Sigma Aldrich. Dichloromethane (DCM; ≥99%) was purchased from JMGS (Odivelas, Portugal).

Collagen type I solution from rat tail was purchased from Sigma Aldrich and acetic acid (≥99%) was acquired from JMGS (Odivelas, Portugal).

Poly-L-Lysine hydrobromide (PLL; MW 30,000-70,000 Da) and the alginate (ALG; alginic acid sodium salt from brown algae, low viscosity) were produced by Sigma Aldrich and purchased from Laborspirit (Loures, Portugal) and Sigma Aldrich, respectively. Chitosan (CHT, Protasan UP CL 213, viscosity 107 mPA s, molecular weight $M_w = 2.7 \times 10^5$ g mol^{-1}, 83% degree of deacetylation; NovaMatrix, Norway). Calcium chloride ($CaCl_2$, anhydrous analytical grade) was purchased from JMGS (Odivelas, Portugal) and produced by PanReac. MES hydrate (>99%) and sodium chloride (NaCl; 99.5%) were purchased from Laborspirit (Loures, Portugal) and produced by Alfa Aesar and LabChem, respectively.

MC3T3-E1 cells were obtained from ATCC, Alpha Modified Eagle's Medium (α-MEM), DPBS(without calcium and magnesium), Calcein-AM, Propidium Iodide (PI) were all purchased from Thermofisher Scientific Inc (Alfagene, Portugal, 48-well plates (non-adherent) were purchased from VWR. And 96-Well White Plates (Non-Treated), without Lid, Flat Well NS were purchased from Corning. DAPI (4',6-diamidino-2-phenylindole, dihydrochloride) and WFI for cell culture were purchased from Thermo Fisher Scientific and rhodamine phalloidin (Thermo Fisher Scientific) was purchased from Alfagene (Carcavelos, Portugal). CellTiter 96 AQ_{ueous} One Solution cell (MTS) from Promega was purchased from VWR. Trypsin-EDTA solution (SIGMA) and formaldehyde solution (SIGMA) was purchased from Laborspirit (Loures, Portugal).

Carbon film 400mesh copper from EMResolutions was used for scanning transmission electron microscopy (STEM) sample preparation.

3.2 Methods

3.2.1. Oleic acid functionalised iron oxide magnetic nanoparticles synthesis and characterization

The aforementioned magnetic nanoparticles (MNPs) were synthesised through a co-precipitation method with minor modifications [1]. Briefly, $FeCl_3.6H_2O$ and $FeCl_2.4H_2O$ (0.046 and 0.023 mol respectively) were dissolved in 150 mL of debbubled miliQ water in a 250mL three-necked flask and heated to 85ºC under vigorous stirring.

To ensure that oxidation didn't occur the solution was bubbled with N_2. Then 20 mL of ammonia solution 25% were added rapidly to the mixture. After 30 min, 1mL of oleic acid were added to the iron solution to modify the Fe_3O_4 magnetic nanoparticles surface and then the mixture was heated to 80ºC. After 1h, the synthesised magnetic nanoparticles were separated magnetically, dialysed against deionised water to remove the excess ammonia and then washed with deionised water and ethanol, frozen at -80ºC and lastly freeze-dried (Lyoquest, Telstar).

To evaluate the size distribution and zeta potential, the measurements were performed in a ZetaSizer Nano ZS (Malvern,Worcestershire, UK).

The samples for STEM were prepared by resuspending the nanoparticles in ethanol and 10 µL of the solution were transferred to a carbon-film copper grid (400 mesh, EM Resolutions, United Kingdom), which was used to evaluate the morphology of the nanoparticles.

3.2.2. Piezoelectrically assisted PCL microparticles loaded with functionalised magnetic nanoparticles (µPCL[MNPs]) production

The production of µPCL[MNPs] consisted on an oil-in-water (O1/W1) emulsion-solvent evaporation technique. The oil phase (O1) was comprised by PCL solutions dissolved in DCM and the aqueous phase (W1) consisted on a PVA solution dissolved in deionised water.

Different conditions will imply different microparticles sizes, hence different formulations were evaluated, namely: PCL concentration in the oil phase and magnetic stirring speed.

Three PCL solutions with different concentrations (1.5, 3 and 5% PCL(w/v)) were prepared by dissolving 1.5g, 3g and 5g of PCL in 100 mL of DCM. Since large quantities of PVA were ought to be used, 5 g of PVA were dissolved in 1 L (0.5 % PVA(w/v)) of deionised water in vigorous stirring (800 rpm) and by heating at 80ºC for at least 5 h to

ensure complete dissolution of the polymer, following with filtration using 0.22 µm syringe filters to remove possible impurities.

Using the OB1 MK3 – Elveflow® Microfluidic Flow Control System, the 8 mL of PCL solution were extruded through a 22-gauge blunt tip needle at a pressure of 5 bar into a 250 mL beaker containing 150 mL PVA (0.5% (w/v)) stirred solution as described in a recent work [2] (Figure 1). The flow of the PCL solution was aimed to the middle of stirring aqueous phase from a height of 8 cm. Initially, PCL microparticles were produced to be used as a comparison to µPCL[MNPs] using the three different PCL solutions.

Then, 8mg of freeze-dried MNPs were resuspended in 2 mL of DCM in a falcon tube and then mixed using a vortex mixer. After this step, depending on the formulation desired, 8mL of PCL solution were added followed with another mixing step.

To facilitate the evaporation of excess DCM, W1 phase was removed until approximately the 50mL mark and then the beakers were placed on an orbital shaker (Thermo Scientific™ Compact Digital Microplate Shaker) at 170 rpm for at least 8h at room temperature inside the fume hood. The microparticles were recovered using a magnet (Supermagnete, Gottmadingen, Germany) and washed 5 times with deionised water to remove PVA and remaining DCM residues.

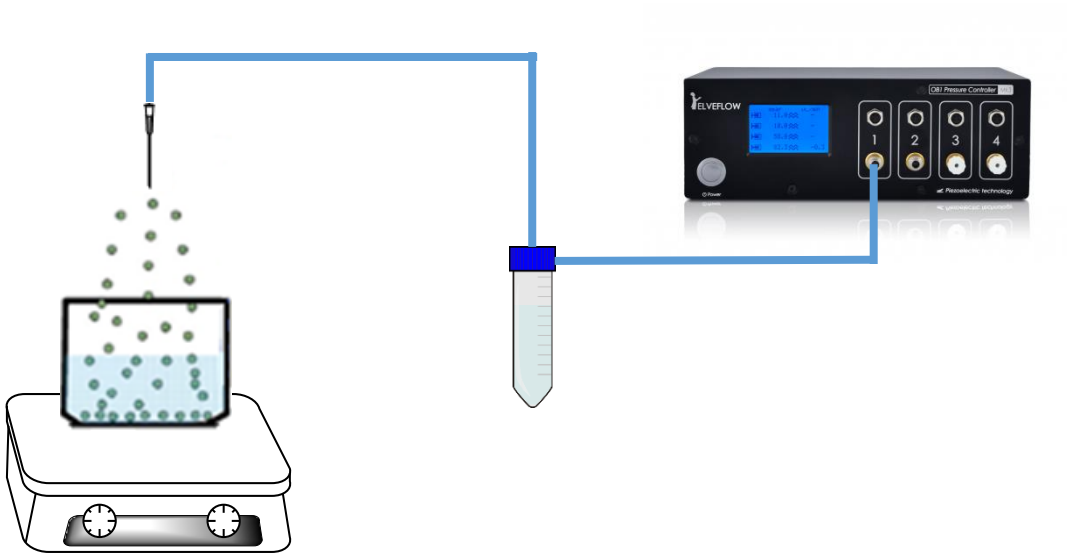

Figure 1. Schematic representation of the microparticles production system

The microparticles were then sieved using stainless steel test sieves with 63 µm and 40 µm mesh test sieves (VWR, Portugal CN: 510-0705; CN-510-0710, respectively) frozen at -80ºC and lastly freeze-dried for at least 48h (Lyoquest, Telstar) and stored.

3.2.3. µPCL[MNPs] surface functionalisation

The coating of µPCL[MNPs] was performed as described in the literature [3,4] with minor modifications.

The microparticles underwent treatment inside a plasma reactor chamber fitted with a radiofrequency generator. To do so, the microparticles were placed in the centre of the chamber and air was used as the working atmosphere. After the pressure of the chamber reached approximately 0.2 mbar, glow discharge plasma was created (previously set at 30 V). Overall, the process occurred for 15 minutes, however, to achieve an even functionalised surface on the particles after 5 minutes the particles were lightly shaken which was repeated three times.

Following the plasma treatment, 450 mg of microparticles were sterilised by UV radiation for 30 min and then immersed in 30 mL of 0.02 M acetic acid containing 1200 µg of collagen I from rat tail for 4h at room temperature. The microparticles were then recovered and washed three times with PBS and stored.

3.2.4 Microparticles characterisation

The morphology and particle size were evaluated using optical light microscopy (Primo Star, Carl Zeiss, Germany). The images acquired were then processed and analysed using the open-source software ImageJ [5]. The microparticles' size distribution was evaluated using ImageJ software (NIH) before and after sieving. The average diameter was determined by measuring 300 microparticles using an algorithm which analysed the microparticles' area.

The microparticles' topography and surface morphology were characterised using scanning electron microscopy (SEM). To do so, a small amount of microparticles were dispersed in deionised water and dropped carefully on top of an aluminium stub containing a plastic tissue culture coverslip which were then dried overnight at 37ºC then sputter coated with gold/palladium and observed in a Hitachi S-4100 scanning electron microscope (Hitachi, Japan) with voltage ranging from 15-25kV at various magnifications.

3.2.5. Production of alginate beads

The alginate beads were produced using an electrospray device (Spraybase®). Different conditions were evaluated namely: alginate concentration and voltage.

Firstly, 2g and 2.5g of alginate were dissolved in deionised water and then using a syringe a few millilitres were extracted and the syringe was connected to a 1mm diameter PTFE tube and place in a Kd Scientific Legato 200 pump on which a 50 mL/h flow rate was selected. The voltage was induced using a Heinzinger LNC 30000-2pos high voltage power supply set to 5, 7.5 and 10 kV according to the desired formulation. 22-gauge blunt tip needle was set at a distance from the collector of 8cm and approximately 1mL of alginate solution was extruded to a 10mL beaker containing 10mL of 0.1M $CaCl_2$. After extrusion, the microgels were ionic-crosslinked in the $CaCl_2$ (pH 6.7) bath for 20 min at 100 rpm.

This procedure was repeated when the alginate solution was mixed with microparticles with a concentration of 30 mg of microparticles per mL of alginate solution.

Using a plastic Pasteur pipette, a few alginate beads were transferred to a glass slide and observed under optic microscope (Zeiss Primo Star) to evaluate their shape, as it was expected to be rounded, and the size distribution (n=20) was determined using ImageJ software (NIH, Bethesda, ML).

3.2.6. Production of liquefied capsules

The liquified capsules are developed from alginate microgels, hence the production procedure has already been described above. However, only 2.0% alginate solution was used while the microparticle ratio was the same as described. Furthermore, all the lab ware, solutions and microparticles involved in this procedure were previously autoclaved, sterilised by UV light or 0.22 μm syringe filters.

The production of the liquefied capsules has been performed as described in the literature [3,4] , however with a few modifications.

Stock solutions of NaCl/MES and NaCl/MES/$CaCl_2$ were prepared by weighing each component separately. The concentration of NaCl in each solution was 0.15 M, MES buffer was 25mM and $CaCl_2$ in the latter stock solution was 0.1 M. The pH of these solutions was corrected to 6.7 and were then stored at 4ºC prior to usage.

292.24 mg of EDTA were dissolved in 50 mL of WFI (20mM) by increasing the pH which was then corrected to 6.7 after dissolving all EDTA. The solutions used to adjust the pH were also prepared with WFI.

To produce the liquified capsules, polyelectrolyte layers were needed. These layers consisted on oppositely charged polyelectrolytes deposition whose polyelectrolytes chosen were PLL, ALG and CHT. PLL and CHT were dissolved in NaCl/MES/$CaCl_2$ solution and ALG was dissolved in NaCl/MES solution to avoid ionic crosslinking with Ca^{2+}. In each solution, 15 mg of the desired polymer were dissolved in 30mL the respective solution, thus the polymer concentration was 0.5mg/mL ultimately the pH was corrected: 6.7 to PLL and ALG solutions and 6.3 for CHT. All the previously mentioned solutions were filtered with a 0.22 µm syringe filter except for alginate used for microgel production whose powder was sterilised under UV light for 30 min and dissolved using sterile deionised water

Prior to capsules' production, the MC3T3-E1 cells were trypsinized using a 0.05% trypsin-EDTA solution, dyed with trypan blue (which colours dead cells dark blue) and counted using a cell counting chamber. $2x10^6$ cells per mL of alginate were used. The cells were then resuspended with 1mL of alginate prior to addition to a plastic flask with microparticles previously weighed and sterilised inside, once again resuspending the mixture. Afterwards, 4 mL of alginate solution were added reaching 5mL of solution to be extruded. Using a 5mL luer-lock syringe (Soft-Ject), the volume was extracted.

An alternative procedure was performed which implied manually pressing a 1mL syringe (Soft-Ject) with a 21G needle to add dropwise to 50mL of 0.1M $CaCl_2$ solution stirred at 150rpm in a 100mL plastic flask, while the remainder of procedure was equal to the one already described.

After producing the alginate microgels, these microgels must be rinsed in NaCl/MES before starting the layer-by-layer assembly. The layers follow a repeating pattern of PLL/ALG/CHT/ALG until reach 12 layers of polyelectrolytes. The deposition of each layers occurred by submerging the alginate microgels for 10 min in each solution followed with rinsing steps with NaCl/MES solution to remove excess Ca^{2+}, once again avoiding alginate crosslinking and wash away the excess of polyelectrolytes.

After the final layer deposition, the microgels were rinsed once again in NaCl/MES solution and submerge in the EDTA solution for 5 minutes. The EDTA

chelated the Ca^{2+} ions from the crosslinked alginate causing liquification which integrity was not compromised due to the polyelectrolyte layers holding it together.

After liquification, the capsules were rinsed carefully two times with NaCl/MES to remove the EDTA and then were rinsed in α-MEM 1%ATB without FBS also two times.

3.2.7. Capsules characterization

To characterise the capsules' morphology of SEM was performed. Before subjecting the capsules to this analysis, they must be dehydrated[4] After dehydration, the capsules were sputter coated with gold/palladium and observed in a Hitachi S-4100 scanning electron microscope (Hitachi, Japan) .

3.2.8. Cell metabolic activity assay(MTS)

To assess the metabolic activity of the cells, a MTS colorimetric assay was used as described by Correia *et al*[3]. This assay is based on the reduction ability of mitochondrial dehydrogenase enzymes to convert the 3-(4,5-dimethylthiazol-2-yl)-5-(3-carboxymethoxyphenyl)-2-(4-sulphofenyl)-2H-tetrazolium (MTS) compound into a cell culture soluble brown formazan product which is observed in viable cells. As already described in the literature[3] but with minor modifications , the capsules (n=5 per well, in triplicate) were placed in a 48-well plate for each time point (day3 and day 7). The assay was performed in a light free environment by adding 300 µL of a 1:6 diluted MTS solution to each well. The plate was protected from light and placed in an incubator at 37ºC and 5% CO_2 atmosphere (Binder Model C170 CO_2) for 4h. After incubation, 100 µL of solution from each well (in triplicates) was removed transferred to a 96-well plate. The absorbance was read at a wavelength of 490nm in a Synergy HTX microplate reader

3.2.9 Live/dead assays

Live/dead assay was performed after 1 day, 3 days and 7 days of capsule incubation as already described in the literature[3]. In live/dead assay, calcein-AM and PI were used. After a hydrolysis process, calcein-AM turning into a green fluorescent marker named calcein which dyes the cytoplasm occurring only in viable cells. On the other hand, PI is membrane impermeant hence binds to the DNA of dead cells. For each time point, the culture medium is removed and replaced with a solution comprised of 500µL of

DPBS,1 µl of calcein-AM and 0.5 µL of PI, which was incubated for 30 min protected from light at 37 °C. Then, the solution was removed and the capsule was washed with PBS and visualized immediately after it in the dark by fluorescence microscopy (Axio Imager M2,Carl Zeiss, Germany). Calcein-AM stained living cells, through a fluorescent filter (fluorescence excitation (λ_{ex}: 494 nm, λ_{em}: 517 nm), appeared bright green. With PI, through a rhodamine filter (fluorescence excitation (λ_{ex}: 535 nm, λ_{em}: 617 nm), dead cells appeared bright red.

3.2.10. DAPI/phalloidin

DAPI stains the double stranded DNA in nuclei which will appear blue. Phalloidin labels F-actin revealing them red and will display the actin filaments in fixed cells. For each time point, capsules were added to a well-plate, the medium was removed and the cells were fixed with 4% formaldehyde solution for 15min at RT. After that, formaldehyde solution was removed and 0.1% Triton X solution was added to permeabilize the cells. The solution was then removed and the capsules were washed with DPBS. To label the cell components, firstly, a solution with 500µL of DPBS and 12.5 µL of phalloidin/rhodamine was added to the wells and was left at RT for 45min before washing with PBS. Subsequently, a solution comprised of 1mL of DPBS and 1µL of DAPI was added to the wells and left at RT for 5 min before washing with DPBS. After washing, the capsules were immediately observed in the dark by fluorescence microscopy (Axio Imager M2,Carl Zeiss, Germany) on which cell nuclei appeared bright blue and F-actin filaments appeared red

4. Results and Discussion

4.1 *In situ* magnetically fixable hydrogel-microcapsular hybrid for bottom-up bone tissue engineering

Subchapter 4.1

This subchapter is based on the article entitled

"In situ magnetically fixable hydrogel-microcapsular hybrid for bottom-up bone tissue engineering"

In situ Magnetically-fixable Cell-loaded Liquefied Microcapsules as Building Blocks for Bottom-up Bone Tissue Engineering

João C.M. Martins, Vítor M. Gaspar[#], Clara R. Correia and João F. Mano[#]

Department of Chemistry, CICECO – Aveiro Institute of Materials, University of Aveiro, Campus Universitário de Santiago, 3810-193, Aveiro, Portugal

[#]Corresponding authors:

Professor João F. Mano
Department of Chemistry, CICECO – Aveiro Institute of Materials
University of Aveiro, Campus Universitário de Santiago
3810-193, Aveiro, Portugal
E-mail: jmano@ua.pt
Telephone: +351 234370733

Dr. Vítor Gaspar
Department of Chemistry, CICECO – Aveiro Institute of Materials
University of Aveiro, Campus Universitário de Santiago
3810-193, Aveiro, Portugal
E-mail: vm.gaspar@ua.pt
Telephone: +351 234370733

Abstract

Cellular encapsulation in semi-permeable liquefied microcapsules holds a tremendous potential for the long-term survival of cell-rich agglomerates after their implantation. Due to their versatility these systems can administered in damaged tissues via minimally invasive surgical procedures and seldom promote a systemic immunological reaction from the host. However, microcapsules tissue fixation and adhesion remain significant issues that hinder their rapid translation. In this work, we propose the development of a hierarchic nano-to-macro magnetically responsive microcapsule as an *in situ* fixable cell delivery system. To prove this concept layer-by-layer surface structured microcapsules containing magnetically responsive microparticles acting as adhesion sites for MC3T3-E1 cells were produced. The magnetically responsive microparticles allowed an easy manipulation of cell-laden microcapsules under a magnetic field in a tissue mimicking microenvironment. As the results demonstrated magnetically responsive microparticles had no cytotoxic effects on cells up to 7 days in culture and allowed for cell spreading and proliferation in the compartmentalized liquefied environment. Overall the magnetically guidable system provides a valuable alternative for cell-rich microcapsules *in situ* fixation during or after tissue implantation.

1. Introduction

Bone related diseases or defects are a currently a major worldwide concern particularly because the overall the number of bone related injuries will increase in the upcoming years in the United States and in the European Union[1,2]. Despite bone tissues have intrinsic regeneration capacities, when the suffered damage exceeds a critical size, bone cannot regenerate by itself. In an attempt to overcome these issues, metals and ceramics have been widely used as implants although with limited performance results[3]. Allografts and xenografts emerged as potential alternatives to hard material-based implants, however they pose a potential risk of disease transmission and are poised by the low number of donor as well as overall number of cells[4]. To overcome these limitations the development of bioactive biomaterials with enhanced biological performance and safety have been developed in the last decades.

Magnetic nanoparticles (MNPs), specifically superparamagnetic iron oxide nanoparticles, and the use of magnetic fields have been widely employed for bone tissue engineering applications over the years. These applications range from enhancing cell proliferation[5] and osteogenic differentiation[6–8] (e.g. via the use of magnetically responsive scaffolds), to growth factors and drug delivery and up even to cell tracking and imaging, some of which have already been tested *in vivo*[9].

The use of spherical hydrogels (either beads or capsules[10]) has raised interest since their shape provides higher area/volume ratio than normal hydrogels and hence promote better nutrients, waste products and O_2 and CO_2. These systems made from natural or synthetic polymers have been studied for cell encapsulation for regenerative purposes promoting *in vitro* osteogenic differentiation[11,12], *in vitro* stem cell chondrogenesis[13,14], *in vivo* stem cell osteogenic differentiation[15,16] and *in vitro* and *in vivo* liver regeneration[17]. These spherical microgels, as reported recently, may have their shape tuned providing a larger surface area improving or tailored by producing a variety of core-shell capsules[18,19].

In this work, a system combing the use of MNPs and liquefied microcapsules as a compartmentalized carrier with hierarchic organization from nanoscale (MNPs), to microscale (microparticles and cells) to macroscale (capsules) is proposed. This unique assembly allowed to produce a magnetically fixable capsular system supporting cell viability in a semipermeable liquefied microenvironment. For this purpose, poly- ε-caprolactone microparticles containing hydrophobic MNPs were initially produced

(µPCL[MNPs]). The resulting magnetic microcarriers surface was then functionalized with collagen I to act as cell adhesion platforms. and encapsulated along with MC3T3-E1 cells in Alginate which then underwent a layer-by-layer (LBL) polyelectrolyte deposition before liquefying the Alginate (Figure 1). The obtained results indicate that bioencapsulated pre-osteoblasts remain viable along time and form cellular agglomerates in the liquefied microenvironment. Importantly, magnetic cell-laden microcapsules were fixable *in situ* in an ex vivo bone model and were able to withstand liquid wash shear forces.

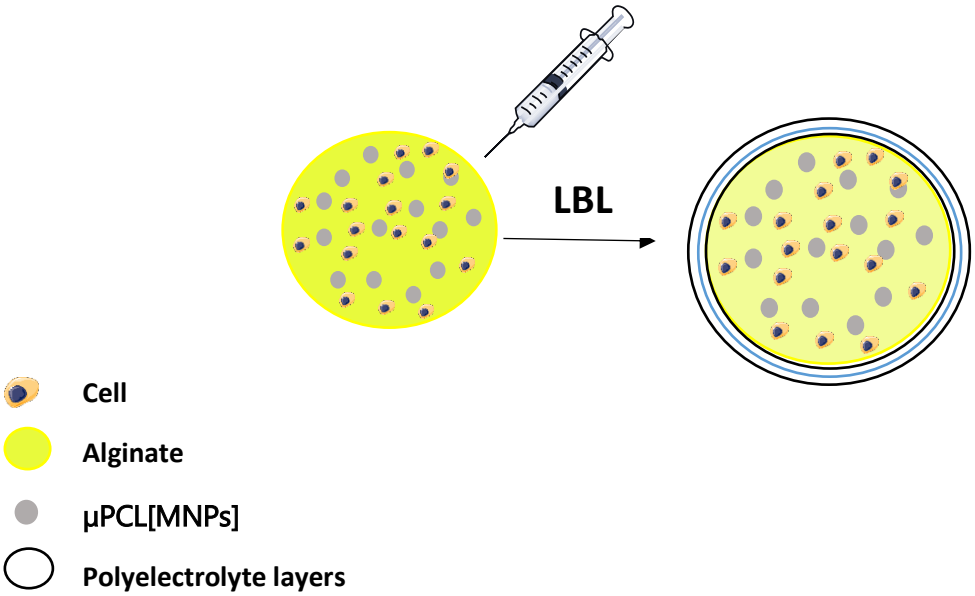

Figure 1. Schematic representation of the capsules production process

2. Materials and methods

2.1. Materials

$FeCl_3.6H_2O$ (≥99%), $FeCl_2.4H_2O$ (98%) and ammonia solution 25% were purchased from Laborspirit (Loures, Portugal) and produced by Sigma Aldrich, Alfa Aesar and LabChem respectively. Oleic acid (Sigma, ≥99%) was purchased from Laborspirit (Loures, Portugal). Neodymium magnet was purchased from Supermagnete (Germany)

Polycaprolactone (PCL; Mn 80 000) and polyvinyl alcohol (PVA; 87-90% hydrolysed, MW-30 000-70 000 and produced by Sigma Aldrich. Dichloromethane (DCM; ≥99%) was purchased from JMGS (Odivelas, Portugal). Collagen type I solution from rat tail was purchased from Sigma Aldrich and acetic acid (≥99%) was acquired from JMGS (Odivelas, Portugal). Poly-L-Lysine hydrobromide (PLL; MW 30 000-70 000 Da) and the Alginate (ALG; alginic acid sodium salt from brown algae, low viscosity) were produced by Sigma Aldrich and purchased from Laborspirit (Loures, Portugal) and Sigma Aldrich, respectively. Chitosan (CHT, Protasan UP CL 213, viscosity 107 mPA s, molecular weight $M_w = 2.7 \times 10^5$ g mol^{-1}, 83 % degree of deacetylation; NovaMatrix, Norway). Calcium chloride ($CaCl_2$, anhydrous analytical grade) was purchased from JMGS (Odivelas, Portugal) and produced by PanReac. MES hydrate (>99%) and sodium chloride (NaCl; 99.5%) were purchased from Laborspirit (Loures, Portugal) and produced by Alfa Aesar and LabChem, respectively.

MC3T3-E1 cells (Clone 4) were obtained from ATCC, Alpha Modified Eagle's Medium (α-MEM), DPBS (without calcium and magnesium), Calcein-AM, Propidium Iodide (PI) were all purchased from Thermofisher Scientific Inc (Alfagene, Portugal, 48-well plates (non-adherent) were purchased from VWR. And 96-Well White Plates (Non-Treated), without Lid, Flat Well NS were purchased from Corning. DAPI (4',6-diamidino-2-phenylindole, dihydrochloride) and WFI for cell culture were purchased from Thermo Fisher Scientific and rhodamine phalloidin (Thermo Fisher Scientific) was purchased from Alfagene (Carcavelos, Portugal). CellTiter 96 AQ_{ueous} One Solution cell (MTS) from Promega was purchased from VWR. Trypsin-EDTA solution (SIGMA) and formaldehyde solution (SIGMA) was purchased from Laborspirit (Loures, Portugal).

2.2 Methods

2.2.1. Functionalized magnetic nanoparticles (MNPs) synthesis and characterization

MNPs were synthesised through a co-precipitation by following a method already described in the literature but with some modifications[20]. Briefly, $FeCl_3.6H_2O$ and $FeCl_2.4H_2O$ (0.046 and 0.023 mol respectively) were dissolved in 150 mL of de-bubbled double deionized and filtered water (miliQ water) in a 250 mL three-necked flask and heated to 85 ºC under vigorous stirring under a N_2 atmosphere. Then, 20 mL of ammonia 25 % solution were added to the mixture. After 30 min, 1 mL of oleic acid was added, and the reaction proceeded for 1h. After synthesis, the nanoparticles were separated using a magnet, dialysed against deionized water for 1 day, recovered, washed with deionised water and ethanol and frozen at -80 ºC before freeze-drying. The size distribution and zeta potential were evaluated through dynamic light scattering (DLS) and the morphology was evaluated through scanning transmission electron microscopy (STEM) by using a Hitachi SU-70 STEM microscope.

2.2.2. MNPs-laden PCL microparticles (µPCL[MNPs]) production

Oil-in-water emulsion solvent evaporation technique was used to produce the microparticles as already reported by our group with few modifications in the protocol[21]. PCL microparticles (µPCL) without MNPs were produced for comparison purposes. Firstly, 8 mg of µPCL[MNPs] were resuspended and 8 mL of PCL solution in dichloromethane were added comprising the oil phase. The aqueous phase was comprised by 0.5% PVA solution. The oil-in-water emulsion was formed by dispersing 8 mL of the oil phase into 150 mL of PVA by using a highly precise piezoelectric-based air pumping system (OB1 MK3 –Microfluidic Flow Control System, Elveflow®, France), at a pressure of 5 bar. Then, the microparticle-containing solution was placed on an orbital stirring plate for 8 h at room temperature inside a fume hood. The microparticles were then recovered by magnetic separation and washed 5 times with deionized water and sieved using stainless steel test sieves to obtain a size range of 40-63 µm. Lastly, the microparticles were frozen at -80 ºC and freeze-dried for at least 48 h and stored.

2.2.3. Magnetic microparticles characterization

Microparticles size distribution and morphology were determined by analysing pictures taken from optical contrast light microscopy (Primostar, Carl Zeiss, Germany) which were then analysed using ImageJ v1.08 (NIH, Bethesda, ML) [22]. The size distribution was obtained by running a segmentation algorithm which analysed at least 300 microparticles.

Microparticles morphology and topography were evaluated by scanning electron microscopy (SEM). For this, microparticles were sputter coated with gold/palladium and observed in a Hitachi S-4100 scanning electron microscope (Hitachi, Japan) with voltages ranging from 15-25 kV, at various magnifications. By using the SU-70 electron microscope equipped with a Bruker EDS equipment, the iron (Fe) was mapped on the volume of µPCL[MNPs].

2.2.4 Magnetic microparticles surface functionalization

The surface coating was performed by using a protocol already established in our group [23,24]. Briefly, the particles were plasma treated inside a plasma reactor chamber fitted with a radiofrequency generator. Air was used as the working atmosphere. Once the pressure inside the chamber stabilized at approximately 0.2 mbar, a glowing charge of plasma was discharged at 30 V for 5 min. Then, the sample was removed from the chamber and shaken gently to ensure a more homogenous surface exposition and the procedure was repeated 3 times. After plasma treatment, the microparticles were sterilized for 30 min under UV light and immersed in 0.02 M acetic acid solution containing collagen I from rat tail overnight at 4 ºC. The particles were then washed in PBS three times.

2.2.5 Production and characterization of Alginate beads

The Alginate beads were produced using an electrospray device (Spraybase®). Different conditions were evaluated namely: Alginate concentration and voltage. Two Alginate solutions; 2% (w/v) and 2.5% (w/v) were used to acquire preliminary data of beads size distribution before LBL capsules production. The production of Alginate beads containing non-magnetic µPCL was also assessed. For each formulation, the Alginate solution with or without µPCL was loaded into a syringe (5 mL), placed in a syringe pump (KD2000) and extruded at a 50 mL/h flow rate. The syringe was connected to a tube (1 mm diameter) with a needle attached at the end contacting with a metal pin

connected through subjected to high voltage. The solution was then dropped into a beaker containing a $CaCl_2$ solution (0.1 M), under stirring at RT.

To evaluate the morphology and the size of the beads, optical microscopy (Zeiss, Primo Star) was used. The diameters of the beads (n=20) were measured using the open-source software ImageJ (NIH, Bethesda, ML).

2.2.6 Cell encapsulation and capsules production

The production of such capsules has already been described and validated in several studies using different cells types and even tested *in vivo* [11,13,15,23,24]. The MC3T3-E1 cells were grown in tissue culture flasks until 90% confluence and trypsinized using a 0.05% trypsin-EDTA solution to detach the cells for 5min at 37ºC and in a 5% CO_2 atmosphere. The trypsin was inactivated with α-MEM and the where then centrifuged at 300 g. The medium was decanted, and the cell pellet was resuspended using a 2% (w/v) Alginate solution. For each mL of Alginate, $2x10^6$ cells were used. The microparticles were mixed in the Alginate/cells solution. The solution was added dropwise by using a 21G needle to a 0.1 M $CaCl_2$ bath under agitation 150 rpm.

The droplets were then transformed into Alginate beads due to ionic cross-linking. The beads were left 20 min under stirring and then washed in a NaCl/MES solution. Then, the beads were immersed in PLL and subsequently in ALG, CHT and ALG again in a repetitive pattern until a total of 12 layers was produced (6 bi-layers). Between each polyelectrolyte layer deposition (which lasted 10 min), a NaCl/MES solution (0.15M NaCl and 25 mM MES, pH 6.7) was used to rinse and wash way the excess of polyelectrolytes. After the layer-by-layer (LBL) polyelectrolyte deposition, a 0.02 M EDTA solution was used to chelate the Ca^{2+} ions from the bead leaving a liquefied environment protected by the polyelectrolyte's membrane becoming a capsule.

2.2.7. Cell metabolic activity assay (MTS)

To assess the metabolic activity of the cells, an MTS colorimetric assay was used. This assay is based on the reduction ability of mitochondrial dehydrogenase enzymes to convert the 3-(4,5-dimethylthiazol-2-yl)-5-(3-carboxymethoxyphenyl)-2-(4-sulphofenyl)-2H-tetrazolium (MTS) compound into a cell culture soluble brown formazan product which is observed in viable cells. As already described in the literature[23] but with minor modifications , the capsules (n=5 per well, in triplicate) were placed in a 48-well plate for each time point (day3 and day 7). The assay was performed

in a light free environment by adding 300 µL of a 1:6 diluted MTS solution to each well. The plate was protected from light and placed in an incubator at 37 ºC and 5 % CO_2 atmosphere for 4 h. After incubation, 100 µL of solution from each well (in triplicates) was removed transferred to a 96-well plate. The absorbance was read at a wavelength of 490nm in a Synergy HTX microplate reader.

2.2.8 Fluorescence microscopy

Live-dead and DAPI/phalloidin staining were performed on each time point using similar protocols already established in our group [23].

2.2.8.1 Live/dead

In live/dead assay, calcein-AM and propidium iodide (PI) were used. After a hydrolysis process, occurring only in viable cells, calcein-AM turns into a green fluorescent marker named calcein which labels the cytoplasm. On the other hand, PI binds to the DNA of necrotic cells. For each time point, the culture medium is removed and replaced with a solution comprised of 500 µL of DPBS,1 µL of calcein-AM and 0.5 µL of PI, which was incubated for 30 min protected from light at 37 °C. Then, the solution was removed, and the capsule was washed with PBS and visualized immediately after it in the dark by fluorescence microscopy (Axio Imager M2, Carl Zeiss, Germany).

2.2.8.2 DAPI/phalloidin

DAPI stains the double stranded DNA in nuclei which will appear blue. Phalloidin labels F-actin revealing them red and will display the actin filaments in fixed cells. For each time point, capsules were added to a well-plate, the medium was removed and the cells were fixed with 4 % formaldehyde solution for 15 min at RT. After this, formaldehyde solution was removed and 0.1% Triton X solution was added to permeabilize the cells. The solution was then removed and the capsules were washed with DPBS. To label the cell components, firstly, a solution with 500µL of DPBS and 12.5 µL of phalloidin/rhodamine was added to the wells and was left at RT for 45min before washing with PBS. Subsequently, a solution comprised of 1mL of DPBS and 1µL of DAPI was added to the wells and left at RT for 5 min before washing with DPBS. After washing, the capsules were immediately observed in the dark by fluorescence microscopy (Axio Imager M2,Carl Zeiss, Germany) on which cell nuclei appeared bright blue and F-actin filaments were stained red.

3. Results and discussion

3.1 Functionalized MNPs synthesis and characterization

Initially, iron oxide nanoparticles were synthesized through a co-precipitation method described by Mahdavi and co-workers[20] with some modifications.

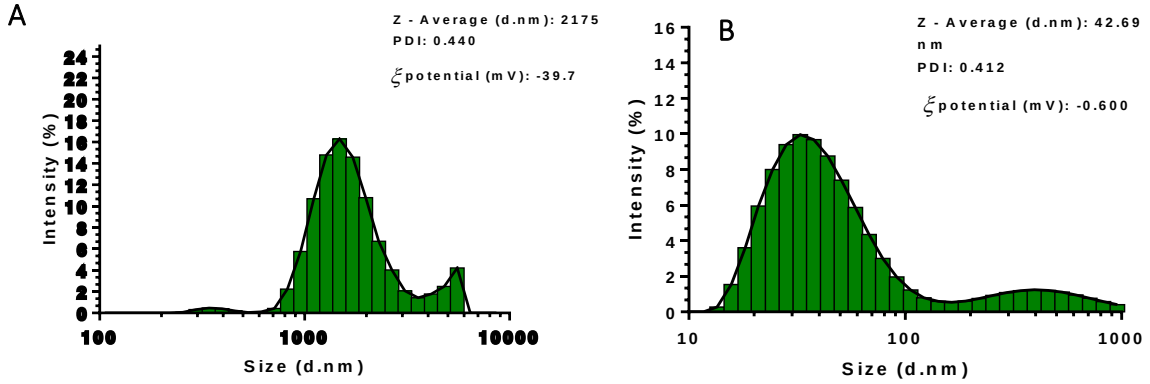

Figure 2. Dynamic light scattering analysis of size distribution of synthesised MNPs, PDI and zeta potential. A) Iron oxide nanoparticles, B) Oleic acid functionalized nanoparticles.

In the first synthesis, the iron oxide particles must not be called nanoparticles since their size was on average 2175 nm (Figure 2). In this synthesis, no oleic acid was used which might explain the enormous hydrodynamic size of the particles along with problems with stirring which was irregular causing the magnetic bar to not move in the centre of the flask. Ideally, to synthesise MNPs the stirring must be mechanical and not magnetic stirring. The different results might have been due to an irregular agitation. To counteract this, the stirring rate had to adjusted to 400 rpm in comparison to that reported originally in the literature (800 rpm). On the other hand, the addition of oleic acid to produce hydrophobic iron oxide nanoparticles yielded formulations with an average nanoparticle size of ~42 nm and an almost neutral zeta potential. STEM analysis of oleic acid iron oxide nanoparticles (MNPs) indicates that the synthesized particles have a quasi-spherical shape (Figure 2), which is in accordance with other literature reports for oleic acid functionalized iron oxide carriers[25].

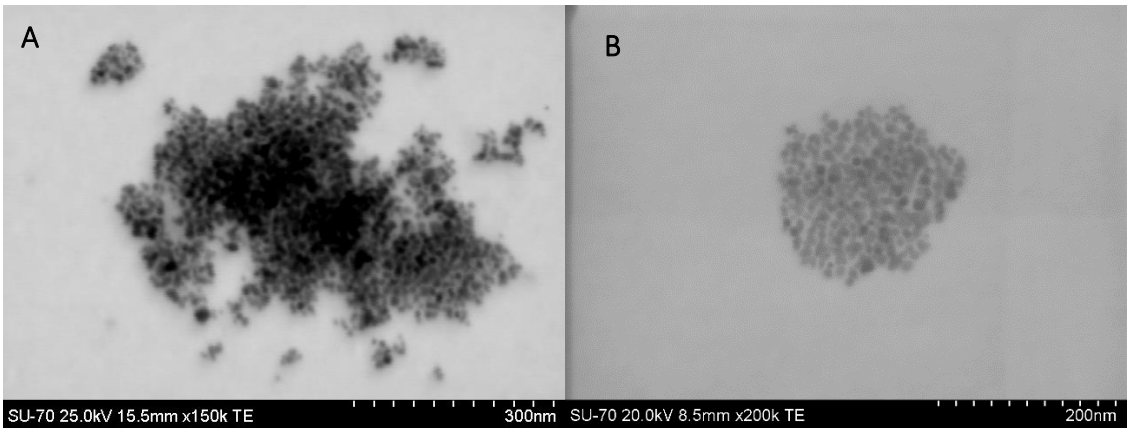

Figure 3 STEM image of MNPs functionalized with oleic acid at different voltages and magnifications 150k (A), 200k (B).

The PDI data obtained for DLS for oleic acid MNPs might have been a result of a small amount of particle aggregates (< 2% intensity in DLS and Figure 3 A) caused by sedimentation or low stability in water during analysis since the zeta potential is -0.600 mV. Zeta potential before and after oleic acid coating may change and values are influenced by pH as previously reported[26],

3.2 Production of MNPs laden PCL microparticles (µPCL[MNPs]) and surface functionalization

The µPCL[MNPs] were produced by oil-in-water emulsion and several formulations were tested since the particle size is influenced by parameters such as polymer concentration and stirring. Prior to µPCL[MNPs] production the desired size range was defined as the minimum to provide enough surface area to promote cell adhesion. On the other hand, the size should be small enough to avoid agglomeration and clogging in the needle while extruding the mixture to produce the cell-laden capsules. Initially, non-magnetic microparticles (µPCL) and magnetic microparticles production was optimized to have the highest yield of synthesized particles within the 40-63 µm range. For this, various formulations were produced, and numerous parameters summarized in Supplementary Table 1, in the Annexes were optimized (Figure 4 to 15). Considering that the selected size was narrow the formulations were optimized to obtain the highest number of particles within the 40-63 µm range.

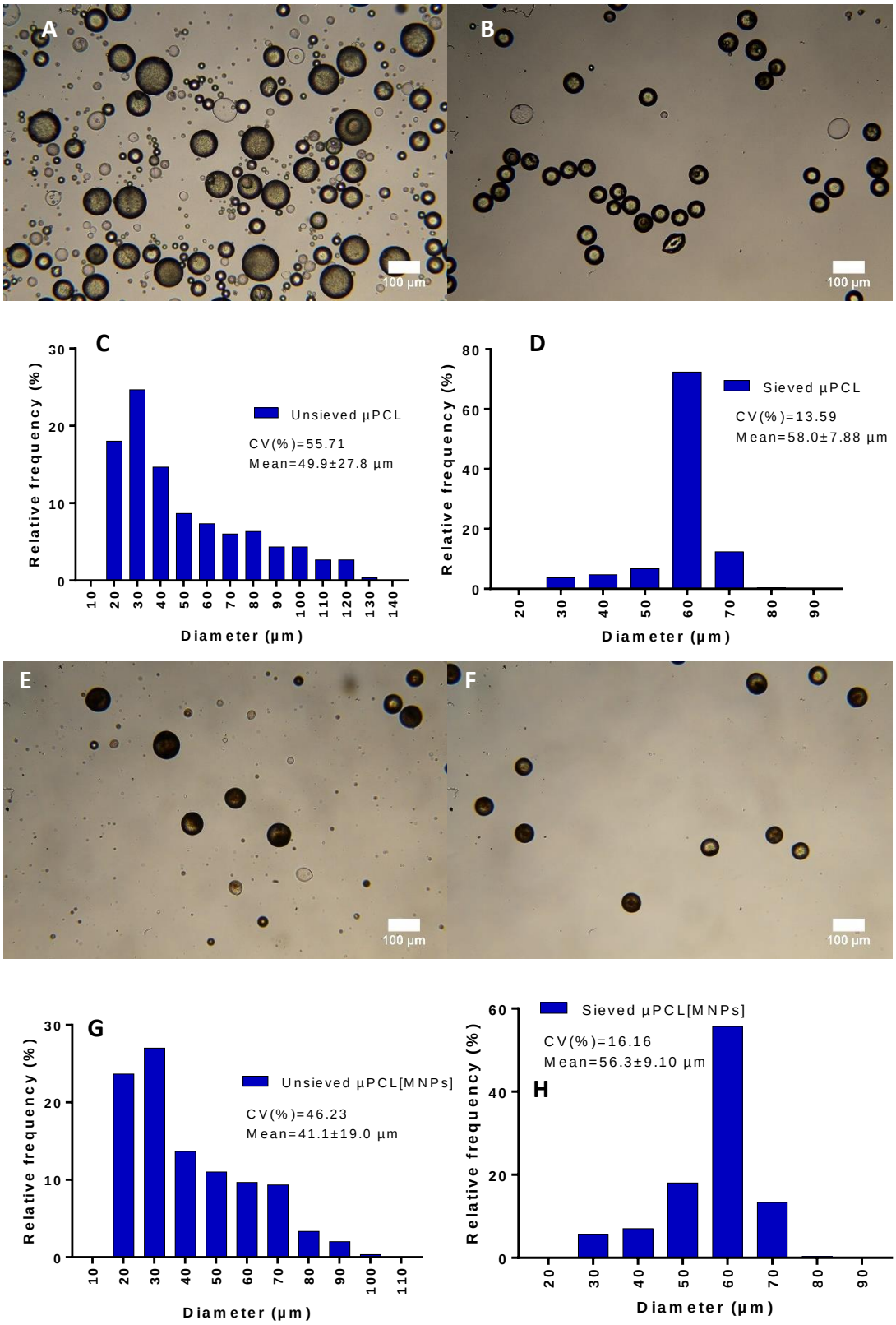

Figure 4. µPCL microparticles produced using a **1.5 %P CL solution** without MNPs (A, B,C and D) and with MNPs (E,F,G and H) at **500 rpm** before sieving (A and E) and after sieving (B and F) with 63 and 40 µm mesh test sieves. Size distribution graphs before sieving (C and G) and after sieving (D and H).

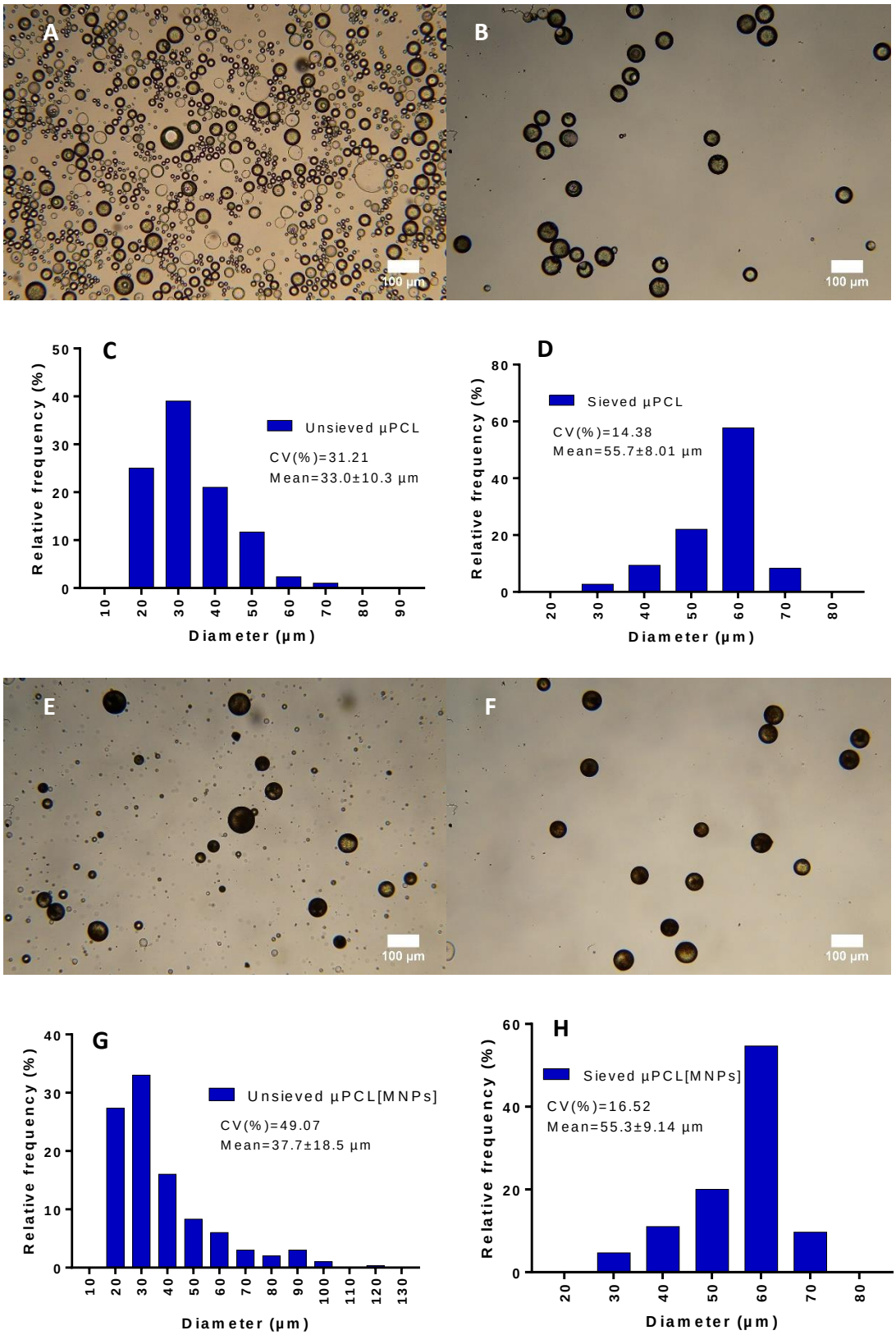

Figure 5. µPCL microparticles produced using a **1.5 %PCL solution** without MNPs (A, B,C and D) and with MNPs (E,F,G and H) at **600 rpm** before sieving (A and E) and after sieving (B and F) with 63 and 40 µm mesh test sieves. Size distribution graphs before sieving (C and G) and after sieving (D and H).

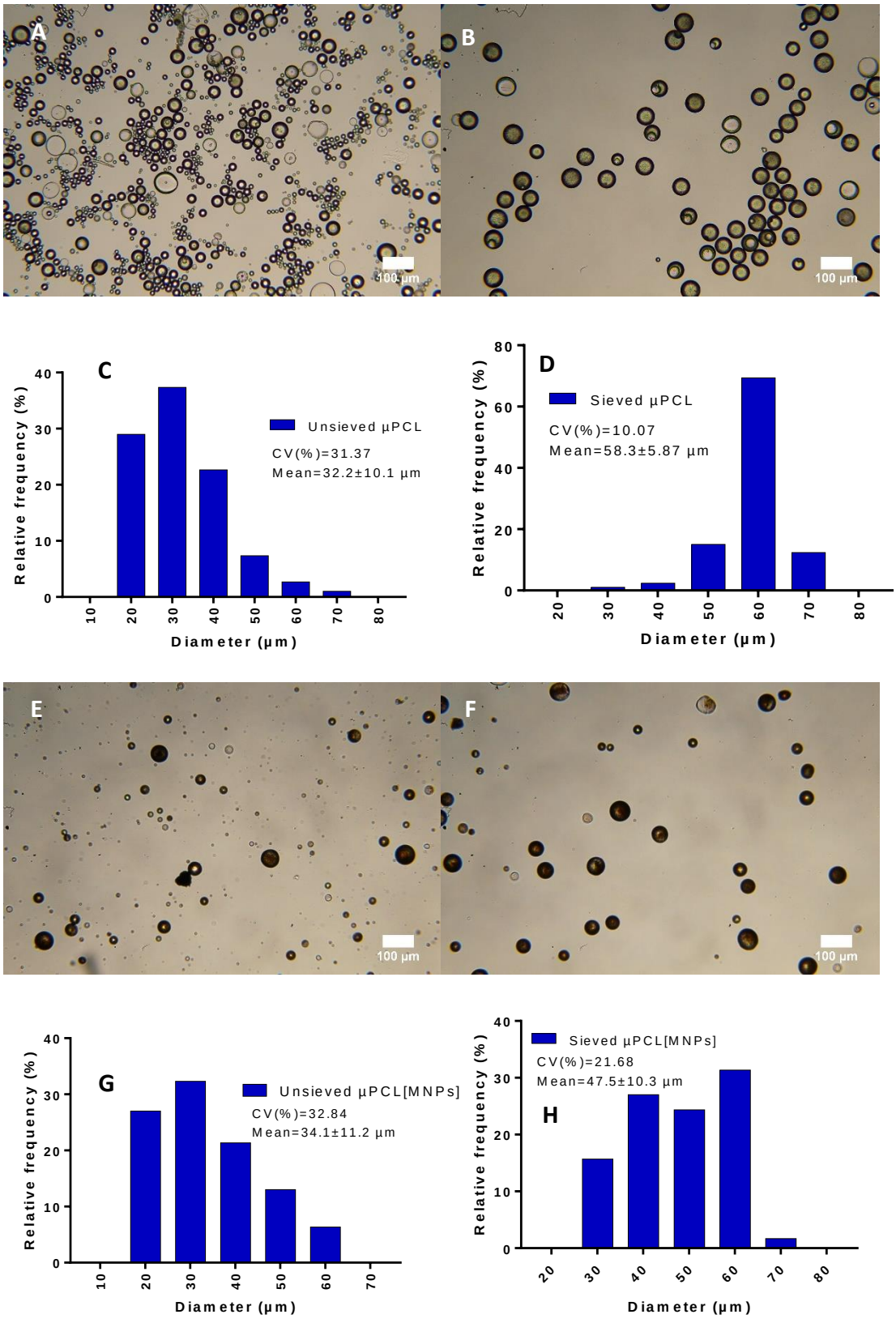

Figure 6. µPCL microparticles produced using a **1.5% PCL solution** without MNPs (A, B,C and D) and with MNPs (E,F,G and H) at **900 rpm** before sieving (A and E) and after sieving (B and F) with 63 and 40 µm mesh test sieves. Size distribution graphs before sieving (C and G) and after sieving (D and H).

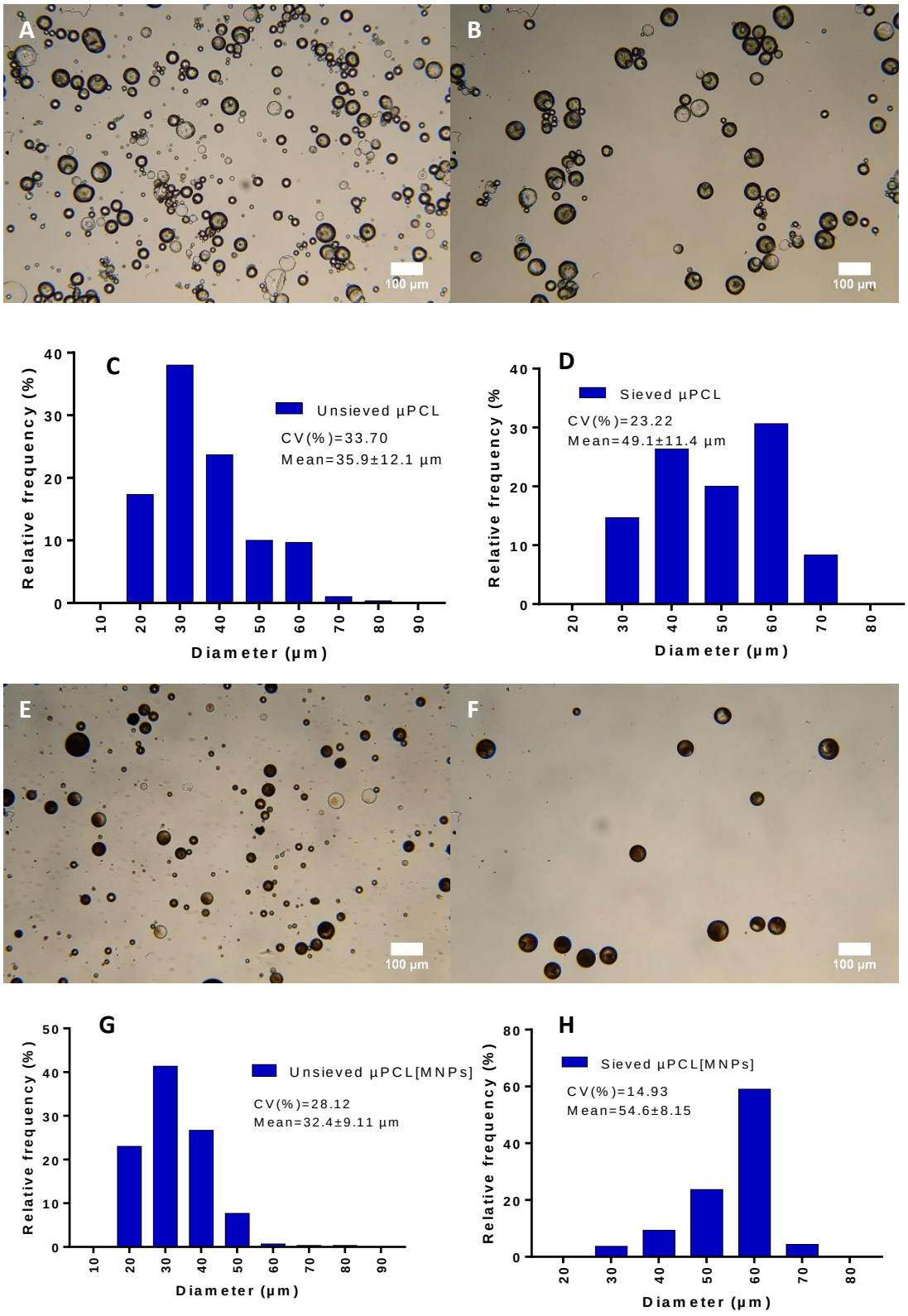

Figure 7. µPCL microparticles produced using a **1.5% PCL solution** without MNPs (A, B,C and D) and with MNPs (E,F,G and H) at **1000 rpm** before sieving (A and E) and after sieving (B and F) with 63 and 40 µm mesh test sieves. Size distribution graphs before sieving (C and G) and after sieving (D and H).

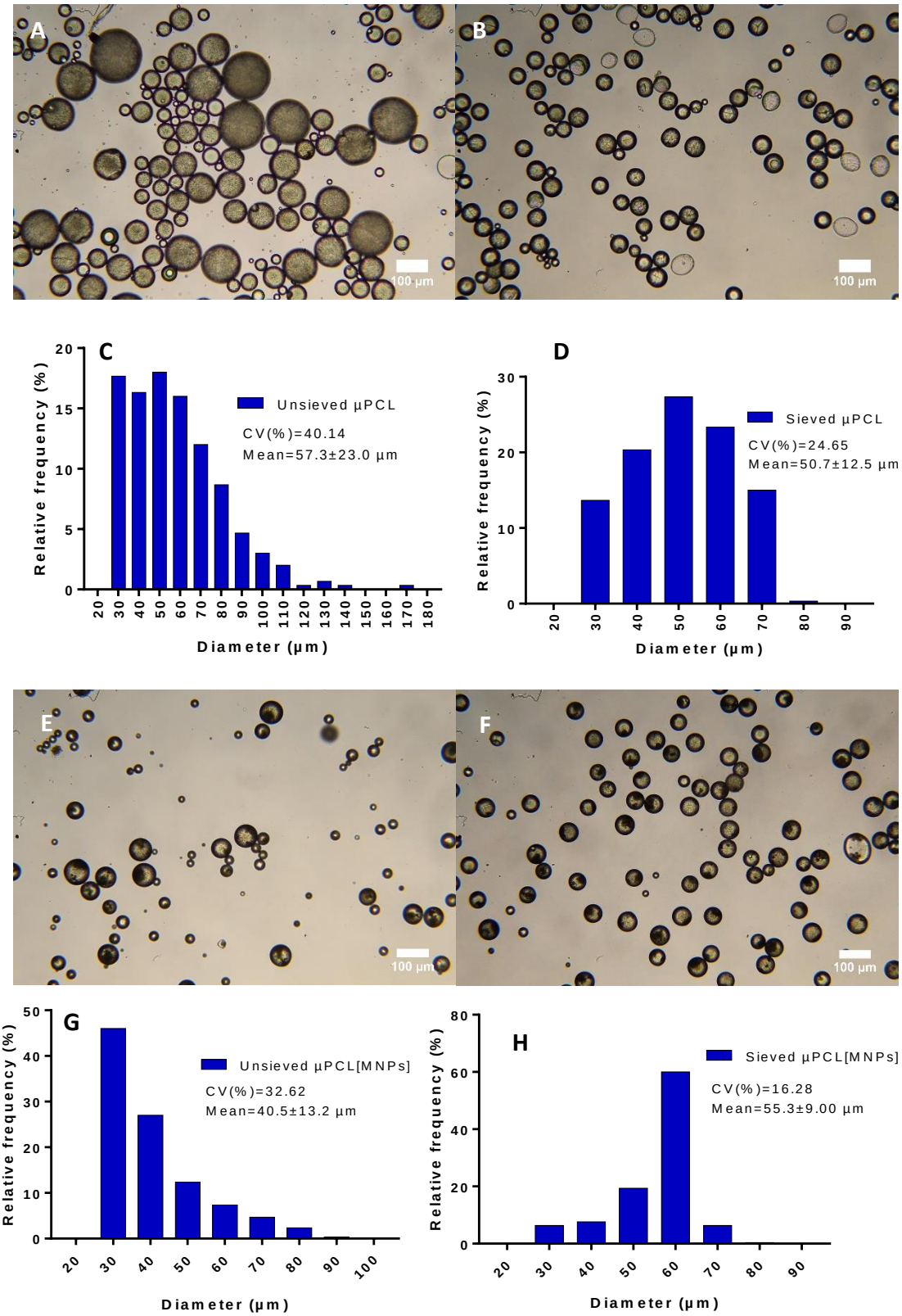

Figure 8. µPCL microparticles produced using a **3% PCL solution at 500 rpm** without MNPs (A, B,C,D) and with MNPs (E,F,G,H) produced before sieving (A and E) and after sieving (B and F) with 63 and 40 µm mesh test sieves. Size distribution graphs before sieving (C and G) and after sieving (D and H).

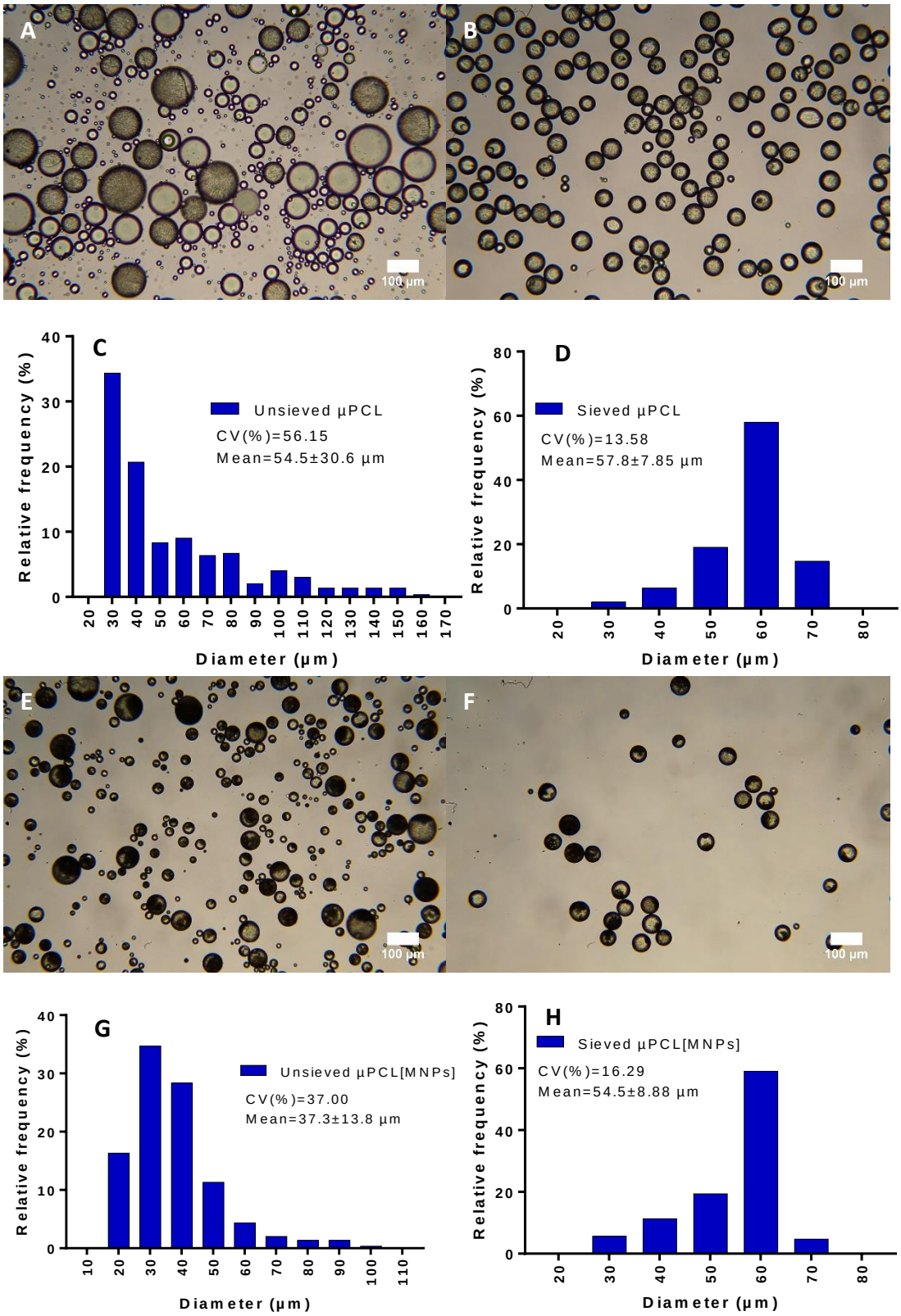

Figure 9. µPCL microparticles produced using a **3% PCL solution at 600 rpm** without MNPs (A, B,C,D) and with MNPs (E,F,G,H) produced before sieving (A and E) and after sieving (B and F) with 63 and 40 µm mesh test sieves. Size distribution graphs before sieving (C and G) and after sieving (D and H).

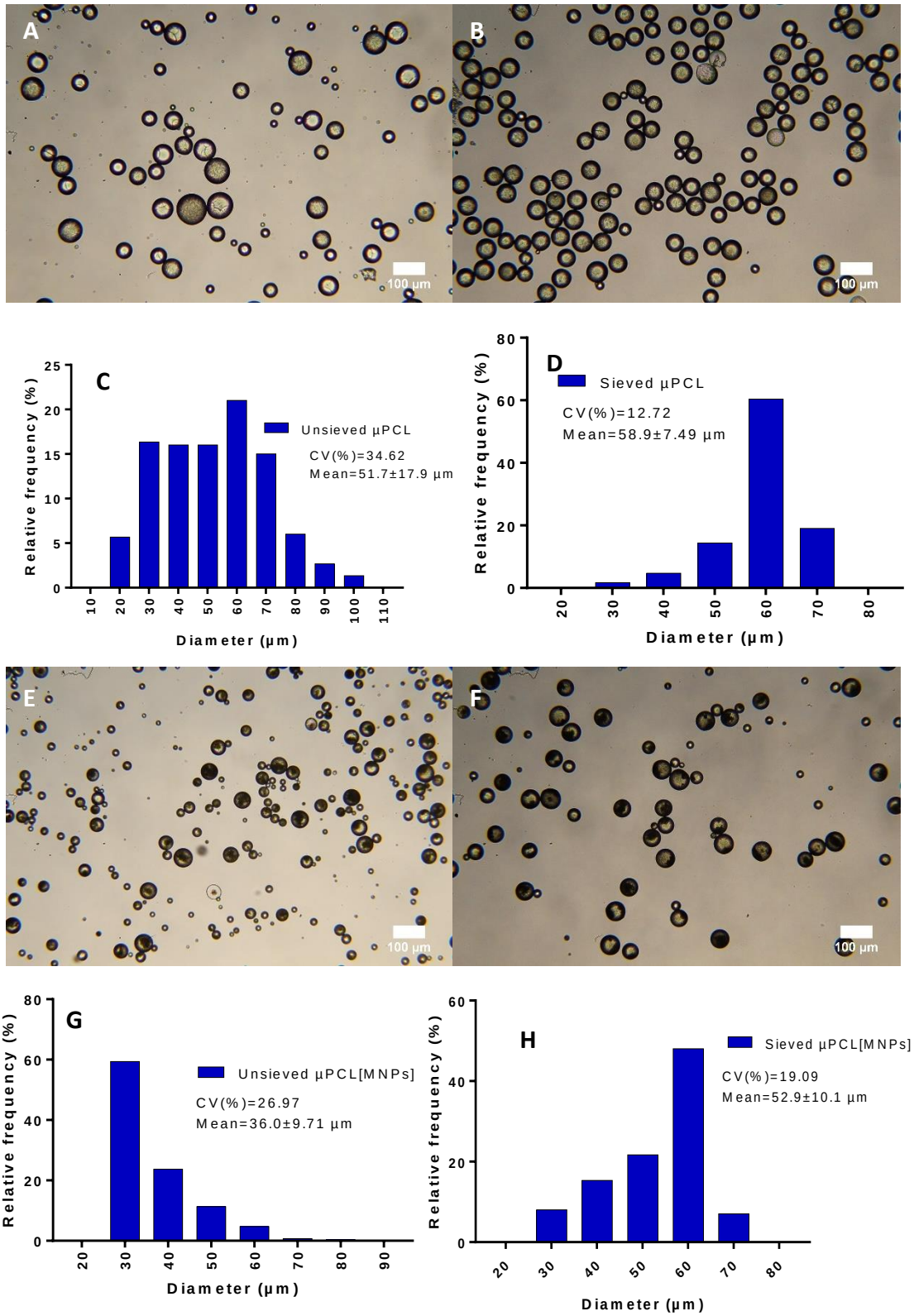

Figure 10. µPCL microparticles produced using a **3% PCL solution at 900 rpm** without MNPs (A, B, C, D) and with MNPs (E, F, G, H) produced before sieving (A and E) and after sieving (B and F) with 63 and 40 µm mesh test sieves. Size distribution graphs before sieving (C and G) and after sieving (D and H).

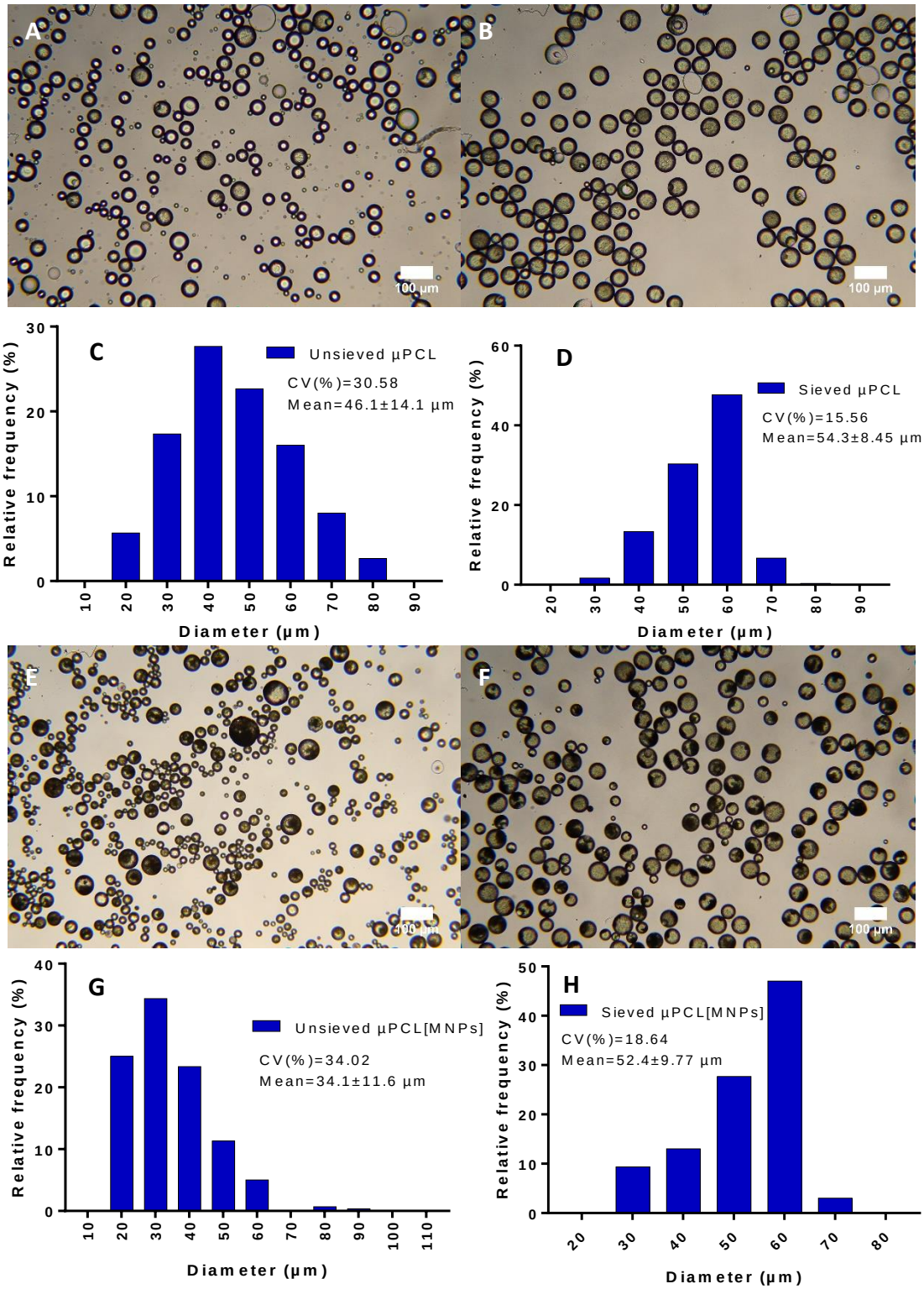

Figure 11. µPCL microparticles produced using a **3% PCL solution at 1000 rpm** without MNPs (A, B,C,D) and with MNPs (E,F,G,H) produced before sieving (A and E) and after sieving (B and F) with 63 and 40 µm mesh test sieves. Size distribution graphs before sieving (C and G) and after sieving (D and H).

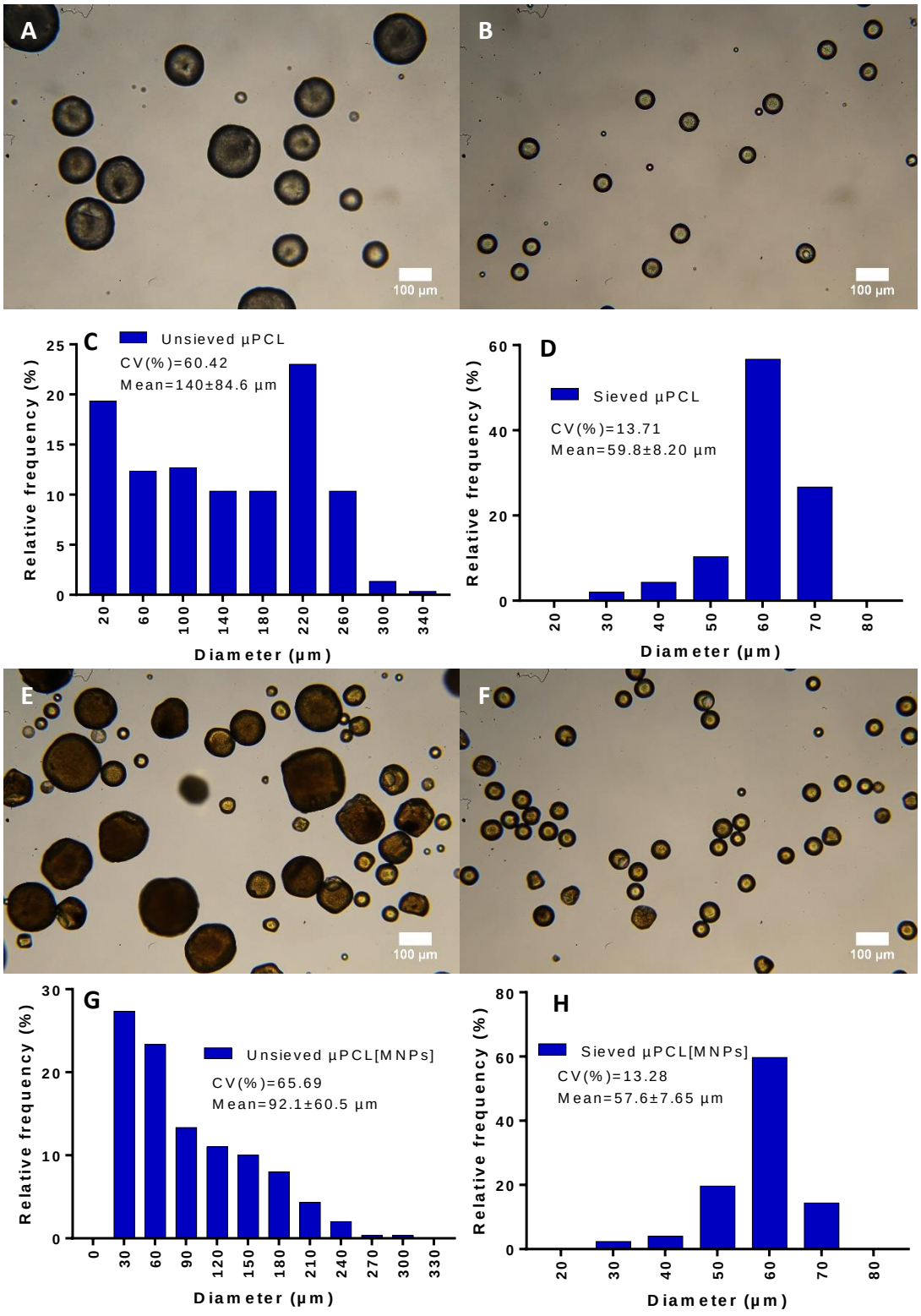

Figure 12. µPCL microparticles produced using a **5% PCL solution at 500 rpm** without MNPs (A, B,C,D) and with MNPs (E,F,G,H) produced before sieving (A and E) and after sieving (B and F) with 63 and 40 µm mesh test sieves. Size distribution graphs before sieving (C and G) and after sieving (D and H).

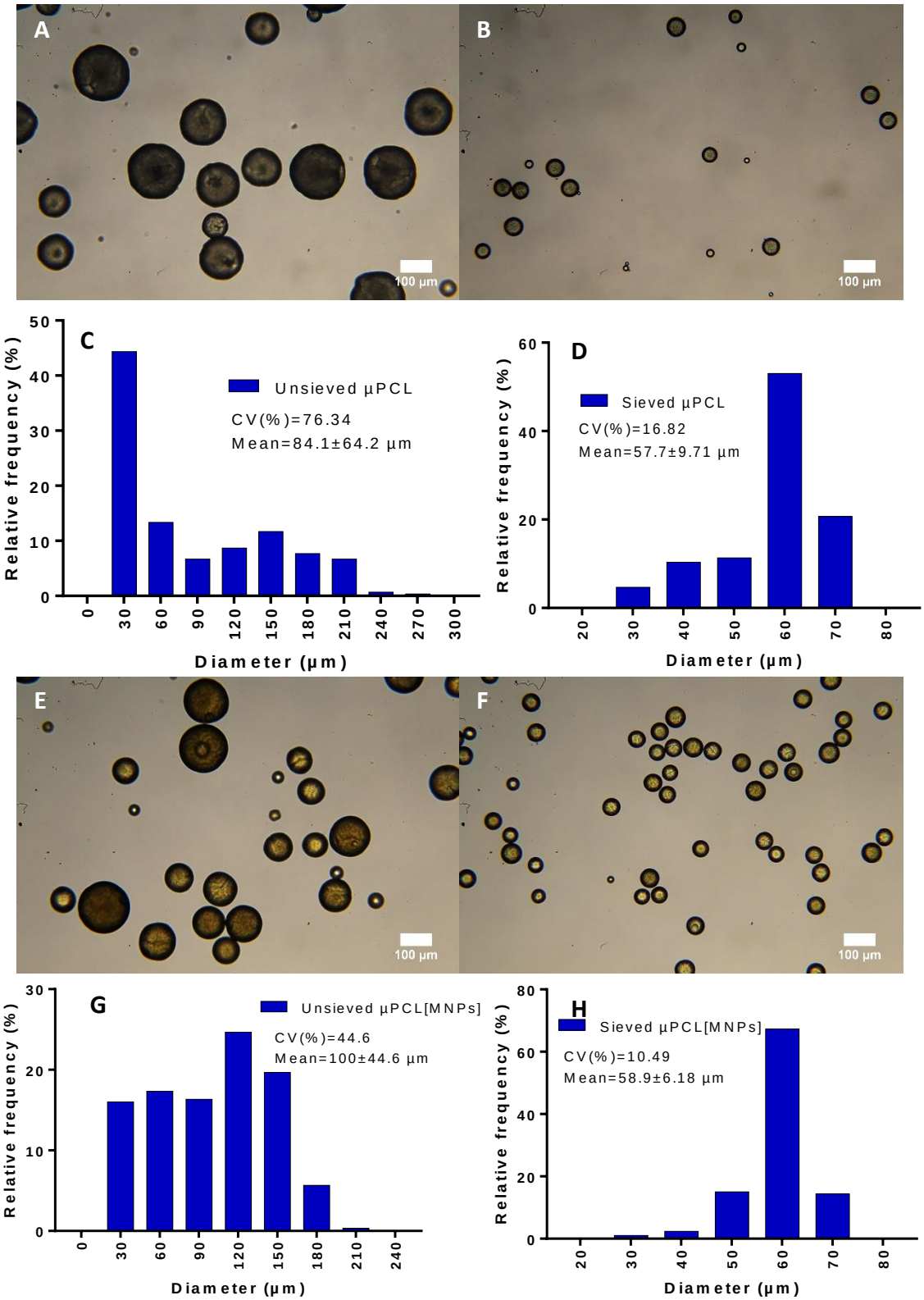

Figure 13. µPCL produced using a **5% PCL solution at 600 rpm** without MNPs (A, B,C,D) and with MNPs (E,F,G,H) produced before sieving (A and E) and after sieving (B and F) with 63 and 40 µm mesh test sieves. Size distribution graphs before sieving (C and G) and after sieving (D and H).

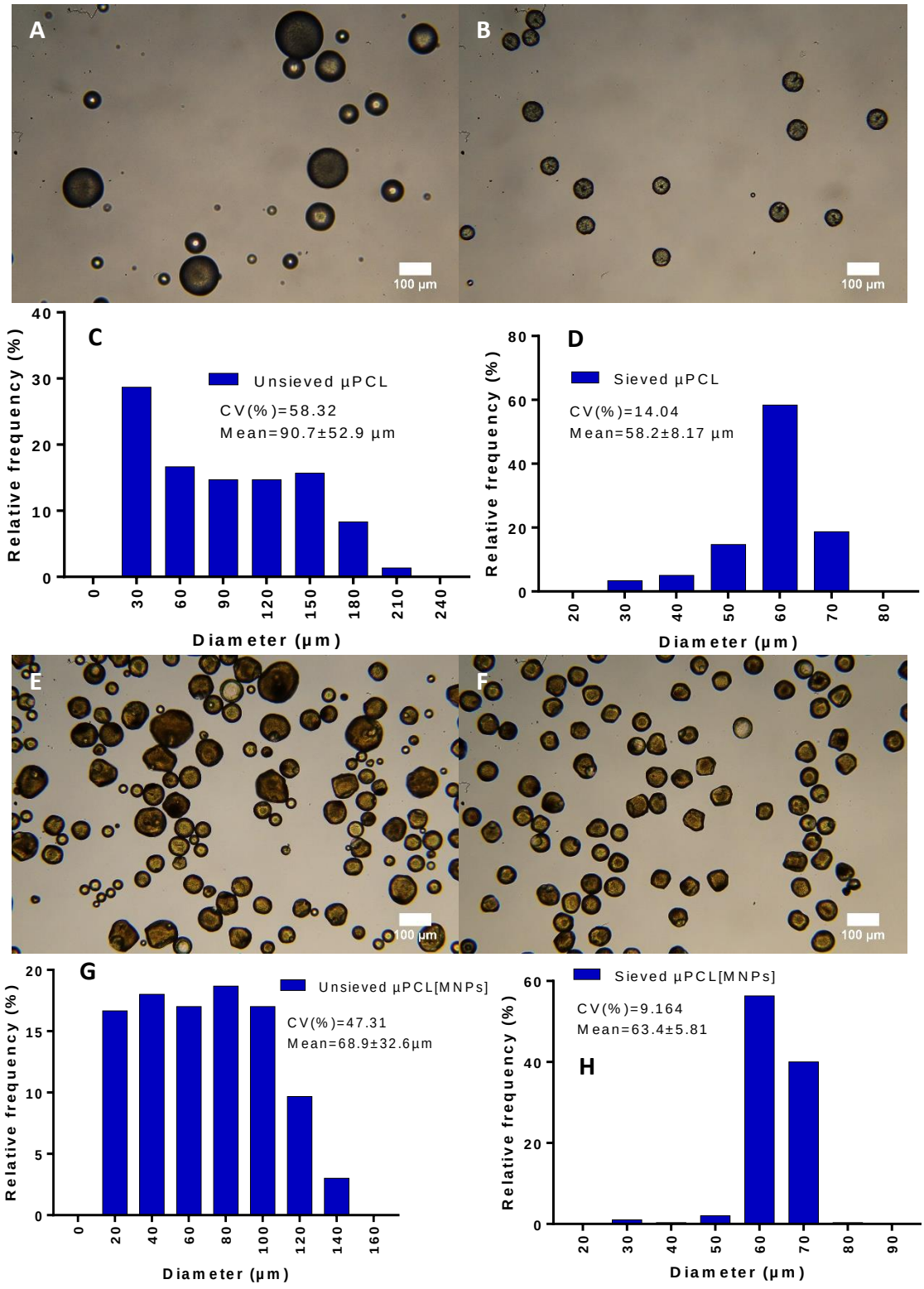

Figure 14. µPCL microparticles produced using a **5% PCL solution at 900 rpm** without MNPs (A, B,C,D) and with MNPs (E,F,G,H) produced before sieving (A and E) and after sieving (B and F) with 63 and 40 µm mesh test sieves. Size distribution graphs before sieving (C and G) and after sieving (D and H).

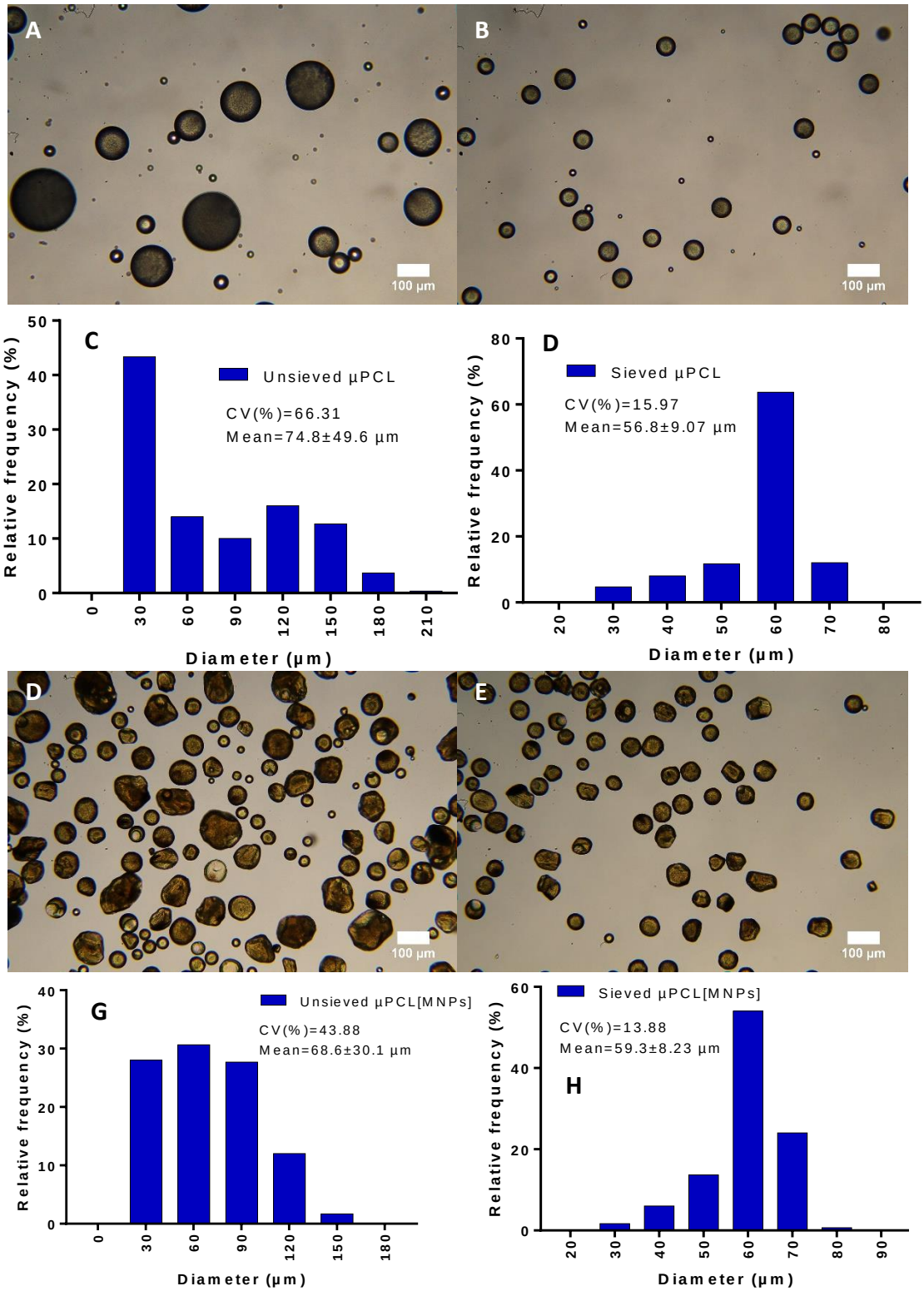

Figure 15. µPCL microparticles produced using a **5% PCL solution at 1000 rpm** without MNPs (A,B,C,D) and with MNPs (E,F,G,H) produced before sieving (A and E) and after sieving (B and F) with 63 and 40 µm mesh test sieves. Size distribution graphs before sieving (C and G) and after sieving (D and H).

As the results demonstrate, in general, higher concentrations of PCL resulted in larger particles and therefore the average particle diameter was affected by this parameter. When 5% PCL solution was used, there was a higher polydispersity, with particle sizes ranging from approximately 20 μm up to 300 μm. Furthermore, when 5 % PCL solution was used in the production of μPCL[MNPs] and a stirring rate of 900 to 1000 rpm, a greater amount of microparticles was non-spherical (Figure 14 and 15). On the other hand, using the lowest concentration of PCL, the microparticles produced were the smallest and the size distribution was as well the lowest that was obtained. However, in all formulations, the particles' size distribution was skewed to values lower than 40 μm. Taking this data into consideration, the microparticles produced with 3% PCL solution were chosen for their more adequate size range even with slightly higher polydispersity than 1.5 % PCL microparticles. The stirring rate influenced microparticles size. Generally, higher stirring rates led to the production of smaller particles and with lower size polydispersity. This might be explained by a more effective agitation process dispersing more evenly the oil phase (PCL) in the water phase (0.5 % PVA). The chosen formulation for μPCL[MNPs] was 3% PCL and 500 rpm because the size distribution (40.5±13.2 μm) and after sieving it produced the larger amount of microparticles hence the yield was higher. Similar average size range has been reported as appropriate to promote cell adhesion on the microparticles surface Moreover, the plasma treatment is crucial to increase the particles surface area providing a larger area on which cells could adhere.[23].

Following this optimization, the morphology and surface topography of μPCL[MNPs] was evaluated through SEM analysis. As the results of Figure 16 demonstrate μPCL[MNPs] display a spherical morphology and a rough surface topography (Figure 16 D). In addition, SEM energy dispersive spectroscopy (EDS) with elemental mapping confirmed the detection of an iron rich area in μPCL microparticles, further corroborating the successful encapsulation of magnetic nanoparticles (Figure 16 B.

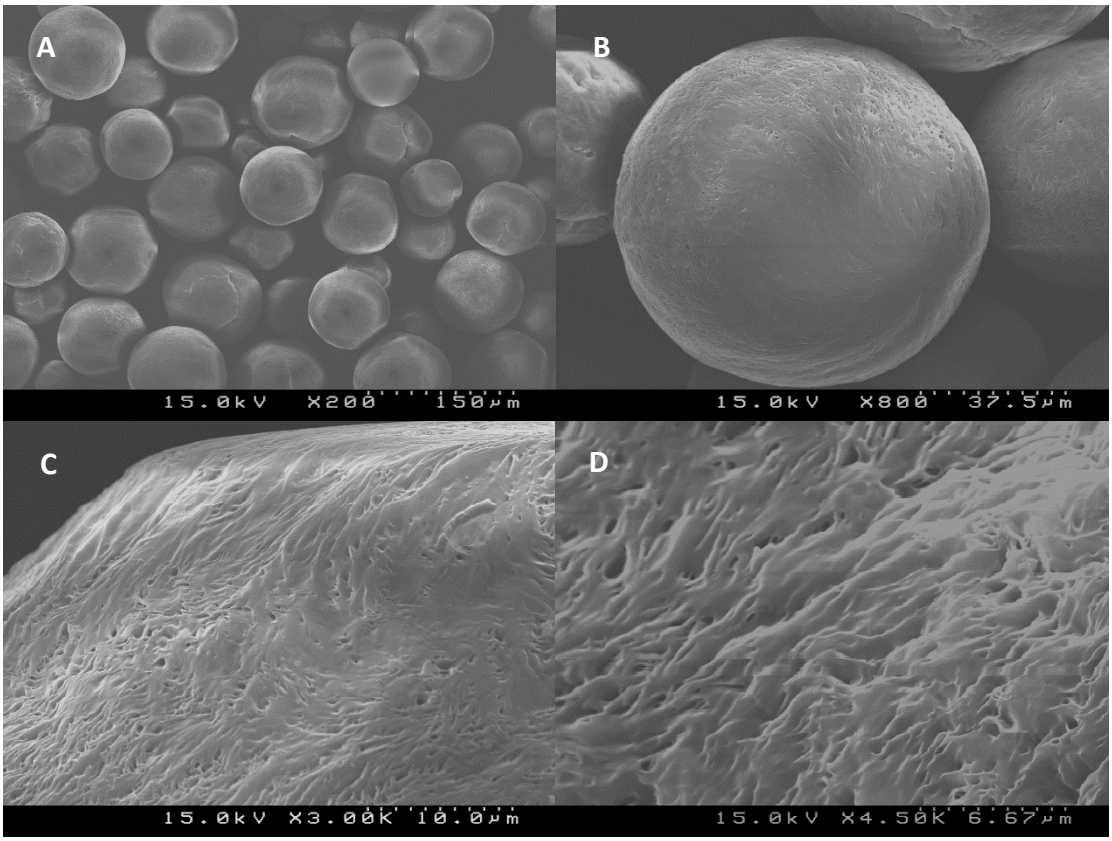

Figure 16. SEM micrographs of µPCL[MNPs] at 15.0 kV with different magnifications 200x (A), 800x (B), 3000x (C) and 4500x (D).

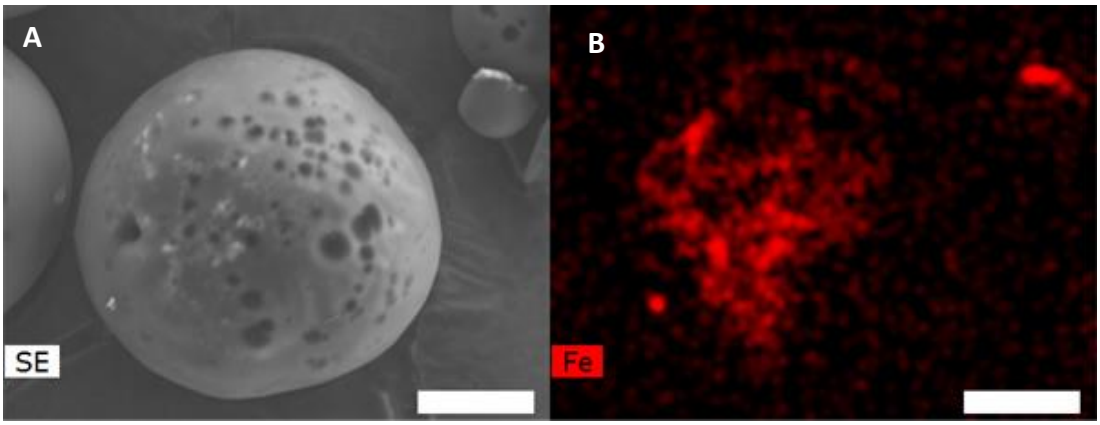

Figure 17. Electron microscopy characterization of MNPs inclusion in µPCL microparticles. Secondary electrons SEM micrographs (A) and Fe ion mapping of MNPs loaded in synthetized µPCL[MNPs] (B).

To further confirm that µPCL[MNPs] were responsive to externally applied magnetic fields the particles were placed in close contact with a neodymium magnet (40-42 MGOe; 318-334 kJ/m³; 1.29-1.32 Tesla). As shown in Figure 18 A, µPCL[MNPs] are readily responsive to magnetization being attracted to the magnet and agglomerating, whereas control non-magnetic µPCL particles remain unaltered and dispersed in solution.

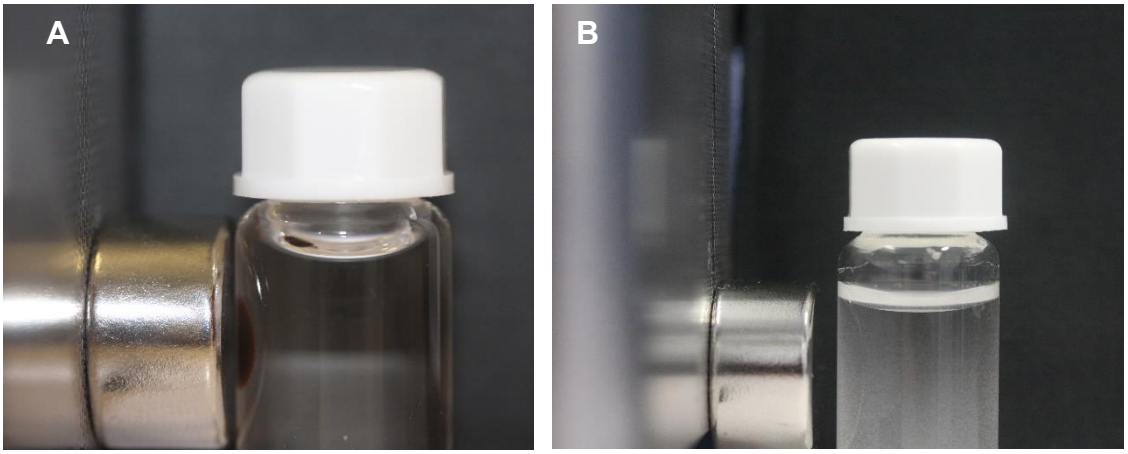

Figure 18. Microparticles response to magnetization. Magnetic µPCL[MNPs] (A) and non-magnetic control µPCL microparticles (B).

Following the successful inclusion of MNPs and the confirmation of microparticles response to magnetic stimuli, PCL particles surface was modified with Collagen I to promote cell adhesion and proliferation. Collagen I addition to PCL surface has previously shown to increase cells adhesion[23,24] and is a crucial aspect if cell culture on these spherical scaffolds is envisioned. Following plasma treatment to render PCL microparticles more hydrophilic they were dispersed in a Collagen I solution and extensively washed. To evaluate collagen deposition microparticles zeta potential was determined. The obtained results demonstrate that pristine PCL microparticles exhibit a negative zeta potential (ξ= -29.4 mV, Figure 19), on the contrary microparticles subjected to collagen coating display a positive zeta potential (ξ= +6.45 mV) indicating therefore the presence of collagen.

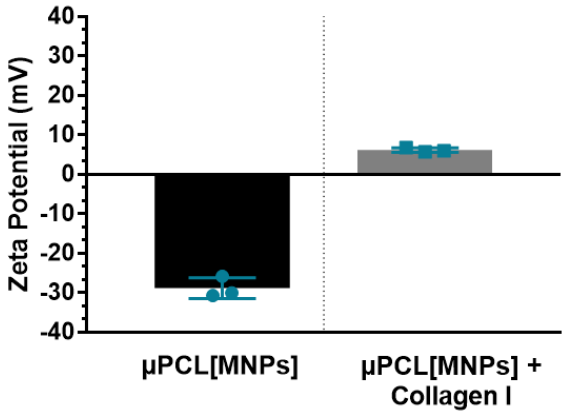

Figure 19. Zeta potential analysis of different microparticle formulations before and after Collagen I surface coating. Data is presented as mean ± s.d., n=3.

Having confirmed the formulation of hybrid nano-in-micro particles the production of Alginate beads were these systems would be further encapsulated was then addressed.

3.3. Production of Alginate beads and Cell-laden LBL microcapsules

Alginate beads production explores the ionotropic gelation occurring between Alginate and divalent cations such as calcium. Preliminary data on beads size was required to choose the proper formulation to for subsequent capsules production. Several formulations were tested as described in Table 1 and portrayed on Figures 20 to 22. All Alginate beads were produced by using the electrospray technique to obtain formulations with very low size variance (%C.V. < 10%).

Table 1. Alginate beads formulation parameters.

Formulation	Voltage (kV)	Average Size (µm)	Alginate % (w/v)	µPCL	% C.V.
B1	5	2169±78.53	2	-	3.62
B2	7.5	715.8±26.28			3.67
B3	10	491.3±25.27			5.14
B4	5	2297±92.53		30 mg of µPCL per mL Alginate	4.03
B5	7.5	775.9±21.92			2.83
B6	10	486.2±26.07			5.36
B7	5	1880±55.44	2.5	-	2.95
B8	7.5	688.4±22.92			3.33
B9	10	499.0±24.59			4.93
B10	5	2082±135.8		30 mg of µPCL per mL Alginate	6.52
B11	7.5	708.7±28.34			4.00
B12	10	580.3±27.23			4.69

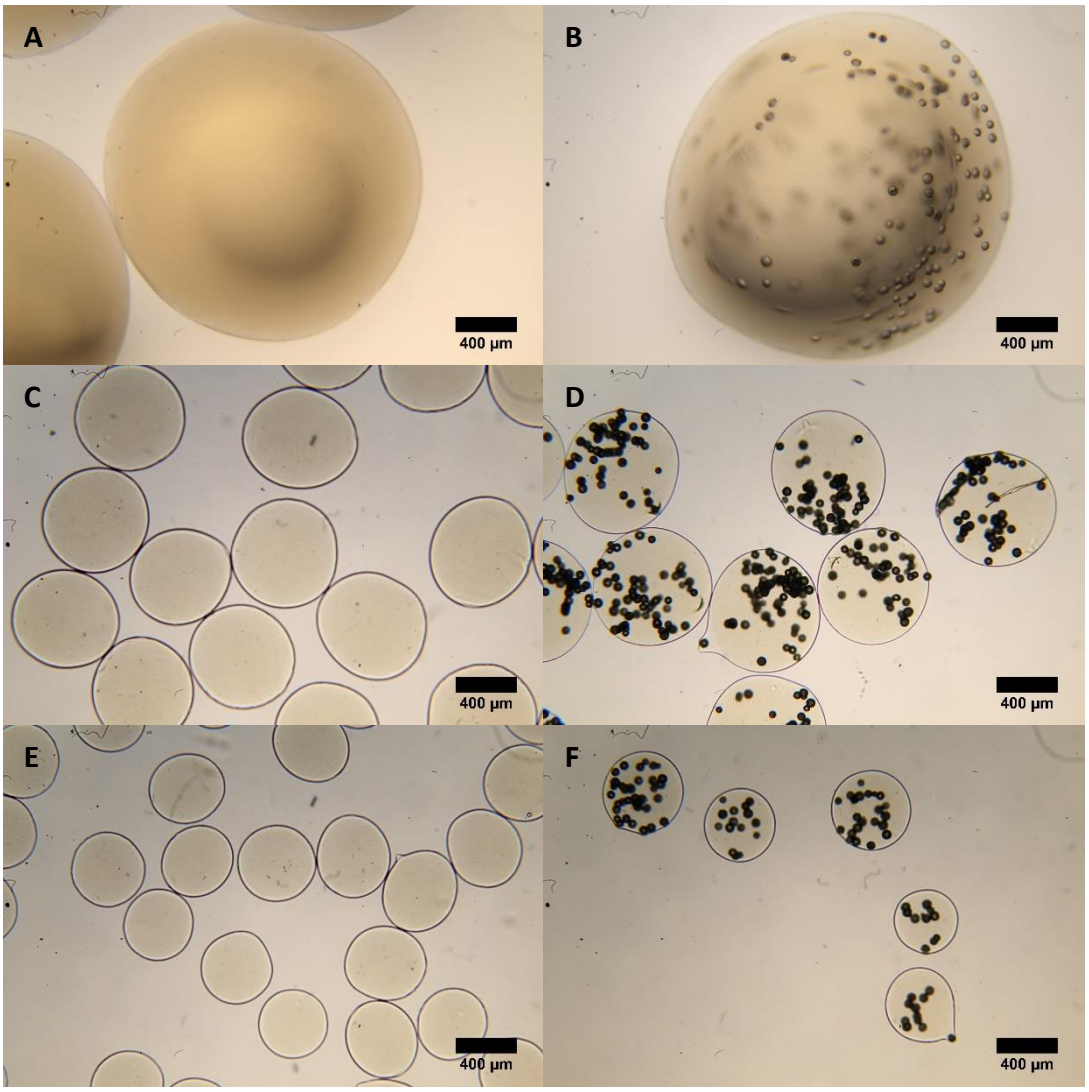

Figure 20. Optical contrast micrographs of Alginate beads produced using **2% Alginate** without µPCL (A,C and E) and with µPCL (B, D and F) with different voltages: 5kV (A and B), 7.5kV(C and D) and 10kV (E and F).

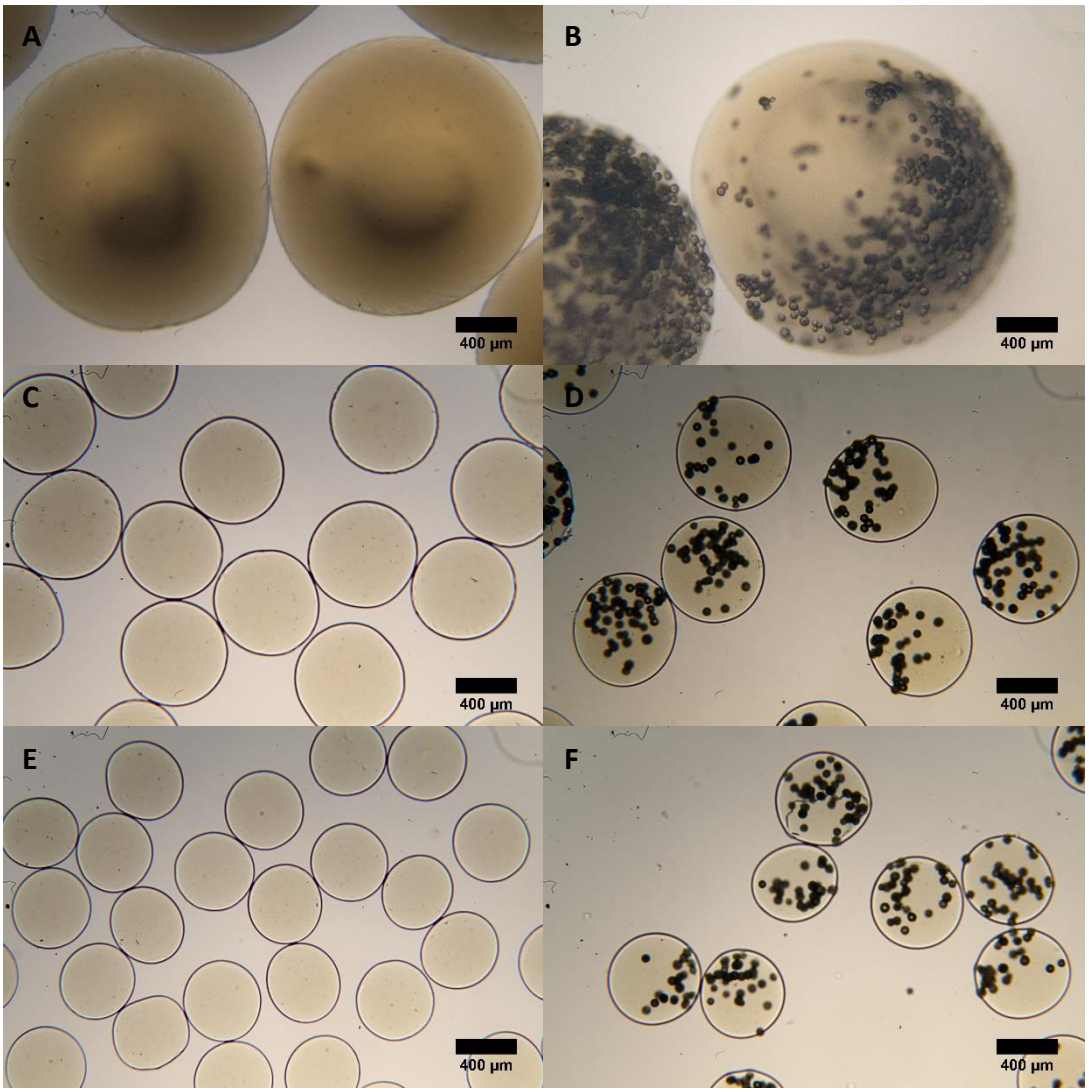

Figure 21. Optical contrast micrographs of Alginate beads produced using **2.5 % Alginate** without µPCL (A,C and E) and with µPCL (B,D and F) with different voltages: 5kV (A and B), 7.5kV(C and D) and 10kV (E and F).

As expected, in most electrosprayed formulations, when the Alginate solution contained µPCL microparticles larger Alginate beads were produced. Generally, the higher the voltage the smaller beads this is in accordance to recent reports[27]. All formulations revealed high monodispersity with size variations ranging only from 2.83 to 6.52 %. Moreover, all Alginate concentrations tested yielded beads with quasi-spherical morphology.

The electrospray assisted production of Alginate beads encapsulating µPCL[MNPs] (µPCL[MNPs]@ALG) was performed by using the optimal conditions of formulation B11. The obtained size distribution was 670.1± 32.51µm and with a size variation of 4.85%. Interestingly µPCL[MNPs]@ALG were slightly smaller but monodisperse and also displayed a spherical morphology (Figure 22A).

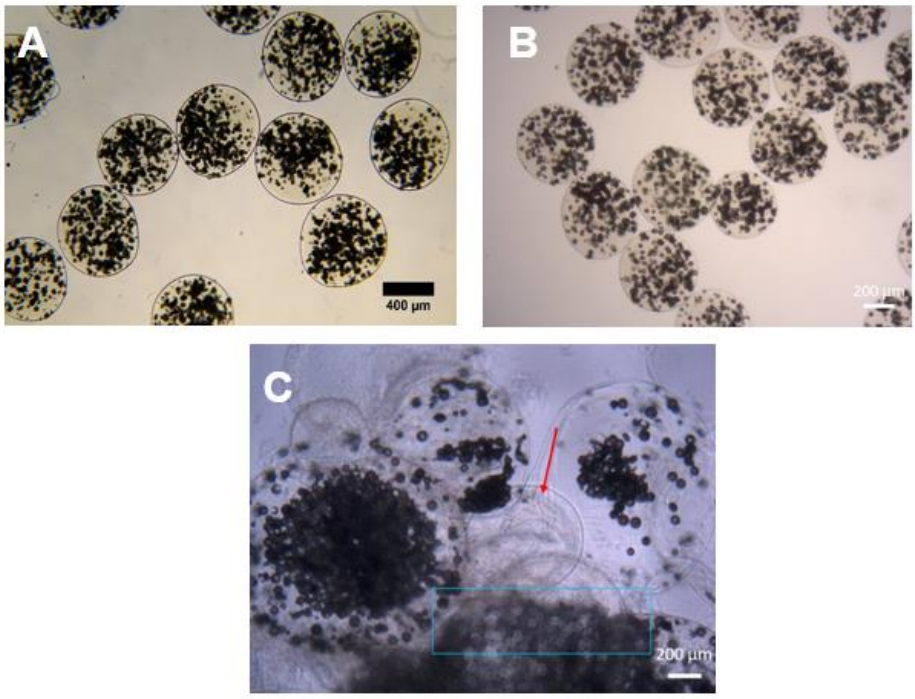

Figure 22. Optical contrast micrograph of electrosprayed hydrophobic µPCL[MNPs]@ALG microgel beads produced by using the parameters optimized for formulation B11 (7.5 kV). Dark spots indicate the presence of magnetic microparticles (A). µPCL[MNPs]@ALG microcapsules produced via LBL surface deposition (B). Effects of system clogging on the formulation of cell laden µPCL[MNPs]@ALG microcapsules. Red arrow indicates blank microcapsules. Blue rectangle indicates non-encapsulated microparticles (C).

Moreover, LBL deposition of oppositely charged polymers and subsequent EDTA calcium leaching from the core as led to the formation of highly robust and stable µPCL[MNPs]@ALG magnetic microcapsules. Despite these results, when MC3T3-E1 cells were included in µPCL[MNPs] Alginate mixtures and electrosprayed, a significant particle aggregation was observed on the electrospray system. This also led to the production of numerous LBL microcapsules without µPCL[MNPs] microparticles due to system clogging (Figure 22 C).

To overcome the former issues, capsules were produced by syringe-based extrusion. In these systems the use of molecular biology grade water to dissolve EDTA was crucial since in preliminary tests using 30 mg of microparticles per mL of 2.5% Alginate solution and using 0.02M EDTA dissolved in standard deionised water, the calcium ions were not chelated, and no capsules were formed. This might be explained by the presence of metal cations in the deionised water which were chelated instead of calcium ions which would not allow the liquefication of the beads all the way through.

The produced capsules size ranged from 2 to 3mm. This is an important parameter that has a key role on implantation or injection *in vivo*. Few years ago, the importance of size of spherical implant materials was reported[28]. The authors determined that spherical implants over 1.5 mm are more biocompatible than smaller implants since smaller implants triggered a more acute foreign body immune response and hence the application of larger spheres might be more effective as cell transplantation mechanisms for biomedical applications.

3.4.1 *In situ* magnetic fixation

To address the feasibility of magnetic force mediated microgels and microcapsules fixation the particles were placed on top of a section of porcine bone and subjected to a fluid displacement. Initially, the microgels and capsules were placed in the bone (Figure 23 and 24) and water was extruded. It was clear that both microgels and microcapsules were removed from their initial location. The same *ex vivo* experiment was repeated in the presence of a neodymium magnet near the top of the microgels and capsules (Figure 23 and 24). Interestingly the microcapsules remained intact in their initial location, indicating that *in situ* magnetic fixation of this system is possible in the context of open surgery/implantation medical procedures.

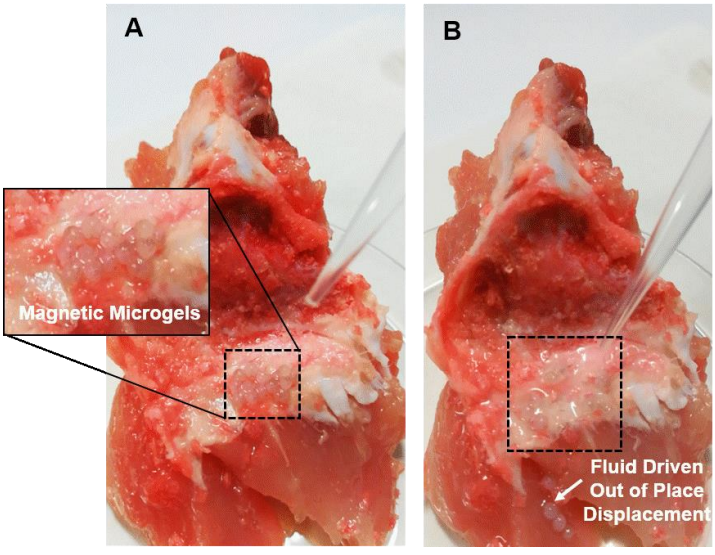

.

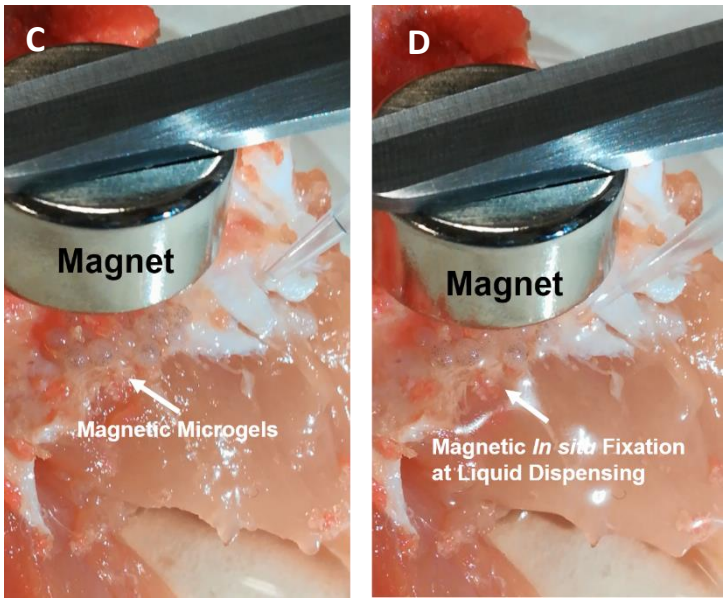

Figure 23. Assessing the feasibility of magnetic fixation of microgels. (A) Microgels prior to fluid flow; (B) Microgels after fluid extrusion; (C) Microgels prior to fluid extrusion with magnetic an applied field ; (D) Microgels after fluid extrusion with an applied magnetic field.

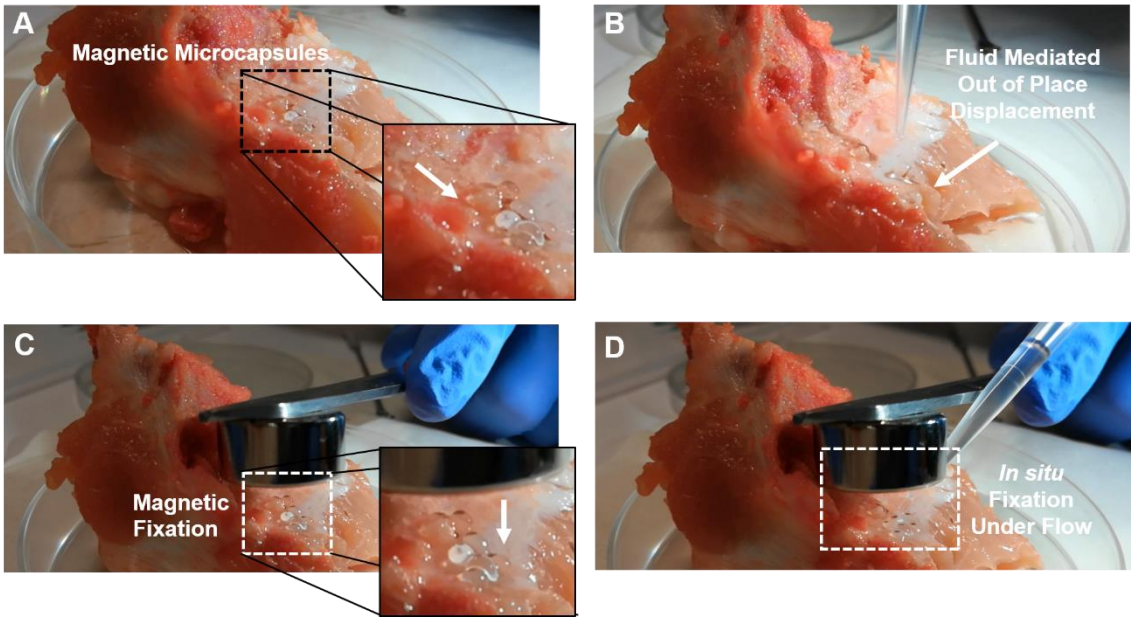

Figure 24. Assessing the feasibility of magnetic fixation of capsules. (A) Capsules prior to fluid extrusion; (B) Capsules after fluid extrusion; (C) Capsules prior to fluid extrusion with magnetic an applied field; (D) Capsules after fluid extrusion with an applied magnetic field.

3.4.2 Cell Bioencapsulation characterization

To evaluate if cells bioencapsulation and magnetic microparticles were not affecting loaded cells a time course live/dead assay was performed. As shown in Figure 25 A and B most of the cells encapsulated remained viable up to 7 days.

By analysing DAPI/phalloidin fluorescence images showed that the µPCL[MNPs] formed aggregates between day 3 and day 7 since the surface of the microparticles was completely covered with cells. The formation of these aggregates was further confirmed by SEM images (Figure 25). These microtissues play a critical role in the biological performance of such systems.

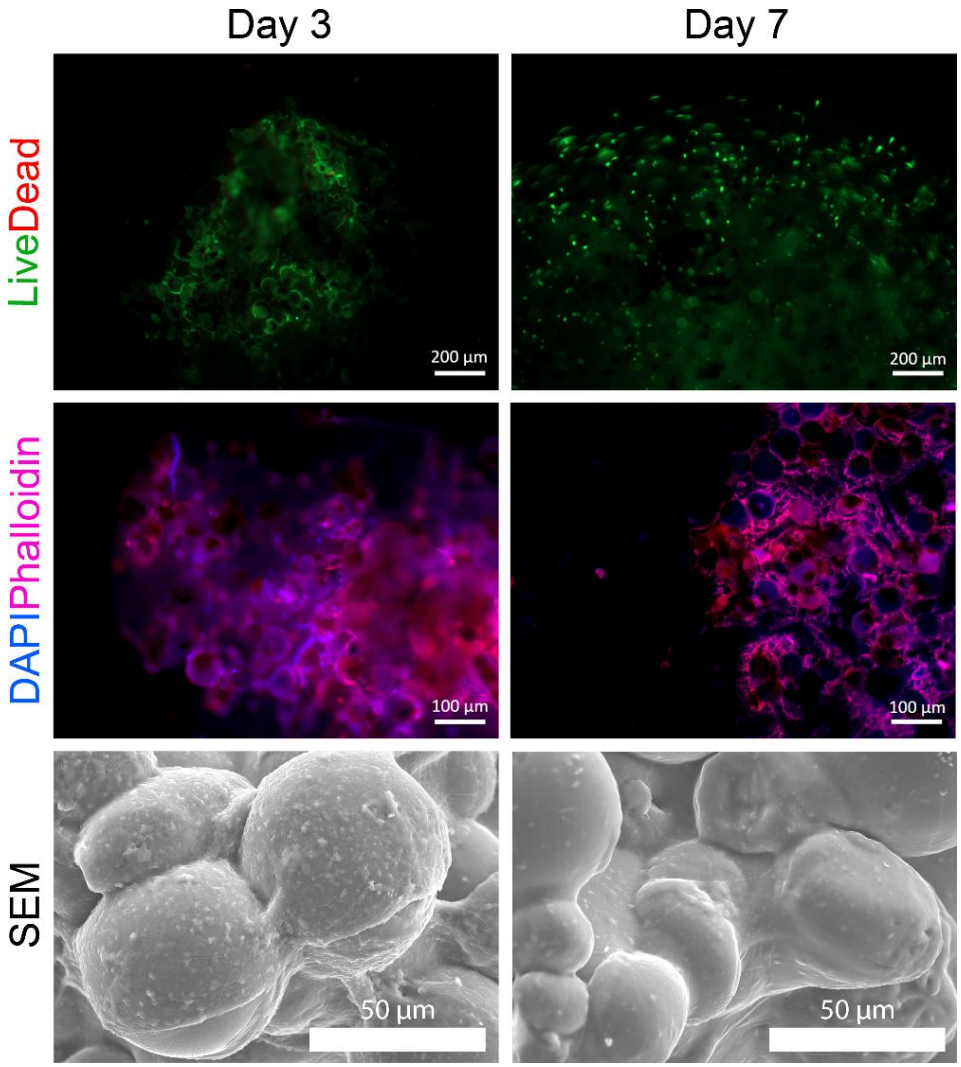

Figure 25. Fluorescence microscopy imaging (Live/Dead; DAPI/phalloidin) of capsules on day3 and day 7 and SEM images showing cells attached to µPCL[MNPs] that were loaded inside the compartmentalized LBL microcapsules.

3.4.2 Cell viability in Magnetic Microcapsules

The mitochondrial metabolic activity of cells was further determined in order to evaluate the feasibility of the system as an implantable medical scaffold- As the results demonstrate (Figure 26), the metabolic activity increased from day 3 to day 7, and as determined in the live/dead assay the MC3T3-E1 were still viable.

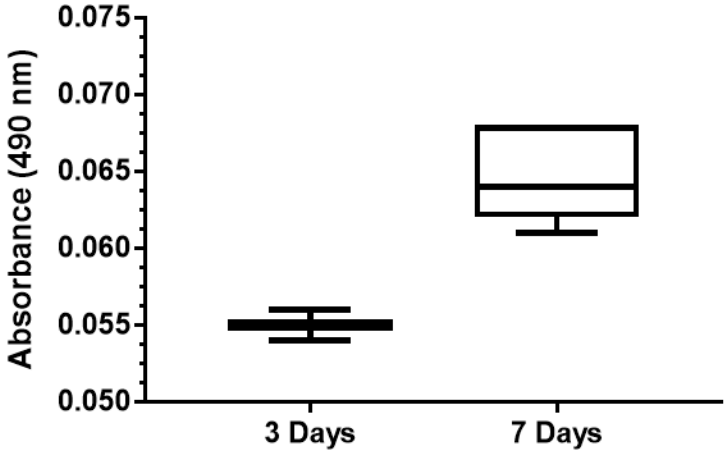

Figure 26. MTS metabolic activity assay performed after 3 days and 7 days by measuring the absorbance at 490nm.

Overall these obtained results showed that the µPCL[MNPs] effectively function as adhesion sites for cell culture and the liquefied environment of the capsules supported MC3T3-E1 culture for 7 days.

Moreover, since any type of cells can adhere to the µPCL[MNPs], different types of microtissues might be created and consequently this system could be applied for drug screening purposes as well. By fixing the capsules within a hydrogel, when implanted or injected *in situ*, the degradation of the capsules could be delayed allowing the proliferation of microtissues potentiating the regeneration of a damaged tissue.

5. Conclusion and future perspectives

Herein we reported the formulation of magnetic microcapsules as an *in situ* fixable cell rich system that can be used for tissue engineering and regenerative medicine applications. The systems demonstrated rapid response to the externally applied magnetic stimuli. Since the system is versatile other cells sources (e.g. stem cells) and cell co-culture (e.g. macrophages and stem cells) could be considered to be used in the future.

Overall, it is envisioned that magnetically fixable capsules will open a new avenue for bioencapsulated scaffolds translation. For this purpose, further *in vivo* studies should be performed on the adhesion of such systems under dynamic *in vivo* conditions.

6. Acknowledgments

The authors would like to acknowledge the support of the European Research Council Grant Agreement No. ERC-2014-ADG-669858 for project ATLAS. The authors also acknowledge the financial support by the Portuguese Foundation for Science and Technology (FCT) through a Post-Doctoral grant (SFRH/BPD/119983/2016,Vítor Gaspar). The authors would like to acknowledge Dr. Sónia Patrício for the help in iron identification by SEM-EDS

6. References

1. Quarto, R. & Giannoni, P. in *Methods in molecular biology (Clifton, N.J.)* **1416,** 21–33 (2016).
2. Hernlund, E. *et al.* Osteoporosis in the European Union: medical management, epidemiology and economic burden. *Arch. Osteoporos.* **8,** 136 (2013).
3. Salgado, A. J., Coutinho, O. P. & Reis, R. L. Bone Tissue Engineering: State of the Art and Future Trends. *Macromol. Biosci.* **4,** 743–765 (2004).
4. Griffin, K. S. *et al.* Evolution of Bone Grafting: Bone Grafts and Tissue Engineering Strategies for Vascularized Bone Regeneration. *Clin. Rev. Bone Miner. Metab.* **13,** 232–244 (2015).
5. Zhu, Y. *et al.* Protein Corona of Magnetic Hydroxyapatite Scaffold Improves Cell Proliferation via Activation of Mitogen-Activated Protein Kinase Signaling Pathway. *ACS Nano* **11,** 3690–3704 (2017).
6. Yuan, Z. *et al.* Development of a 3D Collagen Model for the In Vitro Evaluation of Magnetic-assisted Osteogenesis. *Sci. Rep.* **8,** 16270 (2018).
7. Cai, Q. *et al.* Osteogenic differentiation of MC3T3-E1 cells on poly(l-lactide)/Fe3O4 nanofibers with static magnetic field exposure. *Mater. Sci. Eng. C* **55,** 166–173 (2015).
8. Yun, H.-M. *et al.* Magnetic nanocomposite scaffolds combined with static magnetic field in the stimulation of osteoblastic differentiation and bone formation. *Biomaterials* **85,** 88–98 (2016).
9. Xia, Y. *et al.* Magnetic field and nano-scaffolds with stem cells to enhance bone regeneration. *Biomaterials* **183,** 151–170 (2018).
10. Correia, C. R., Reis, R. L. & Mano, J. F. Design Principles and Multifunctionality in Cell Encapsulation Systems for Tissue Regeneration. *Adv. Healthc. Mater.* **7,** 1701444 (2018).
11. Correia, C. R. *et al.* Semipermeable Capsules Wrapping a Multifunctional and Self-regulated Co-culture Microenvironment for Osteogenic Differentiation. *Sci. Rep.* **6,** 21883 (2016).
12. Hou, Y. *et al.* Injectable degradable PVA microgels prepared by microfluidic technology for controlled osteogenic differentiation of mesenchymal stem cells. *Acta Biomater.* **77,** 28–37 (2018).
13. Correia, C. R., Gil, S., Reis, R. L. & Mano, J. F. A Closed Chondromimetic Environment within Magnetic-Responsive Liquified Capsules Encapsulating Stem Cells and Collagen II/TGF-β3 Microparticles. *Adv. Healthc. Mater.* **5,** 1346–1355 (2016).
14. Li, F. *et al.* Cartilage tissue formation through assembly of microgels containing mesenchymal stem cells. *Acta Biomater.* **77,** 48–62 (2018).
15. Correia, C. R. *et al. In vivo* osteogenic differentiation of stem cells inside compartmentalized capsules loaded with co-cultured endothelial cells. *Acta Biomater.* **53,** 483–494 (2017).

16. Zhang, S., Xu, K., Darabi, M. A., Yuan, Q. & Xing, M. Mussel-inspired Alginate gel promoting the osteogenic differentiation of mesenchymal stem cells and anti-infection. *Mater. Sci. Eng. C* **69,** 496–504 (2016).

17. Chang, S. H. *et al.* In vitro and *in vivo* study of the application of volvox spheres to co-culture vehicles in liver tissue engineering. *Acta Biomater.* **63,** 261–273 (2017).

18. Bjørge, I. M. *et al.* Tuneable spheroidal hydrogel particles for cell and drug encapsulation. *Soft Matter* **14,** 5622–5627 (2018).

19. Costa, A. M. S. & Mano, J. F. Solvent-Free Strategy Yields Size and Shape-Uniform Capsules. *J. Am. Chem. Soc.* **139,** 1057–1060 (2017).

20. Mahdavi, M. *et al.* Synthesis, Surface Modification and Characterisation of Biocompatible Magnetic Iron Oxide Nanoparticles for Biomedical Applications. *Molecules* **18,** 7533–7548 (2013).

21. Ferreira, L. P., Gaspar, V. M. & Mano, J. F. Bioinstructive microparticles for self-assembly of mesenchymal stem Cell-3D tumor spheroids. *Biomaterials* **185,** 155–173 (2018).

22. Schneider, C. A., Rasband, W. S. & Eliceiri, K. W. NIH Image to ImageJ: 25 years of image analysis. *Nat. Methods* **9,** 671–5 (2012).

23. Correia, C. R., Reis, R. L. & Mano, J. F. Multilayered Hierarchical Capsules Providing Cell Adhesion Sites. *Biomacromolecules* **14,** 743–751 (2013).

24. Correia, C. R., Sher, P., Reis, R. L. & Mano, J. F. Liquified chitosan–Alginate multilayer capsules incorporating poly(l -lactic acid) microparticles as cell carriers. *Soft Matter* **9,** 2125–2130 (2013).

25. Wang, J. *et al.* Synthesis and antitumor efficacy of daunorubicin-loaded magnetic nanoparticles. *Int. J. Nanomedicine* **6,** 203–11 (2011).

26. Soares, P. I. P. *et al.* Iron oxide nanoparticles stabilized with a bilayer of oleic acid for magnetic hyperthermia and MRI applications. *Appl. Surf. Sci.* **383,** 240–247 (2016).

27. Rutkowski, S., Si, T., Gai, M., Frueh, J. & He, Q. Hydrodynamic electrospray ionization jetting of calcium Alginate particles: effect of spray-mode, spraying distance and concentration. *RSC Adv.* **8,** 24243–24249 (2018).

28. Veiseh, O. *et al.* Size- and shape-dependent foreign body immune response to materials implanted in rodents and non-human primates. *Nat. Mater.* **14,** 643–651 (2015).

RESULTS AND DISCUSSION

5.General conclusions and Future Perspectives

The use of 3D culture to recapitulate *in vivo* has paramount importance in tissue engineering studies to achieve the most reliable responses.

Throughout this thesis the assembly of a compartmentalized system for cell encapsulation was studied by starting with the nanoscale (MNPs), the microscale (µPCL and µPCL[MNPs] and lastly with macroscale (capsules).

Overall, the capsules exhibited a good capacity to maintain cell viability and metabolic activity as it was demonstrated by the MTS assay and fluorescence imaging. When placed in porcine bone it was evident that when there was not a magnetic field applied, the capsules were washed away by fluids and when the magnetic field was applied it was possible to fixate them to the site even after disturbance.

In the future, this system could be implanted and fixated in an injured site coupled with stem cells to promote regeneration or even by releasing growth factors and cytokines to promote such regeneration. For this specific application the system herein developed can be improved by for example using co-cultures that could potentiate the pro-osteogenic potential. Moreover, it will be important to address the host response upon implantation to these systems, such insights have already been demonstrated by our group but further investigation regarding the long-term effects and capsules degradability could be of interest for the final application.

6. References

1. Mahdavi, M. *et al.* Synthesis, Surface Modification and Characterisation of Biocompatible Magnetic Iron Oxide Nanoparticles for Biomedical Applications. *Molecules* **18,** 7533–7548 (2013).

2. Ferreira, L. P., Gaspar, V. M. & Mano, J. F. Bioinstructive microparticles for self-assembly of mesenchymal stem Cell-3D tumor spheroids. *Biomaterials* **185,** 155–173 (2018).

3. Correia, C. R., Reis, R. L. & Mano, J. F. Multilayered Hierarchical Capsules Providing Cell Adhesion Sites. *Biomacromolecules* **14,** 743–751 (2013).

4. Correia, C. R., Sher, P., Reis, R. L. & Mano, J. F. Liquified chitosan–alginate multilayer capsules incorporating poly(l -lactic acid) microparticles as cell carriers. *Soft Matter* **9,** 2125–2130 (2013).

5. Schneider, C. A., Rasband, W. S. & Eliceiri, K. W. NIH Image to ImageJ: 25 years of image analysis. *Nat. Methods* **9,** 671–5 (2012).

7. Annexes

Supplementary Table 1 – Microparticles production formulations . F# represents a formulation and S# corresponds to the same formulation after sieving

Formulation	%PCL	V_{PCL}	Pressure	Needle	MNPs	% PVA	V_{PVA}	Tubing	Beaker	RPM	Size distribution(µm)	%variation
F1	1.5	8.0	5 bar	22G	-	0.5	150 mL	1mm	250mL	500	49.9±27.8	55.71
S1					-						58.0±7.88	13.59
F2					0.8mg/mL						41.1±19.0	46.23
S2					0.8mg/mL						56.3±9.10	16.16
F3					-					600	33.0±10.3	31.21
S3					-						55.7±8.01	14.38
F4					0.8mg/mL						37.7±18.5	49.07
S4					0.8mg/mL						55.3±9.14	16.52
F5					-					900	32.2±10.1	31.37
S5					-						58.3±5.87	10.07
F6					0.8mg/mL						34.1±11.2	32.84
S6					0.8mg/mL						47.5±10.3	21.68
F7					-					1000	35.9±12.1	33.70
S7					-						49.1±11.4	23.22
F8					0.8mg/mL						32.4±9.11	28.12
S8					0.8mg/mL						54.6±8.15	14.93
F9	3.0	8.0	5 bar	22G	-	0.5	150mL	1mm	250 mL	500	57.3±23.0	40.14
S9					-						50.7±12.5	24.65
F10					0.8mg/mL						40.5±13.2	32.62
S10					0.8mg/mL						55.3±9.00	16.28
F11					-					600	54.5±30.6	56.15
S11					-						57.8±7.85	13.58
F12					0.8mg/mL						37.3±13.8	37.00
S12					0.8mg/mL						54.5±8.88	16.29

F13	3.0	8.0	5 bar	22G	-	0.5	150mL	1mm	250mL	900	51.7±17.9	34.62
S13					-						58.9±7.49	12.72
F14					0.8mg/mL						36.0±9.71	26.97
S14					0.8mg/mL						52.9±10.1	19.09
F15					-					1000	46.1±14.1	30.58
S15					-						54.3±8.45	15.56
F16					0.8mg/mL						34.1±11.6	34.02
S16					0.8mg/mL						52.4±9.77	18.64
F17	5.0	8.0	5 bar	22G	-	0.5	150mL	1mm	250mL	500	140±84.6	60.42
S17					-						59.8±8.20	13.71
F18					0.8mg/mL						92.0±60.5	65.69
S18					0.8mg/mL						57.6±7.65	13.28
F19					-					600	84.1±64.2	76.34
S19					-						57.7±9.71	16.82
F20					0.8mg/mL						100±44.6	44.60
S20					0.8mg/mL						58.9±6.18	10.49
F21					-					900	90.7±52.9	58.32
S21					-						58.2±8.17	14.04
F22					0.8mg/mL						68.9±32.6	47.31
S22					0.8mg/mL						63.4±5.81	9.164
F23					-					1000	74.8±49.6	66.31
S23					-						56.8±9.07	15.97
F24					0.8mg/mL						68.6±30.1	43.88
S24					0.8mg/mL						59.3±8.23	13.88